MAGNETOSPHERIC VLF LINE RADIATION

by

Keith Howard Yearby

A thesis submitted to the University of Sheffield for the degree of Doctor of Philosophy

Department of Physics,

The University,

Sheffield 10   August 1982

Magnetospheric VLF Line Radiation
by K.H. Yearby

Summary

        Magnetospheric VLF Line Radiation (MLR) is a broad
band VLF emission (typically 1 kHz wide centered on 3 kHz)
which has line structure in its spectrum. The events studied
were received durring 1977-80 at Halley, Antarctica and also
in the geomagnetically conjugate region (Newfoundland). The
occurrence of Halley MLR events as a function of local time
and geomagnetic activity and the differences in MLR activity
between Halley and Siple, Antarctica are discused. An MLR
event received on 26 June 1978 may be the result of
magnetospheric amplification of VLF radiation of harmonics
from electrical power lines (PLHR) in the conjugate region;
the radiated power required was estimated to be 50 mW. Most
Halley MLR events do not have any direct relation with PLHR
although in several of the generation mechanisms discused
PLHR may have an indirect role.

        A series of measurements of the electromagnetic
field near to several power transmission lines in
Newfoundland were made to determine the magnitude of the
unbalanced harmonic currents and the skin depth in the
ground, which in turn were used to estimate the strength of
PLHR entering the magnetosphere. The largest radiated power
determined for a single line was 500 nW in the range 2.7 to
3.7 kHz although much larger powers may be radiated from the
more industrialised regions further west.

        A description of the VLF receiver and some
improvements made to it is given followed by a review of
spectrum analysis techniques and a description of some
methods used for the work on PLHR and MLR .

Acknowledgements

I would foremost like to express my thanks to my supervisors Prof. T.R. Kaiser and Dr. K. Bullough and to Dr. A.J. Smith for their guidance and advice on all aspects of my research without which the work presented in this thesis would not have been possible. I am grateful to Dr. J.P. Matthews for making the quiet band theory available to me prior to publication and for advice on the subject of MLR, and to Dr. H.J. Strangeways for advice and for help in the search for MLR events. I would like thank V. Sonwalkar of Stanford University for information on MLR activity at Siple.

I am grateful to Mr. J.C. Hakes for preparing the equipment for the Newfoundland expedition and participating in the field work and for his help in the VLF laboratory. I would like to thank the staff of the physics department and in particular Mr. P. Hughes, Mr. A. Strong, Mr. M.R. Ashworth and Mr. I.D. Smith for their help, and also the staff of the University computing services.

I thank the British Antarctic Survey for providing some of the analysis equipment, and the men at Halley during 1977-80 for operating the VLF receiver. I also thank the Science Research Council for financing the Newfoundland expedition and the analysis equipment and also for providing me with a research grant.

I am grateful to Mr. J.A. Thompson for writing an interactive graphics program used to produce many of the figures and for typing the text into a computer for word

Contents

.

Chapter 1   Introduction

The work described in this thesis is concerned with magnetospheric VLF line radiation. This is a broad band VLF emission which exhibits line structure. The emissions, at Halley, are typically of 1kHz bandwidth centered between 2 and 4 kHz, with a spacing between adjacent spectral lines of about 60 Hz . They last between 1 minute and 30 minutes. The 60 Hz spacing is one reason why attempts have been made to associate magnetospheric line radiation (MLR) with power line harmonic radiation (PLHR).

When considering the possible effects of PLHR on the magnetospheric wave environment, it is important to know the intensity of PLHR entering the magnetosphere. Measurements of VLF radiation from power lines have been carried out recently by Yoshino (quoted by Boerner 1981), Hayashi et al. (1978) and Barr (1979) using ground based, balloon and rocket experiments. To assess the possible relation of the MLR events received at Halley to PLHR in the conjugate region, Newfoundland, a series of measurements were made there during June 1980 to estimate the radiated power. This work is fully described in chapter 4.

The MLR events, which are studied in chapter 5, have been received principally at Halley, Antarctica (75.5 S, 26.9 W), although some events were also received in the conjugate region, Newfoundland.

The VLF receiver is described in chapter 2 which includes an account of some recent modifications and a discussion of the methods used for calibration.

Spectrum analysis has been used extensively for the work presented in chapters 4 and 5 and so in chapter 3 there is a review of spectrum analysis techniques. This is followed by a description of some methods developed specifically for the analysis of VLF data and an outline of a design for a future VLF analysis system.

Line radiation of magnetospheric origin has been observed at Siple, Antarctica (75.9 S, 84.2 W) (Helliwell et al. 1975) and also at the conjugate, near Roberval, Quebec (48.4 N, 72.3 W). In this case there appeared to be a definite relationship between the magnetospheric lines and the power line harmonics radiated from power lines in the Roberval area, which were observed on the data recorded at Roberval. However, the frequencies of the magnetospheric lines were not exactly those of the power line harmonics, (ie. odd multiples of 60 Hz) but were 20 to 30 Hz higher in frequency than the closest PLHR line.

Magnetospheric line radiation received at Halley does not usually have a definite relationship to PLHR. The line spacings are very variable, usually between 50 and 120 Hz, and the lines are observed to drift in frequency by as much as 100 Hz in one minute. Power line harmonics do not exhibit such sustained drifts and so the magnetospheric lines cannot be locked onto power line harmonics. Also MLR is observed less often at Halley than at Siple and at different local times.

There is much controversy at present about the extent to which PLHR influences the wave activity in the magnetosphere (Tsurutani and Thorne 1981). Some authors consider PLHR to have a catalytic role in the generation of chorus. Luette et al. (1977) examined the geographical distribution of chorus detected by the OGO-3 satellite and found that the highest probability of occurrence corresponded to industrialised regions. This effect was attributed to PLHR. However, Russell (1980) has shown that the observed localisation in the geographical distribution of chorus may be due to a convolution of the spatial distribution of chorus with the spatial coverage of the OGO-3 satellite, which has an 89 day period associated with its orbit. However, Luette et al. (1980) have re-examined their data to check if the observed peaks in chorus occurrence were due to biased sampling and concluded that they were not.

Tsurutani et al. (1979) have criticised the work of Luette et al. (1977) on the grounds that they over-sampled the data. This resulted in the geographical variations appearing more statistically significant than they really were. They also found no evidence of geographical localisation of chorus using OGO-5 data. However, they only examined the ELF band where earlier work (Bullough et al. 1976, Tatnall et al. 1978) has shown that no localisation would be expected.

Luette et al. (1979) analysed the starting frequencies of chorus elements received on OGO-3, and found these to be within a few hertz of power line harmonics frequencies. Further, it was found that emissions detected over the eastern USA and Canada were controlled by 60 Hz harmonics whereas those over Western Europe were controlled by 50Hz harmonics. On the Alaska - New Zealand meridian starting frequencies of both 50 and 60 Hz were observed.

Park and Helliwell (1977) have suggested that PLHR may have a catalytic role in the generation of whistler precursors. Precursors with starting frequencies equal to 60 Hz power line harmonics have been observed at Siple and Roberval.

A weekly variation in VLF activity at Siple, Antarctica was reported by Park and Miller (1979) who found a minimum in activity on Sundays corresponding to reduced electrical power usage in the conjugate region, Roberval, Quebec. They measured the intensity of VLF emissions, which were thought to be mainly chorus, in the band 2 - 4 kHz. This result has been criticised by Thorne and Tsurutani (1981) who showed that the observed local time dependence of the activity observed at Siple is not consistent with the local time dependence of chorus observed by satellite (OGO-5) and concluded that the former activity was mainly hiss. Secondly they point out that ground based measurements are not representative of magnetospheric chorus as a whole since many of the waves do not reach the ground. However, Park and Miller (1981) point out in reply that the spacial

11

and frequency coverage of the OGO-5 satellite is quite different from that of the Siple VLF receiver and so the occurrence of chorus measured by the two receivers would be expected to be different. In any case, the Sunday minimum still provides evidence of man made control on the VLF activity at Siple.

During 1972 an automatic VLF receiver similar to that on Ariel 4 was operated at Halley, which logged the peak, mean and minimum amplitudes in a number of frequency bands. Analysis of the minimum amplitude in the range 2.7 to 3.7 kHz showed a small (0.6dB) but significant decrease in activity on Sundays (Yearby et al. 1981). However, subsequent checks on the receiver showed that the indicated amplitude in the above band was also influenced by signals from VLF transmitters in the 10 to 20 kHz range, and so the unlikely possibility that the variation was due to VLF transmitters cannot be ruled out.

From studies using the Ariel 3 and 4 satellites Bullough and Kaiser (1979) report a zone of sustained VLF emission at 3.2 kHz over North America and its southern geomagnetic conjugate, which they attribute to PLHR. Although Lyons (1978) has demonstrated a striking similarity between the distribution of thunderstorm activity and the observed VLF maximum over North America, the integrated mean signal intensity due to sferics, even in the world's most active thunderstorm areas is 10 to 20 dB below the observed VLF maximum. Bullough (1981) also points out that at the principal thunderstorm centers in North America (Colorado

and Florida) thunderstorms are present on 70% of all days in the summer, implying that there are a significant number of occasions when storm activity is low. Since the sustained VLF emission was present in 100% of passes this cannot have been due to thunderstorm noise. Therefore, PLHR remains the most likely source of the VLF emission.

Bullough and Cotterill (1982) have recently made detailed studies of the character of the emission observed over North America and its conjugate, the Atlantic and other locations. The character of the emission was identified by curves of the frequency (in the statistical meaning) distribution of amplitudes for the peak, mean and minimum amplitudes observed within a 28 second period in each of the frequency bands studied (1kHz wide bands at 3.2 and 9.6 kHz). A comparison of the emissions observed in the invariant latitude range $45^{o}<\Lambda<55^{o}$, to the west of 10° invariant longitude (American mainland), with the corresponding region to the east (North Atlantic) and their respective conjugate regions is particularly interesting. Although the sferic wave field (measured using the 9.6 kHz band) was significantly weaker in the southern conjugate of both regions compared with the north (a similar situation was observed for 3.2 kHz in the eastern region) almost identical emissions were detected in the western region and its conjugate. This difference is explained by assuming the presence of almost permanent multi-hop propagation conditions over the western region but not over the eastern region, which requires a mechanism for maintaining the

permanent duct structure required. Lefeuvre and Bullough (1973) found that ducts could be sustained by VLF emission and the consequent particle precipitation; the VLF emission in this case may be the result of magnetospheric amplification of PLHR (which would be radiated over the American mainland but not over the Atlantic).

Complementary to measurements of PLHR intensity are experiments to determine the power threshold for a coherent input signal such as PLHR to cause a magnetospheric effect. Active experiments using a VLF transmitter can provide an estimate of this. Park and Chang (1978) used the VLF transmitter at Siple to radiate simulated power line harmonics and found that a radiated power of 0.5 W per harmonic was sufficient to stimulate a magnetospheric effect. Helliwell et al. (1980) report a minimum radiated power of 1 W required for wave growth and triggering.

Transportable VLF transmitters have been operated in New Zealand by Koons et al. (1978), in Alaska by Dowden et al. (1978) and in Norway by Garnier et al. (1981), the latter using a borrowed power line as an antenna.

2.1 The VLF Receiver (Brief Description)

The VLF goniometer receiver electronically synthesises the signal that would be received from a rotating loop aerial using the signals from two perpendicular stationary vertical loop aerials. The goniometer principle is used to determine the direction of arrival of the received signals as described by Bullough and Sagredo (1973). A block diagram of the receiver is shown in figure 2.1.

The preamplifier (described by Francis 1979) uses low noise field effect transistors in a cascode configuration to achieve a sensitivity of 8×10^{-18} $Wm^{-2}Hz^{-1}$ at 1 kHz using loop aerials of 58 m^2 area. A smaller (5.34 m^2) portable loop aerial system is also available with a sensitivity of 2.5×10^{-16} $Wm^{-2}Hz^{-1}$. The dynamic range of the preamplifier is very large so that signals as strong as 120 pT RMS (at 5 kHz) can be received without distortion using the large loop aerials, or as strong as 700 pT using the small loop aerials. This means that filters to remove the signals received from the very powerful VLF transmitters in the 10 to 20 kHz range can be placed after the preamplifier within the main receiver. These signals have to be filtered out since they would otherwise over modulate the tape recorder or require the recording level to be reduced to the extent that the signal to noise ratio for the natural VLF signal would be degraded by tape noise. A 42 dB per

Figure 2.1

V.L.F. GONIOMETER

BLOCK DIAGRAM

JUNE 1979
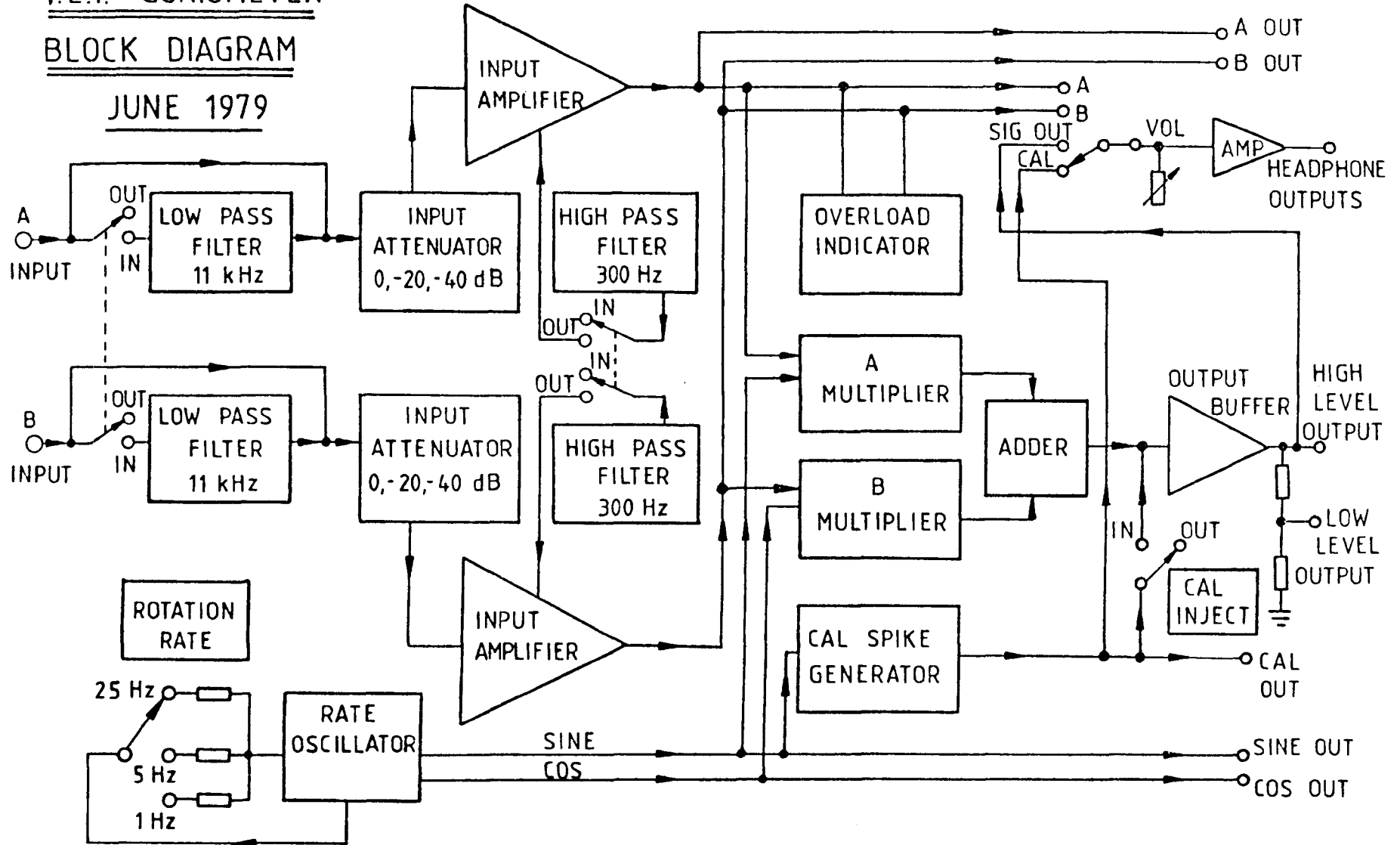
octave low pass filter with a cutoff frequency of 11 kHz and a 6 dB per octave high pass filter with a cutoff frequency of 300 Hz are provided, which may be switched in or out as required. Also available is a switched attenuator providing 0, 20 or 40 dB attenuation between the preamplifier and the goniometer. When using the 40 dB setting, the maximum signal that can be received without distortion is determined by the preamplifier.

The multiplication by sine and cosine required in the goniometer process is now performed using analogue multiplier integrated circuits rather than the Hall effect multipliers described by Bullough and Sagredo (1973). The rotation phase reference is recorded on the second track of the tape recoder using a 9.5 kHz carrier with the same modulation phase as a signal received from the North-South direction. An IRIG B time code is also recorded on this track using a 1 kHz carrier.

2.2 Preamplifier Resonance Correction

2.2.1 Introduction

The preamplifier described by Francis (1979) had a strong resonance peak between 1 and 2 kHz (fig 2.2a). This was known to be due to the self capacitance of the input transformer secondary winding forming a resonant circuit with its shunt inductance and the transformed inductance of the loop aerial. The transformer was required to match the low impedance of the aerial (0.3 Ω) to the high impedance of the FET preamplifier (20 MΩ). This required the transformer to have a very large number of secondary turns (13,000) which resulted in the significant self capacitance.

The resonance was undesirable on two counts; firstly it increased by up to 20 dB the dynamic range of the received signals which often resulted in over modulation of the tape recorder at the resonant frequency. Secondly, associated with the peak in the amplitude response are phase shifts of up to 90°. Since the resonance will not be exactly the same on each channel of the preamplifier some differential phase shift will occur between the two channels. When the signals are summed in the goniometer after multiplying by sine and cosine the combined signal will not correctly represent the signal from a single rotating loop. Therefore, measurements of the bearings of signals near the resonant frequency may not give correct results.

2.2.2 Low Input Impedance Preamplifier

One solution to the problem would be be to use a low input impedance preamplifier which would firstly damp the resonance and secondly, since the transformer turns ratio required would be much less, the self capacitance of the secondary winding would be much reduced and the resonant frequency increased to outside the frequency range of the receiver. The Stanford University VLF receiver (Paschal 1980) uses this method to achieve a flat frequency response down to 1 kHz.

A VLF preamplifier was constructed using a ZN459 very low noise amplifier integrated circuit, which has an input impedance of 7 k Ω, an equivalent input noise resistance of 40 Ω and a gain of 1000. A transformer was wound using the standard primary windings of 6 turns (for large loop aerials) and a secondary of 900 turns to match the loop impedance to 7 k Ω.

The gain and noise response for this preamplifier as a function of frequency are shown in figure 2.2b. Comparing figure 2.2a with figure 2.2b it is observed that below about 7 kHz the signal to noise ratio of the ZN459 preamplifier is slightly inferior to that of the FET preamplifier, whereas above 7 kHz the reverse is true. The ZN459 preamplifier has a low frequency roll off, with the -3 dB point at 2.4 kHz but is otherwise flat to within $\pm$1 dB from 3 kHz to 20 kHz. The flat response results from the increasing inductive reactance of the loop (2 Ω at 5 kHz compared with the input impedance of the amplifier 0.3 Ω)

PREAMPLIFIER FREQUENCY RESPONSE
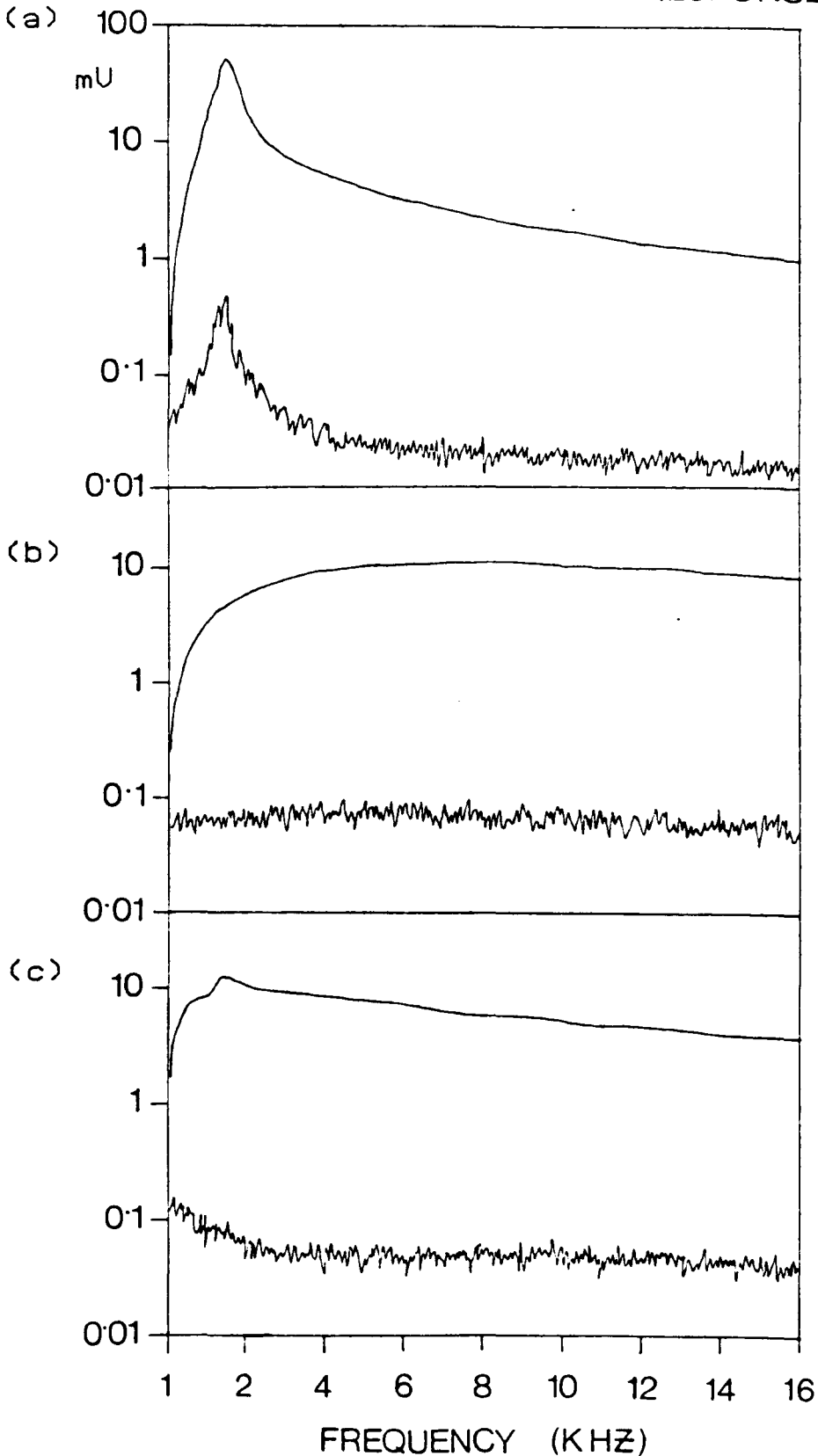
Figure 2.2 . Frequency responses of the uncorrected FET preamplifier (a), the ZN459 preamplifier (b) and the corrected FET preamplifier (c). The vertical scale is the output for a received signal of 1 pT RMS (smooth line) and the noise in a 100 Hz bandwidth with no input signal (jagged line).

compensating for the increased EMF induced in the loop as the signal frequency increases, since both are proportional to frequency. The ZN459 preamplifier is inherently free from bumps in the amplitude and phase response curves, which would make it ideal for use in direction finding systems, especially those which use the electric field component since they require a matched phase response between the electric and magnetic field preamplifiers.

A disadvantage is that the maximum undistorted output from the ZN459 preamplifier is 2 V p-p corresponding to a received field strength of 12 pT RMS (for large aerials) at 5 kHz. This is an order of magnitude less than the maximum signal that the FET preamplifier can handle which means that the filter to remove the strong high frequency signals may need to be placed before a ZN459 preamplifier. This is less satisfactory for two reasons: firstly, the filters will introduce a small loss in the pass band, further reducing the signal to noise ratio, and secondly, the filters could not easily be switched in or out if the preamplifier was used in a remote location.

2.2.3 Correction Circuit to FET Preamplifier

For the above reasons it was decided not to use the ZN459 preamplifier, but to add a response correction network to the FET preamplifier.

Preliminary experiments showed that a parallel tuned circuit, shunted by a resistor to control the Q, placed in the feedback loop of the preamplifier would, with

19

careful adjustment, completely remove the resonance peak. A similar circuit had been developed by Jones (private communication) for the FET preamplifier used with a mumetal rod aerial for a rocket experiment, but in that case the resonance peak was not as sharp as that which occurs with loop aerials. Also, to retain the symmetry of the differential design, two LC circuits were used for each channel of the preamplifier which complicated construction and alignment. The circuit finally employed (figure 2.3) used only a single LC circuit, while retaining the symmetry of the differential amplifier. The previous common source resistor has been split into two resistors each of double the value (labelled 2RS) with the LC circuit placed between them. The 100 k ohm preset resistor allows the Q of the LC circuit to be adjusted to match the resonance, and the two fixed resistors R_{F1} and R_{F2} may be selected for correct DC bias conditions. The capacitor was chosen so that the LC circuit approximately matched the frequency of the resonance with the final adjustment made by adjusting the inductor.

Precise alignment of the corrector circuit is difficult to achieve since the resonance peak, which it has to match, will vary slightly depending on the characteristics of the loop aerials to which the preamplifier is connected. However, it is usually possible to obtain a response such as that shown in figure 2.2c with a peak to peak ripple in response around the resonance of less than 3 dB. On dynamic range considerations this is a considerable improvement on the 20 dB peak which is present

Figure 2.3

CIRCUIT OF V.L.F. PREAMPLIFIER

(ONE CHANNEL ONLY)   SEPT 1979

Q1,Q2,Q3,Q4 : 2N4869A

L : 0.59H LA1228 1170 t 45 SWG

C : typ. 0.02 µf (Select on test)

RF1,RF2 : typ. 560Ω (Select on test)
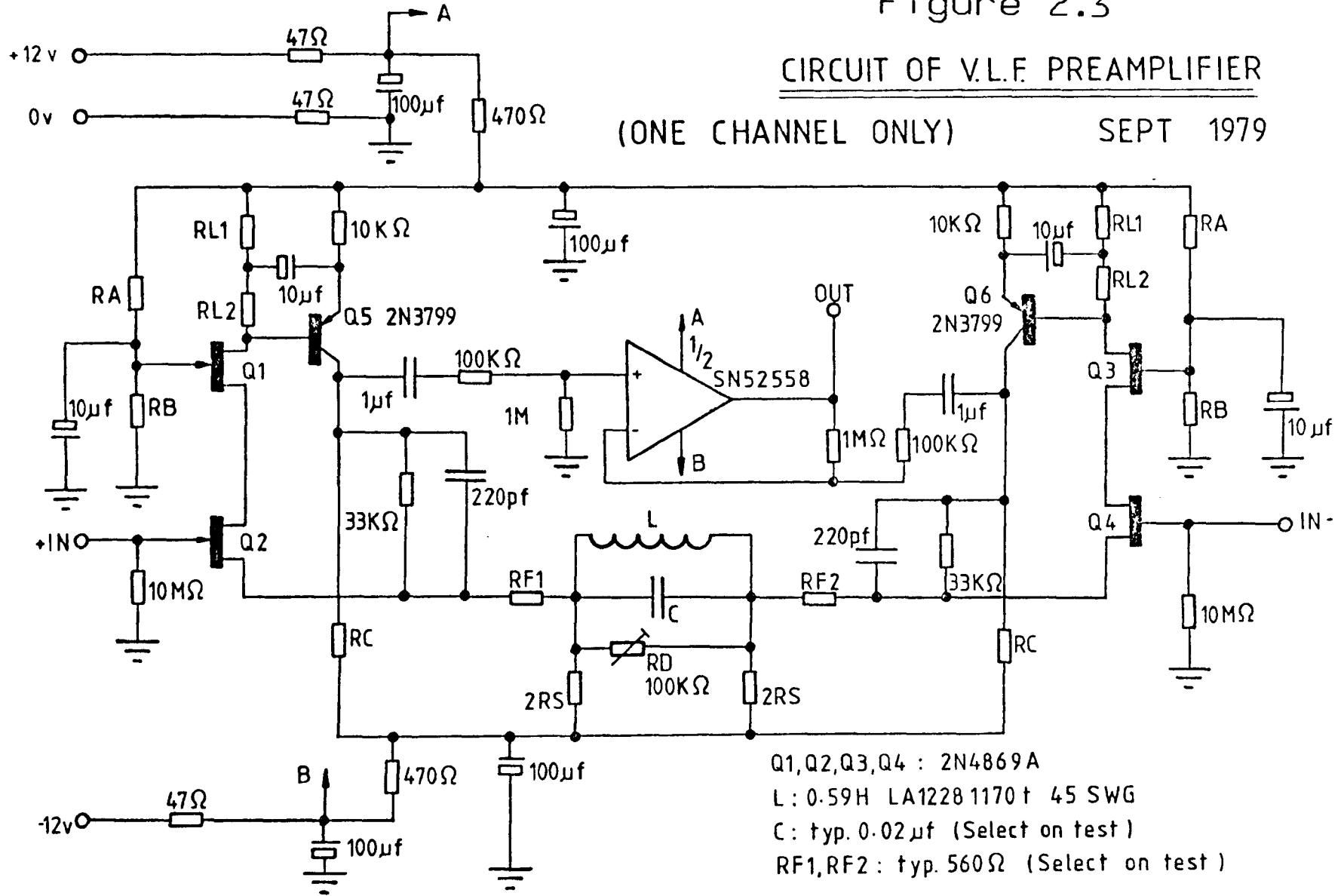
without the correction circuit, but the phase response will still make bearing measurements near the resonance suspect.

2.3 Calibration of VLF Receiver using a Distant Source

Three methods for calibrating the VLF receiver are described in Bullough and Sagredo (1973). The method normally employed is the small calibration coil positioned in the centre of the loop aerials. The current required in the calibration coil to simulate a received signal of a certain strength is determined by consideration of the mutual inductance of the coil and a loop aerial. However, the actual field present in this case is very different to that of a VLF radio wave and it is not known to what extent the mutual inductance is affected by induction in the metal mast present.

To simulate as closely as possible the magnetic field component of a VLF radio wave, a distant calibration coil was used to provide a nearly uniform field over the area of the loop aerial. The small loop aerial system (5.34 m^2 area per loop) was set up (see figure 2.4) at an electromagnetically quiet site in the Derwent valley near Sheffield (National Grid Reference SK145936) on the 6th of May 1981. A local calibration coil (100 turns, 10 cm mean diameter) was clamped to the mast in the usual way. The equivalent field strength for the small loop aerials is given by the following equation (A.J. Smith private communication) where N_c and A_c are the number of turns and area of the of the calibration coil and A is the area of the loop aerials.

Figure 2.4

CALIBRATION OF VLF RECEIVER
USING A DISTANT SOURCE

(a) Geometry

RECEIVER AND
TAPE RECORDER

SMALL LOOP AERIALS

30 m

COIL

CALIBRATION
SIGNAL SOURCE
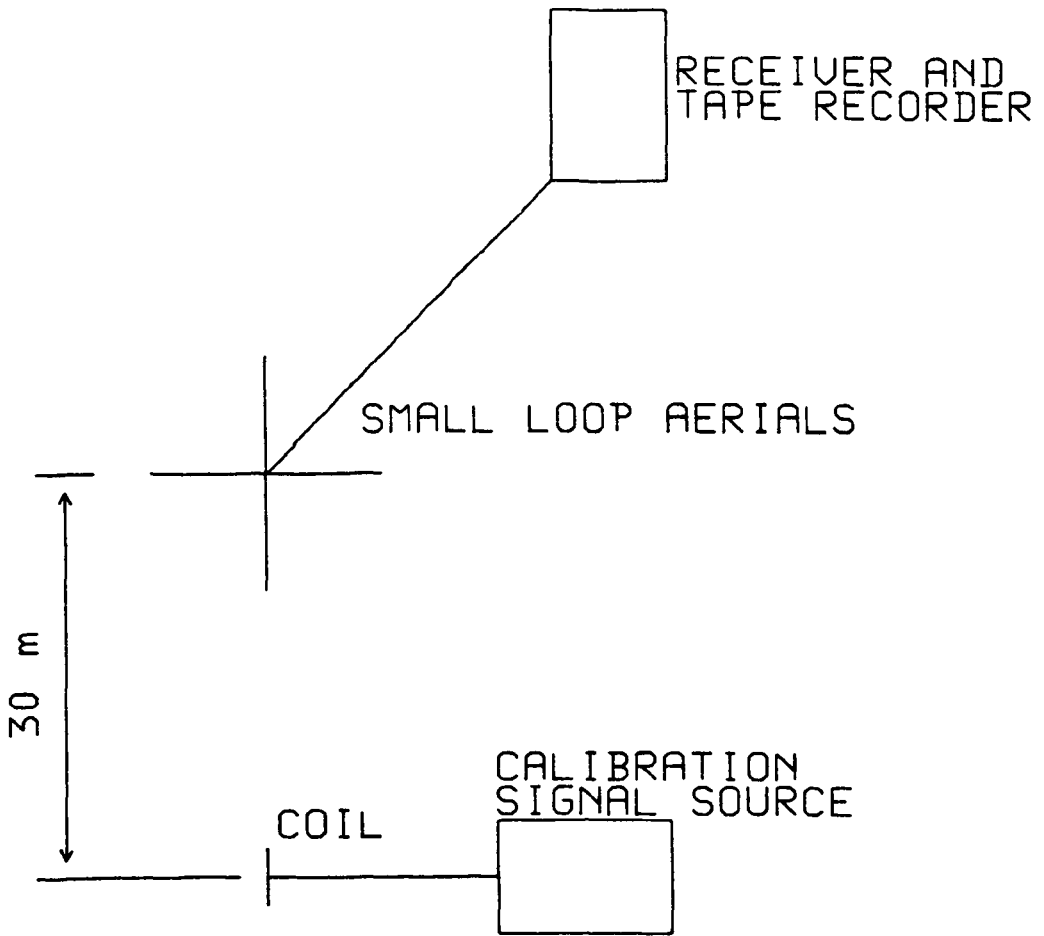
(b) Electrical connections to coil

COIL

MICROVOLTMETER

4R

POWER AMPLIFIER
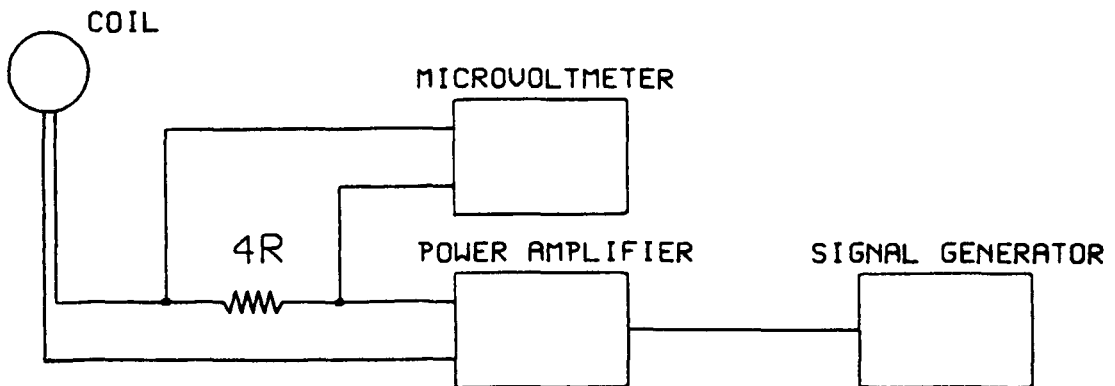
SIGNAL GENERATOR

$$B = 1.042 \frac{\mu_o N_c A_c I}{A^{3/2}}$$
(2.3.1

The coil was connected to a signal generator adjusted for a 1 V RMS sine wave output via a 75 k Ω series resistor to give an equivalent field strength of 1.16 pT, which was much larger than the ambient background.

A second toroidal coil (20 turns, 67 cm diameter) was set up 30 m away from the centre of the loop aerials and mounted in a vertical plane containing the aerials. The sine wave output of a signal generator was connected to a battery operated power amplifier, which in turn was connected to the calibration coil via a 4 ohm resistor. An AC voltmeter was used to monitor the voltage across this resistor and hence the current in the coil. The field at the centre of the loop aerials was determined using the standard formula for the field in the plane of a circular coil where a is the radius of the coil of n turns and r is distance of the field point from its centre (for r>>a).

$$B = \frac{\mu_o n I a^2}{4 r^3}$$
(2.3.2

A current of 50 mA was used which gives a field of 1.3 pT at the centre of the loop aerials. The variation of the field over the area of the aerials is only about $\pm$ 10% and so the average field will be close to the value at the centre.

Two sets of calibrations were done, the first using the standard method, ie. with a calibration coil at the centre of the loop aerials, and the second using a distant source as described above. In each case signals of frequencies 1, 2, 5, and 10 kHz with arrival azimuths of 0 to 180 degrees in 10° steps were simulated. For the local calibration coil this was done by rotating the coil to each position required, but for the distant calibration coil the aerial system itself was rotated to give the required angle between north-south loop and the calibration coil. In each case a 15 second tape recording was made of the signal received by the goniometer for each simulated arrival azimuth.

In the laboratory the tapes were analysed using the filter bank and correlator on the whistler analyser (Smith et al. 1979) to determine the apparent arrival azimuth of the signals. The apparent arrival azimuth of signals simulated by the two methods differed by less than eight degrees, and usually less than 5 degrees. Some of this error can be attributed to errors in the positioning of the calibration coil or loop aerials and some due to slight variations in the frequencies of the calibration signals. The latter changes the apparent bearing since the frequency dependent group delay response of the filters used to select the signal for analysis causes a phase shift of the goniometer modulation.

Additionally, the received signal intensities were compared using the Unigon FFT analyser with the peak measurement program described in section 3.2. Taking into account the different magnitude of the simulated signals in each case the amplitudes of the received signals (for the same nominal amplitude of simulated incident VLF wave) agreed to within 0.5 dB at 1 kHz whereas at 10 kHz the signal from the local calibration coil was 3 dB lower than that from the distant source. The latter difference may be due to induced currents in the mast reducing the mutual inductance between the calibration coil and aerial loop.

For both amplitudes and bearings, the measurements agreed to within the error limits usually required and so the above tests provided a reassuring validation of the use of the local calibration coil.

2.4 Digital Calibration Tone Generator

2.4.1 Introduction

The existing calibration tone generator used with the VLF receiver has the disadvantage of generating only a single frequency and so when making measurements at any frequency far removed from that of the calibration tone, an accurate knowledge of the frequency response is required. Also the amplitude and frequency of the calibration tone are not precisely controlled. To overcome these problems, a digital calibration tone generator was designed which generates 5 tones simultaneously at frequencies of 488.28, 976.56, 1953.13, 3906.25 and 7812.50 Hz and each equivalent to a received strength of 1 pT RMS when the generator is connected to the calibration coil.

2.4.2 Circuit Description

The circuit (figures 2.5 and 2.6) generates the wave form by sequentially transferring the contents of a 1024 x 8 bit block of read only memory into an 8 bit digital to analogue converter, the output of which is buffered before it is fed to the calibration coil.

The data stored in the read only memory at address A is given by the integer part of D(A) in the following formula.

$$D(A) = 128 + [40(\sin x + \sin 2x + \sin 4x + \sin 8x + \sin 16x)]$$

where $x = 6.136 \times 10^{-3}$ A

Figure 2.5 DIGITAL CAL TONE GENERATOR,
1MHz OSC. AND COUNTER
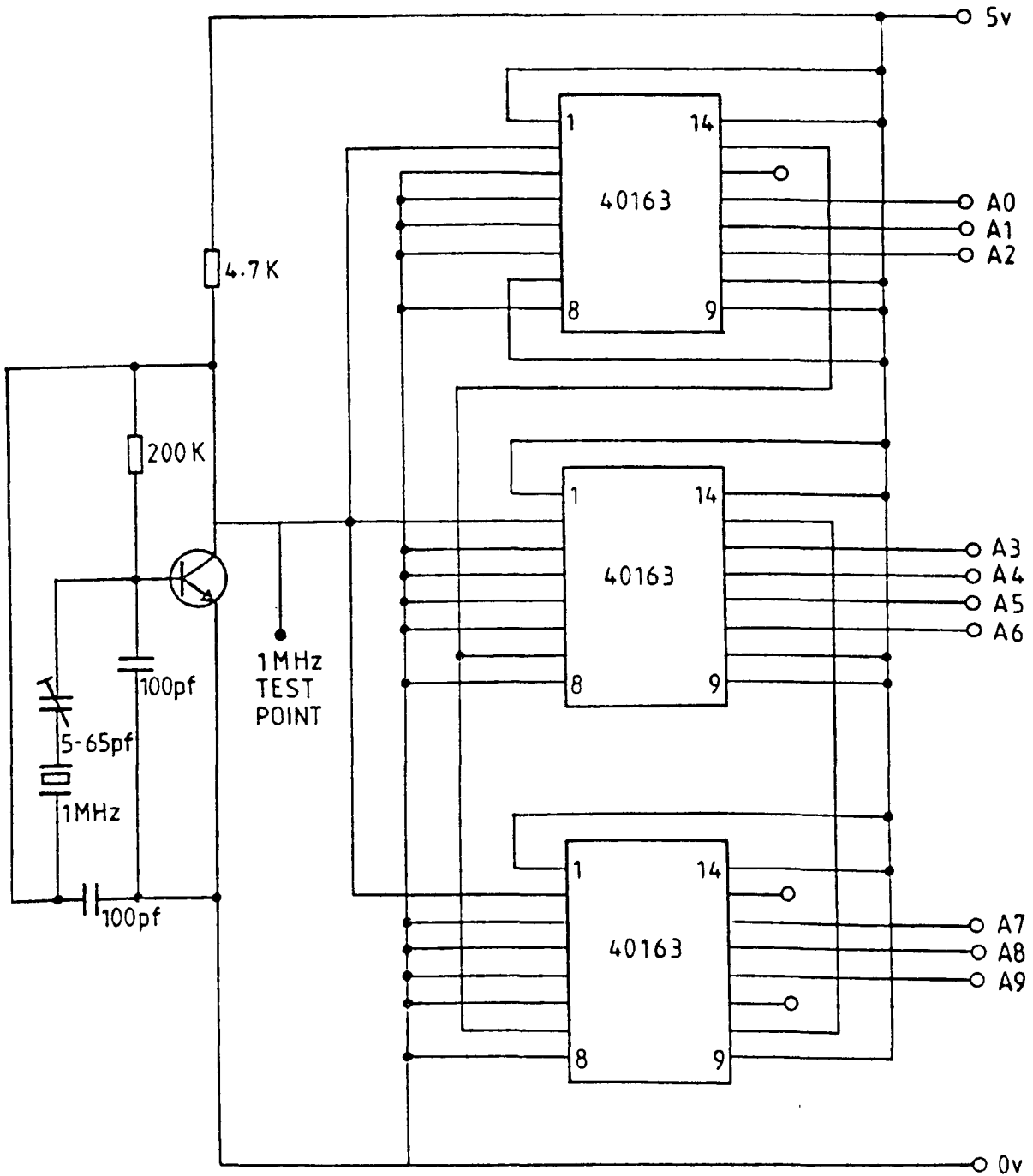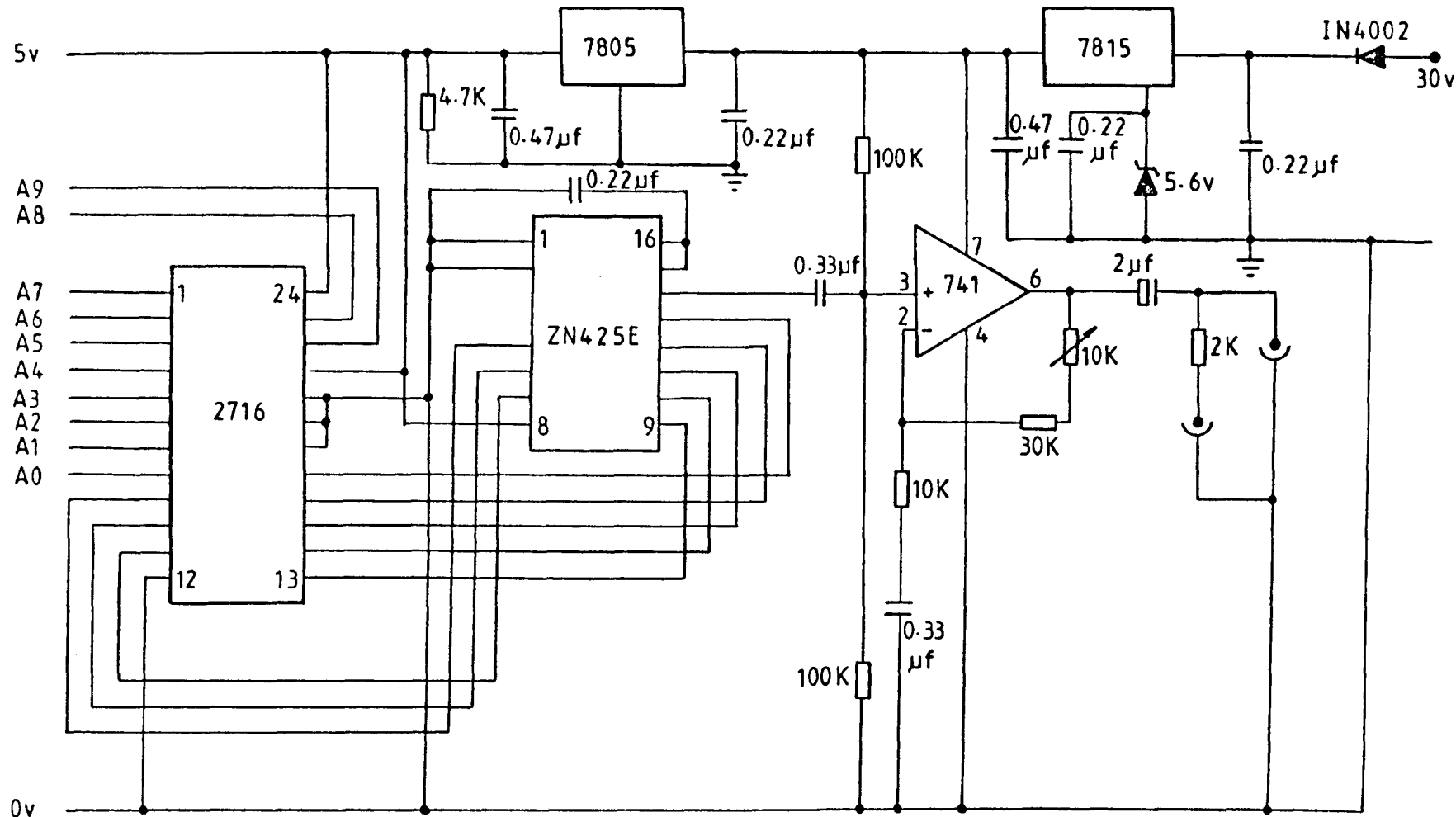
Figure 2.6

DIGITAL CAL TONE GENERATOR.
EPROM, D/A, AMPLIFIER, POWER SUPPLIES
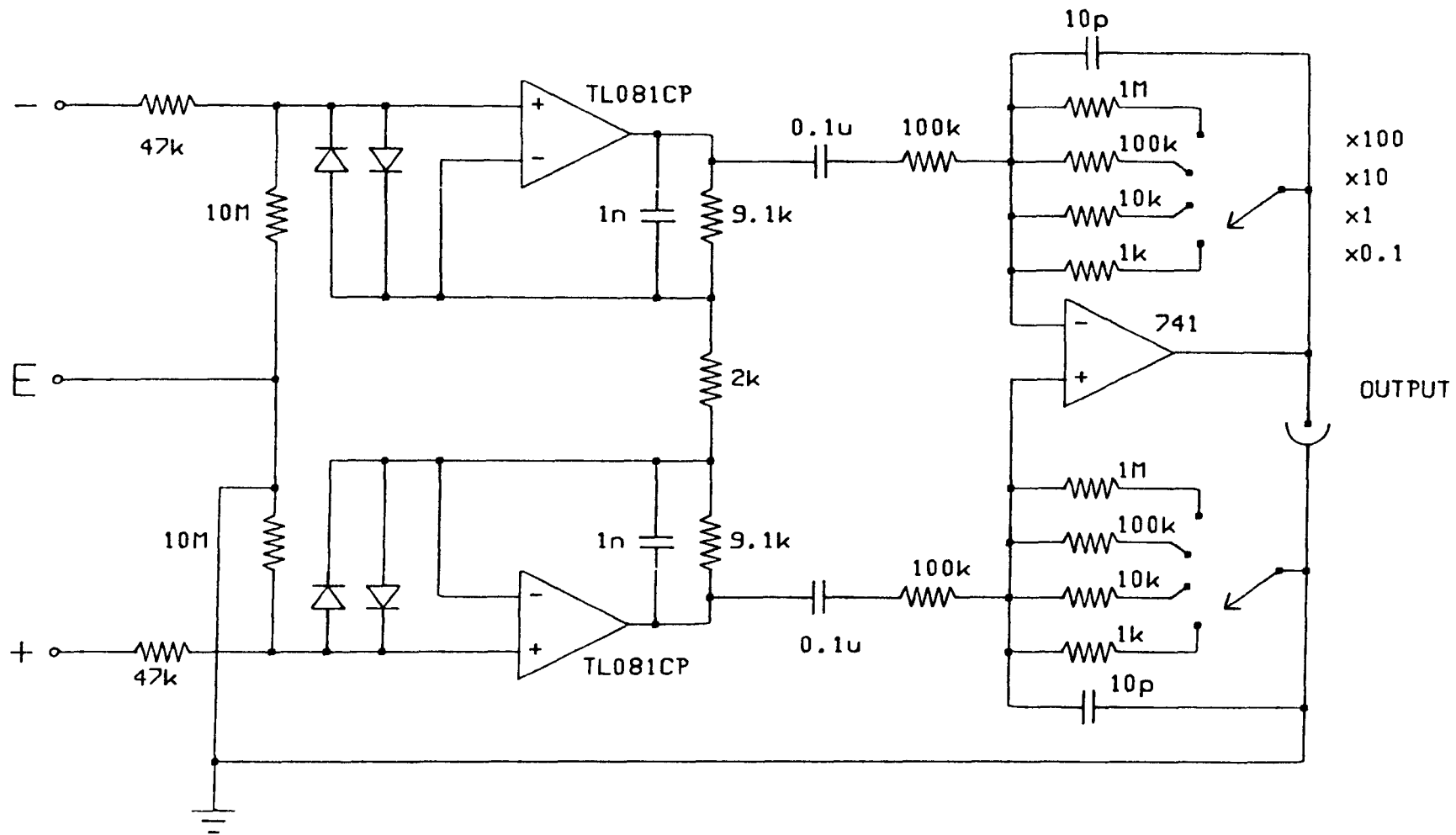
Figure 2.7 . Circuit of the Electric Field Preamplifier

A 1 MHz crystal oscillator is the frequency standard for this device. This feeds a twelve bit synchronous counter using 3 4016B CMOS integrated circuits. The least significant output from the counter is not used; the next ten outputs supply the A_0 to A_9 addresses of the EPROM. The chip select line of the EPROM is wired low resulting in the data at the selected addresses being permanently available at the outputs. The latter are directly connected to the inputs of the ZN425E digital to analogue converter.

The output from the D to A converter has a peak to peak amplitude of 2.5 V. It is amplified so that each of the five sine wave components in the resultant waveform has an amplitude of 1 V RMS. This is done by a 741 operational amplifier used in an AC coupled single supply rail configuration. The peak to peak amplitude at this point should be 8.83 V. The output of the amplifier is connected to the calibration coil via a 2 kΩ series resistor to give the required current in the coil.

The power supply to the unit is derived from a 30 V input. This is first reduced to 20 V using a 7815 regulator with its reference input taken to +5 V. The output amplifier is supplied from this source, which is then reduced to +5 V (using a 7805 regulator) for the digital circuits. The two regulators are mounted on the case to provide a heat sink.

2.4.3 Accuracy

Three methods were employed to check the accuracy of the calibration tone generator. Firstly it was connected to the Unigon FFT analyser which was set to the 20 kHz range. The peak measuring program (see section 3.2) was then used to determine the amplitude and frequency of all lines in the spectrum. The relative amplitudes of the five main frequencies were the same to within 0.25 dB, while the amplitude of the largest unwanted harmonic (15,625 Hz) was 39.5 dB lower.

The absolute amplitude was checked both by measuring the output on a true RMS digital voltmeter, which should read 2.236 V RMS, and by measuring the amplitudes of the individual tones using a tuned AC voltmeter. The absolute amplitudes were accurate to 0.25 dB by both methods.

2.5 Electric Field Preamplifier

As part of the work described in chapter 4, on the radiation of VLF radio wave energy from power lines, it was required to record the electric field in the ground near to the power lines. For this purpose an electric field preamplifier (circuit in figure 2.7) was constructed. The input terminals were connected to copper rod earth electrodes placed in the ground a few tens of metres apart. Since the resistance of the earth connections may be quite high, a high impedance amplifier is required so that the true voltage will be measured. The circuit uses two TL081CP FET input operational amplifiers in the non-inverting mode to give an input impedance of 10 MΩ in parallel with a few pF . The 47kΩ resistors in series with the inputs, in conjunction with the input capacity, form simple low pass filters to reduce the gain of the preamplifier at RF. The first stage has a differential gain of 10 times to ensure that the noise in the first stage dominates over noise in the second stage. A common feedback resistor is used so that the common mode gain is unity. The 1 nF capacitors reduce the differential gain above 17 kHz.

The second stage consists of a 741 operational amplifier used in the differential mode with switched feedback resistors providing overall gains between 0.1 and 100 times.

Tests on the preamplifier showed that the equivalent input noise resistance was 1 MΩ. This is sufficiently good that natural VLF emissions were received

29

when the preamplifier was used during the Baie Verte power line measurements.

2.6 Deployment of Receivers at Halley and Newfoundland

2.6.1 The VLF Receiver at Halley

A VLF receiver is installed permanently at Halley, Antarctica. Large loop aerials are used since the lower level of interference from sferics and PLHR makes the increased sensitivity worthwhile. To reduce interference from the power system on the base the receiver is located 1.6 km west of the base. The VLF signal is returned to base (via a UHF telemetry link) where it is recorded on a Revox model A77 stereo tape recorder. A Datum time code generator/reader type 9300 supplies BCD time information to a programmer which controls the recording, and IRIGB time code to the 2nd track of the tape recorder.

2.6.2 Newfoundland VLF Receivers

Synoptic recordings were made at St. Anthony (see figure 4.10) and Deer Lake in Newfoundland between the 17th of June and the 2nd of July inclusive. At each site the VLF receiver used small loop aerials and the top cut and bottom cut filters were switched in. One minute in five recordings were made simultaneously with recordings at Halley. A Uher stereo tape recorder was used which, together with the rest of the receiver, was powered and controlled by the Programmable Power Supply (PPS) described in appendix A. This in turn was powered from a 55 Ah 12V car battery. A Systron-Donner time code generator provided the timing information to the PPS and the IRIGB time code which was

recorded on track 2 of the tape recorder. A block diagram of the system is shown in figure 4.5.

The St. Anthony receiver was located at a place called Lower Cove on the old road from St. Anthony to Deer Lake (51°33' N, 56°04' W), about 40 km NW of St. Anthony town. There was no detectable interference from PLHR at this site, the nearest electrical power being at the fishing village of Big Brook 6 km away. A site in this area was chosen to be fairly close to the geomagnetic conjugate of Halley.

A second site was required approximately 250 km distant for the purpose of triangulation on the ionospheric exit points of the VLF signals. A site 23 km NNE of Deer Lake at Deadwater Brook was chosen (49°22' N, 57°21'W). Interference from PLHR was detectable but acceptably weak. The nearest mains electricity was 4 km distant and the nearest high voltage line 14 km.

Chapter 3   Spectrum Analysis

3.1 Review of Spectrum Analysis Techniques

Spectrum analysis, or Fourier analysis, in which the variation of some variable as a function of a parameter (usually time) is considered as the sum of a series of sinusoidally varying functions, is a powerful and often used tool in science. This is because many physical systems are most easily analysed in terms of sinusoidal functions; for example the simple harmonic oscillator has a displacement that is a sinusoidal function of time. The analysis of wave particle interactions in the earth's magnetosphere frequently requires a spectrum analysis of the wave observed either in the magnetosphere by a satellite or on the ground. A discussion of the various techniques that have been used is presented in the first half of this chapter. This is followed by a description of special techniques developed for the work presented in later chapters of this thesis and for a future all-digital VLF analysis system.

Spectrum analysis techniques are based on filters, either analogue or digital, which pass only a narrow range of frequencies. One simple way to construct a spectrum analyser is to use a single filter which is swept in frequency across the range of interest. The output of the filter is rectified and smoothed and applied to the Y input of an oscilloscope while the X axis sweeps in time with the filter frequency, resulting in an amplitude versus frequency display. This method has the disadvantage that it does not

work in real time; that is, if an event occurs at one frequency while the filter is tuned to another it will not be indicated. This means simple swept frequency analysers can only be used for signals with a stationary or very slowly changing spectral content.

However, by storing a section of the waveform to be analysed and replaying it many times in succession, swept filter analysers can be used on non-stationary signals. The filter is swept (or stepped) by a frequency of the order of its bandwidth each time the wave form is replayed.

This principle is used in the Kay-Electric Sonagraph analyser which produces a spectrogram (see figure 3.1 for example) covering 2.4 seconds in time (x axis) and 8kHz in frequency (y axis), with the amplitude at a particular time and frequency represented by a grey scale. The input waveform is recorded on a magnetic drum and then replayed at 12 times recording speed while a filter (bandwidth 45 or 300 Hz) sweeps slowly across the frequency range. The time sample is replayed 390 times during the 1.3 minutes required for analysis.

Another analyser which uses this principle is the Federal Scientific Corporation model UA-6 'Ubiquitous' analyser used by Coroniti et al (1971) in their analysis of banded chorus and by the Stanford group. This produces a spectrum in real time by storing a sample of the waveform in a high speed digital loop.

HALLEY   24   JUNE   1977
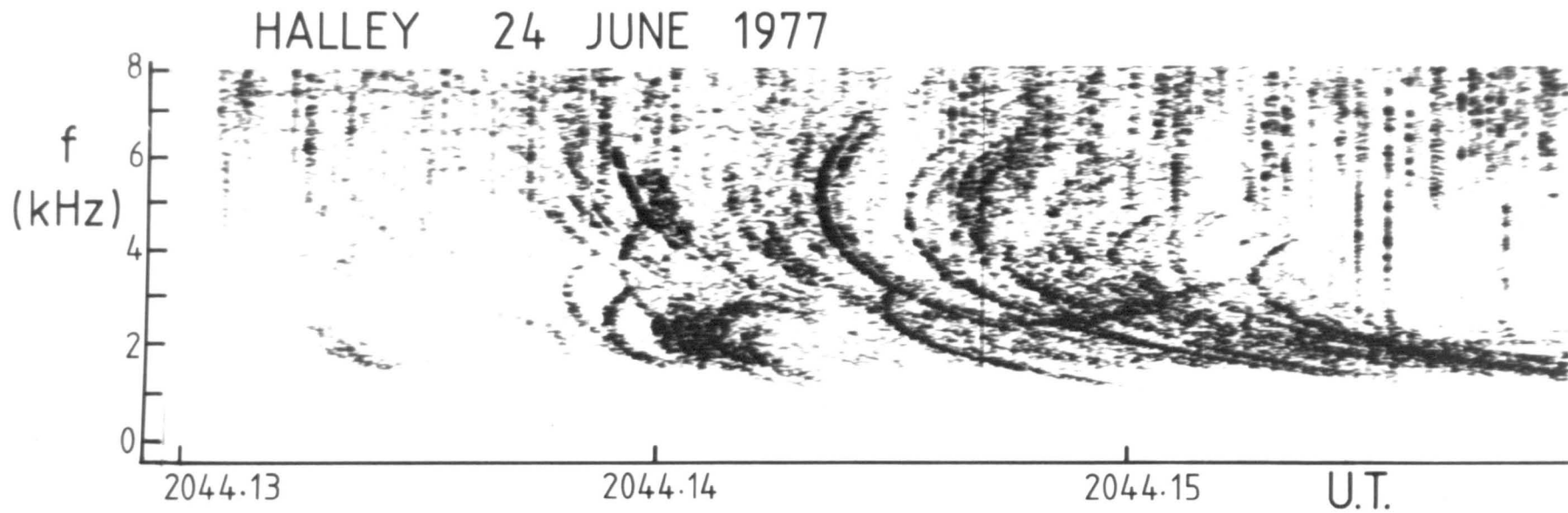
Figure 3.1 . An example of a Sonogram showing
a group of whistlers.

Rather than using one filter which is swept in frequency we could use as many fixed frequency filters as we require points in the frequency domain. In this way we can have a real time spectrum analyser just by applying the input signal to all filters in parallel. A 64 channel filter bank analyser is used in the Sheffield University whistler analyser described by Smith et al. (1979), which uses filters with a 320 Hz bandwidth in the range 0 - 20 kHz. This analyser produces a real time spectrum continuously with the output displayed on a long persistence oscilloscope. A similar analyser using 18 filters of 500 Hz bandwidth covering 1 to 10 kHz was built for use at Halley to monitor VLF activity. The Spectran real time analyser uses this principle to produce a real time spectrum analysis over a 20kHz bandwidth using 480 magnetostrictive filters of 50 Hz bandwidth, the outputs of which are selected in turn using a rotating capacitative commutator.

All the methods described so far have, either wholly or partly, used analogue methods to perform the spectrum analysis. Modern analysers use a digital approach. The input waveform is sampled at regular intervals and the value of each sample stored in digital form. The power spectrum may then be obtained by computing the discrete fourier transform (DFT) of the auto-correlation function of the data. This method used to be the standard method of digital spectral analysis (Blackman and Tukey 1958) as it requires less calculation than computing the DFT directly, since there are usually considerably fewer points in the

auto correlation function than in the time series. It is still used on satellites, with the correlation performed on board, thus reducing the quantity of data to be telemetered to the ground. This technique is described by Jones (1979).

The introduction of the fast fourier transform (FFT) algorithm by Cooley and Tukey (1965) has considerably speeded up the DFT calculation and it is now usual to calculate the DFT of the time series directly.

The processing of the digital data may be done using a general purpose computer to calculate the FFTs, as was done by Stiles (1974). However, unless a very powerful computer is used it is not possible to process data in real time by this method and so its application is limited to the analysis of selected events rather than the production of continuous spectrograms covering a long period of time.

The alternative way to process the digital data is to use a special purpose FFT analyser. These are now made by many manufacturers and besides the hardware to compute the FFT they also generally contain the input sampling and digitising circuits and also digital to analogue converters to convert the digital spectrum into an analogue form for display. However most of these analysers have real time bandwidths of only 1 to 2 kHz and so are not suitable for processing 10kHz bandwidth VLF data.

The two analysers which have been used for the work described in this thesis are both FFT analysers; they are the Unigon model 4512 and the Spectral Dynamics SD350 which have real time bandwidths of 12kHz and 60kHz

respectively. The former has a fixed transform size of 1024 samples in the time domain and produces a spectrum of 512 lines in a frequency range that may be varied from 10Hz to 40kHz. This analyser can also provide phase information on the signals present; some uses for this are discussed later. The SD350 has a transform size which is variable between 64 and 2048 and produces spectra of 25 to 800 lines. The frequency range is variable from 10 Hz to 300 kHz. The analyser can be connected to a separate hard copy unit which produces a continuous spectrogram similar to the 2.4 second segments produced by the Kay-Electric sonograph. With both analysers the frequency range may be translated upwards to cover a band of frequency not starting at zero to allow a small range of frequency to be analysed in detail. On the Unigon 4512 this is achieved using a separate frequency translator unit, whereas the SD350 has the facility built in.

To detect signals with a slowly changing spectral content in the presence of noise (such as the MLR events discused in chapter 5) it is useful to average the spectra of successive time samples. The FFT analysers mentioned above have facilities for averaging a number of spectra to obtain one averaged spectrum, but to observe any (slow) change in the spectral content of the signal a series of averages of successive groups of spectra are required. This may be done using a computer (or microprocessor) to average the digital output of a spectrum analyser. The use of a 6800 microprocessor to average and process the digital spectra

produced by the Unigon FFT analyser is discussed in appendix B.

Alternatively the averaging may be done photographicaly by making a spectrogram with a compressed time scale (see figure 5.1 for example). Compressed time scale spectrograms are made using an oscilloscope camera with the film in slow continuous motion (typically 25mm per minute). The output of a real time analyser is used to intensity modulate the oscilloscope beam which is deflected in a direction at right angles to the film movement, synchronously with the frequency sweep of the analyser. The film takes about 0.2 seconds to move a distance equal to the diameter of the image of the oscilloscope spot, in which time the analyser outputs five spectra; thus the image on the film will be a running mean of about five spectra. In addition to the photographic averaging which takes place on a compressed time scale spectrogram the eye is able to recognise structure in such a spectrogram that would not appear significant in a single spectrum viewed alone.

The use of the discrete fourier transform for spectrum analysis brings two new problems that do not occur with the simple analogue filter analysers. One results from the fact that the input is sampled at discrete intervals; if the input contains any frequencies greater than half the sampling frequency (known as the Nyquist frequency), then they will appear in the spectrum reflected below the Nyquist frequency (Blackman and Tukey 1958). This is known as aliasing. Therefore it is essential that the input does not

contain frequencies above the Nyquist frequency and so the signal is usually passed through a low pass filter prior to sampling.

The second problem is due to the finite length of the input record used for analysis and the fact that the DFT treats the record as repeating indefinitely. If the input contains only frequencies which have a whole number of cycles in the record, or if the signal is a transient with zero amplitude at the ends of the record all is well. Otherwise there will be a discontinuity at the ends of the record which results in side bands appearing in the spectrum. To reduce this effect the input record is normally multiplied by a weighting function which reduces smoothly to near zero at the ends of the input record. The Hanning weighting function (after Julius von Hann), as used on the Unigon 4512 analyser, is a commonly used one. The input sample at position θ within the input record ($0 =< \theta =< 2\pi$) is multiplied by W in the following equation.

$$W = 0.5 - 0.5 \cos\theta \qquad (3.1.1$$

Stiles (1974) used the Hamming weighting function (after R.W. Hamming).

$$W = 0.54 - 0.46 \cos\theta \qquad (3.1.2$$

The two functions give similar results, but the Hamming function results in a slightly sharper main peak, whereas

the side lobes fall off more rapidly with the Hanning function.

When analysing non stationary signals using the DFT it is desirable to have adjacent time samples overlapping so that all points in the time series are used in at least one spectrum with a reasonably large weighting factor. The term 'redundancy' (R) is used to refer to the degree of overlapping present. Figure 3.2a shows the weighting applied to a time series with no overlapping present (R=1), and figure 3.2b shows each time sample overlapping half of the next one (R=2). In the former case, events that occur at times arrowed will not be recorded in any spectrum. For this reason an analyser real time bandwidth of about twice the signal bandwidth is required.

Another method of digital spectrum analysis is the maximum entropy method (MEM). This method was originally proposed by Burg (1967) and is described in detail by Ulrych and Bishop (1975). The latter paper also contains a listing of a Fortran program to calculate a maximum entropy spectrum. Supporters of the maximum entropy technique claim that it produces spectra of higher resolution than other methods (Radoski et al 1975) but this is only the case if the resolution is limited by the length of the time series available for analysis. The advantage of the MEM technique then being that it does not require a weighting function to be applied to the data and so can use all of it to full significance, whereas methods that do apply a weighting function reduce the significance of the data at the ends of

40

Figure 3.2

WEIGHTING OF TIME SERIES PRIOR TO FFT

In case (a) events that occur at times arrowed will not
be recorded in any spectrum, where as in case (b) all data
is processed with a weighting factor of 0.5 or greater.

(a) NON-OVERLAP PROCESSING (R=1)

(b) OVERLAP PROCESSING (R=2)

WEIGHTING

TIME
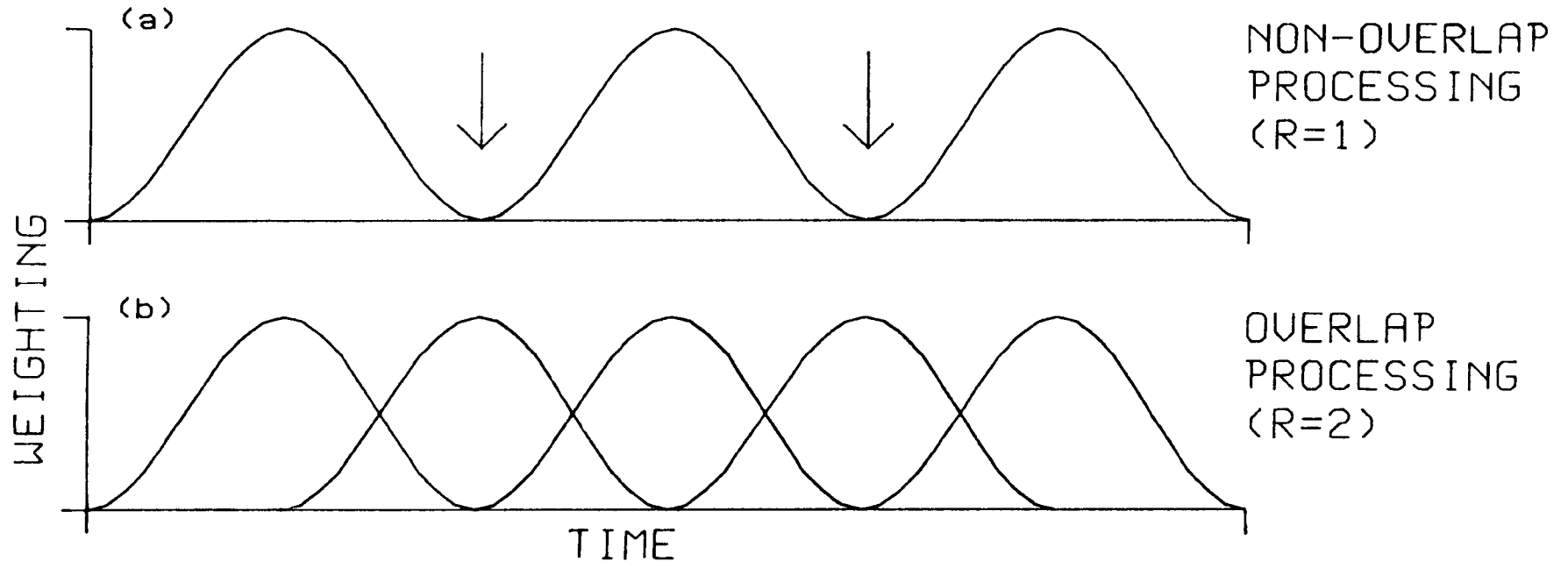
the sample. The MEM technique has the disadvantages that the spectra obtained depend on an a priori assumption about the data and that under certain conditions spontaneous line splitting can occur. Solutions to these problems have been proposed by Akaike (1969) and Fougere (1977).

3.2 Interpretation of Spectra

After spectrum analysis we have a value of spectral amplitude as a function of frequency and time. This still requires interpretation to estimate the amplitude of the signal being analysed as a function of frequency and time. Often we assume that the signal consists of one or several discrete components which may vary in both frequency and amplitude as a function of time, and then what we require are frequency-time profiles for each component. One way to determine a frequency time profile is to make a spectrogram in which the spectral amplitudes are represented by varying shades of grey (fig 3.1) or different colours (fig 3.3), and then to scale the profile of the signal by eye.

There are, however, more rigorous methods for determining frequency time profiles. Four of these are compared by Kodera et al (1978). The first two are the amplitude maximum of the spectrum (MS) method in which the frequency at which the spectral amplitude is a maximum is computed as a function of time, and the amplitude maximum of the envelope method (ME) in which the time of the spectral amplitude maximum is computed as a function of frequency. The Moving Window method determines the curve along which the gradient of the amplitude in frequency-time space is a minimum. The three methods all give similar results fairly close to the frequency-time law of the original signal provided that the product of the frequency excursion of the signal with its duration is much larger than one, and that
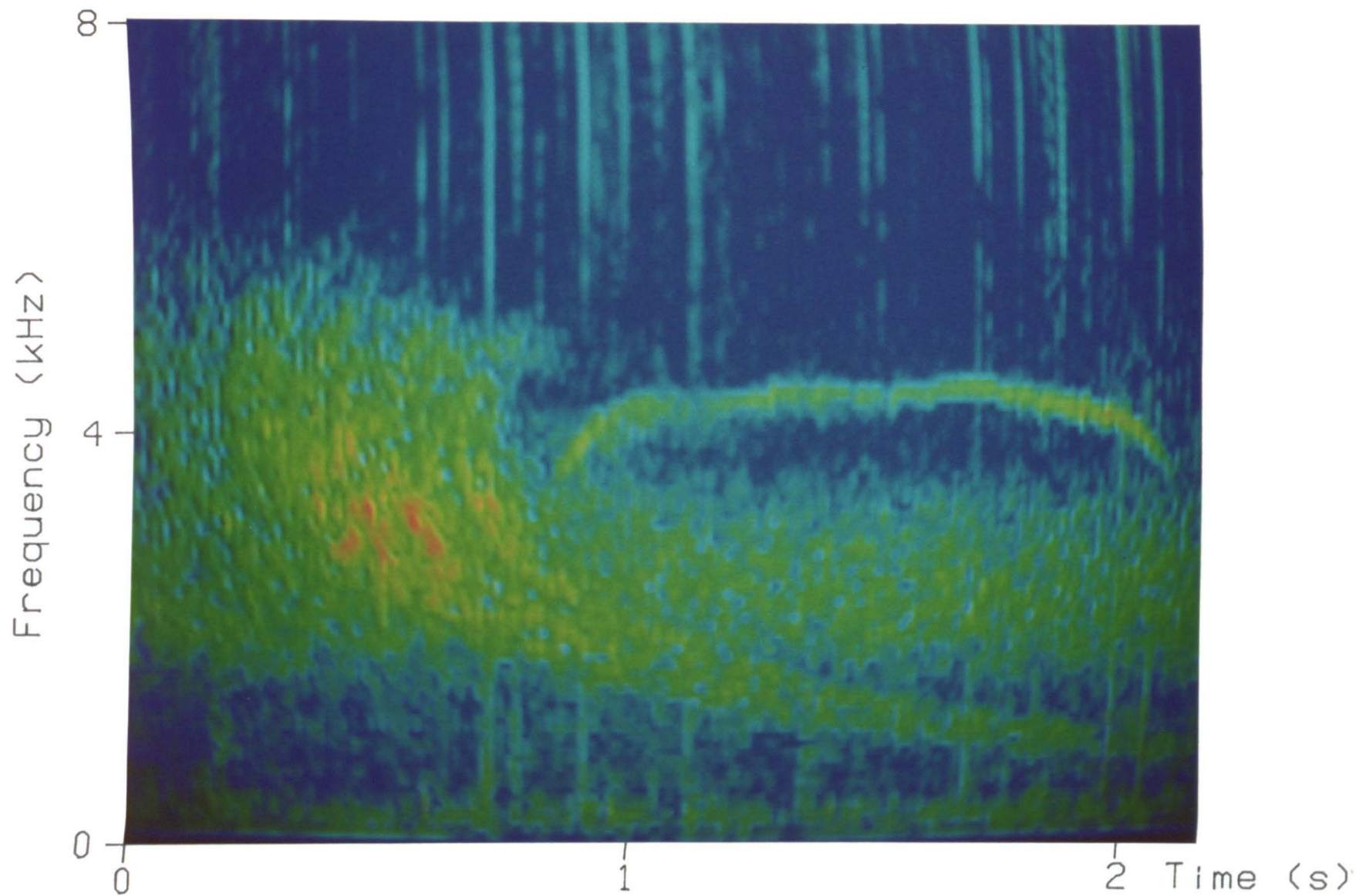
Figure 3.3 . A colour spectrogram of a whistler received at Halley on 27 June 1980 at 1930 UT .

the width of the frequency window is chosen to be of the order of the square root of the time derivative of the frequency. When the former criterion is not fulfilled, the frequency time profile obtained becomes very sensitive to the choice of the frequency window. The fourth method, the modified moving window method (MMWM), is not as sensitive as the other three to the choice of the width of the frequency window and will still work when the duration frequency excursion product is only 2 or 3. The MMWM is also better at resolving two signals closely spaced in frequency or time, which would be useful for determining the individual frequency-time profiles of multi-component whistlers for example. However, in practice, the MMWM is more difficult to use than the other three methods since, as well as the spectral amplitude, it also requires the derivatives of the phase with respect to time and frequency.

The choice of the correct time or frequency window width is important for the correct interpretation of the signals. Stiles (1975) has shown that the banded structure in the chorus studied by Coroniti et al(1971) was an artefact of the analysis system caused by the use of too wide a time window.

Jones (1973) has shown that by using the phase information present in the cross-spectrum (a cross-spectrum is the DFT of the cross-correlation function of two signals) between the components of a VLF signal received on two antennas, signals may be observed that would be lost in the noise on a conventional magnitude spectrogram. This

technique may be used for signals recorded on the ground or on spacecraft. On the ground the noise is mainly due to sferics and other sub-ionospheric signals that have nearly linear polarisation and so give in phase signals on two orthogonal antennas and near zero phase in the cross spectrum. Magnetospheric signals are usually elliptically polarised resulting in non-zero phases in the cross-spectrum.

For the work described in chapters 4 and 5 a technique has been developed for automatically measuring the amplitude, frequency and bandwidth of signals which change only slowly in amplitude and frequency. By applying it to several spectra calculated at successive times it may be used to find frequency time profiles by the MS method described above. First a spectrum of the signal is produced (using the Unigon FFT analyser) and the magnitude of each point in the spectrum stored in digital form. A computer program (appendix C.1) then examines the spectrum between specified frequency limits to look for peaks and then calculates the frequency, amplitude and bandwidth of each peak found. The identification and measurement of a peak in the spectrum are based on equations A13, A11 and A12 in Stiles (1974) which are written in modified form as 3.2.1, 3.2.2 and 3.2.3 below.

The amplitude A of a spectral peak is given by

$$A = (P_j)^{1/2} \qquad\qquad (3.2.1$$

where
$$P_j = \sum_{i=j-N}^{j+N} A_i^2$$

P_j is the power contained in 2N + 1 spectrum points centered on the jth point. A_i is the amplitude of the ith point. The frequency f of a spectral peak is given by

$$f = f_j + \delta_j \, \Delta f \qquad\qquad (3.2.2$$

where
$$\delta_j = \frac{\sum\limits_{i=j-N}^{j+N} (i-j) A_i^2}{P_j}$$

Δf is the frequency interval between adjacent spectrum points. $f_j (=j\Delta f)$ is the frequency of the jth point. $\delta_j \Delta f$ represents the frequency offset of the peak from that of the jth point.

Finally for the bandwidth we have

$$BW = 2\Delta f (B_j - \delta_j^2 - 1/3)^{1/2} \qquad\qquad (3.2.3$$

where
$$B_j = \frac{\sum\limits_{i=j-N}^{j+N} (i-j)^2 A_i^2}{P_j}$$

The -1/3 term in the expression for the bandwidth corrects

45

for the analyser resolution bandwidth. With this correction and Hanning weighting , BW=0 for a monochromatic signal.

The program has been checked experimentally firstly using band limited white noise from a noise generator and band pass filter (Hewlett Packard wave analyser model 3581A) and secondly using monochromatic signals; it gives satisfactory results.

Three criteria are used to identify a peak. Firstly the amplitude of the central component is required to be above a certain threshold. This is a simple test that allows a program to quickly skip over sections of the spectrum with low amplitude. Secondly we require the magnitude of the δ_j parameter in equation 3.2.2 to be less than 0.5. The magnitude of this parameter will only be small when the spectral amplitudes in this summation are fairly symmetrical about the centre component. Values greater than 0.5 indicate that frequency of the peak is nearer $(j\pm1)\Delta f$ rather than $j\Delta f$, requiring the value of j to be changed.

Thirdly the B_j parameter in equation 3.2.3 is used to ensure that a candidate peak is sufficiently sharp. The threshold required for B_j depends on the value of the N parameter and also whether only narrow lines are to be taken as peaks or whether the program is being used to find broad peaks such as those in magnetospheric line radiation events. A monochromatic line gives B_j =1/3 in the absence of noise, whereas equal spectral amplitudes for the 2N+1 points give B_j = N(N+1)/3. A threshold of B_j = N(N+1)/4 was found to give good results for spectra containing narrow lines, and

this is the criterion normally used in the program. B_j = N(N+1)/3.5 was required to pick out magnetospheric lines and this is easily obtained by editing the program.

The best value for the N parameter also depends on the characteristics of the lines being measured. For accurate measurements as much as possible of the power in the spectral line should be within the 2N+1 points used for analysis, which suggests using large values of N. However, large values of N increase the contribution of random noise and possibly allow interference from adjacent spectral lines and so a compromise may be necessary. The value of N should be greater than or equal to 2 since even a single constant frequency generally gives significant amplitudes in 4 adjacent spectrum points which would not all be included in the summations if N=1.

In use it has been found that N=2 gives the best results for both power line harmonic induction lines (narrow) and broad magnetospheric lines. This differs from the value of N=3 used in the equations given by Stiles, but since in both cases Δf was 10Hz and the closest spacing between adjacent lines was ~60Hz, some interference from adjacent lines might be expected with N=3.

3.3 Spectrum Analysis of Goniometer Data

The application of spectrum analysis to VLF data recorded using a goniometer is complicated by the action of the goniometer, which causes amplitude modulation of the signal at $2f_g$ where f_g is the goniometer rotation frequency, and causes any line in the spectrum to be split into a doublet with one component at $f+f_g$ and the other at $f-f_g$ where f is the signal frequency.

The amplitude modulation is seen when Δf, the width of the frequency window, is greater than f_g, and the line splitting when Δf is less than f_g.

The modulation effect is used in the usual method of determining the bearing of the received signal in which the phase of the modulation envelope is measured. To see a good modulation envelope we require Δf to be several times f_g and this limits the frequency resolution that can be obtained.

The splitting of lines into doublets can make interpretation of the spectrum difficult when there are lines present with separations of the order f_g. A description follows of a method developed to remove the splitting caused by the goniometer and to determine the bearing of the signals while maintaining detailed frequency resolution.

The goniometer system electronically synthesises the signal that would be received from a rotating loop aerial, by using signals from two perpendicular stationary vertical loop aerials. Consider a plane vertically polarised

electromagnetic wave incident on loop aerials aligned N-S and E-W. Suppose the wave normal makes an angle θ to the N-S direction. The EMFs induced in the loops are given in equation 3.3.1, where V_o is a constant depending on the size of the loops and the amplitude of the wave.

$$V_a = V_o \sin\omega t \cos\theta \; , \quad V_b = V_o \sin\omega t \sin\theta \qquad (3.3.1$$

In the goniometer these signals are multiplied by $\sin\omega_g t$ and $\cos\omega_g t$, where ω_g is the goniometer angular rotation frequency, and then added to give V_g.

$$V_g = V_o (\sin\omega t \cos\theta \sin\omega_g t + \sin\omega t \sin\theta \cos\omega_g t) \qquad (3.3.2$$

Further manipulation of equation 3.3.2 ,

$$V_g = V_o [\cos(\omega t - \omega_g t - \theta) + \cos(\pi + \omega t + \omega_g t + \theta)] \qquad (3.3.3$$

shows that the goniometer signal contains components at $\omega - \omega_g$ and $\omega + \omega_g$. The phase constant π appearing in the second term of the right hand side of 3.2.3 signifies that for $\theta = 0$ the components are out of phase at the time origin which is at the minimum of the modulation envelope.

The bearing information is contained within the phase of the two components but the latter cannot be measured directly since there is no phase reference at the signal frequency. However, the phase difference between the two terms is $2\omega_g t + 2\theta + \pi$. The phase, 2θ, can be deduced by comparing the phase difference to the goniometer rotation reference $\sin\omega_g t$. Therefore the two components may be

filtered out using narrow band filters (which must have equal phase shifts) and the phases measured to determine the bearing. Hence the filter bandwidth for the bearing measurement can be as narrow as required.

A digital fourier transform spectrum analyser may be used to perform the filtering if it is used to produce a complex spectrum which contains phase information on the signals present in the input wave form. The measured phase ϕ_i of a signal $\cos(\omega t + \alpha)$ in point i of the spectrum is given by equation 3.3.4 (t=0 at the start of the sample, t=T at the end).

$$\phi_i = \alpha + \pi \left[\frac{\omega}{\omega_o} - i \right] \quad ; \quad \omega_o = \frac{2\pi}{\Delta t} \equiv 2\pi \Delta f \qquad (3.3.4$$

Note that a signal is only within the pass band of a spectrum point if $i-1 < \omega/\omega_o < i+1$. The measured phase for the two components resulting from goniometer splitting on a received signal, and for a reference $\cos(2\omega_g + \pi)$ are given in equations 3.3.5 to 3.3.7 . The quantities i and r represent the spectrum point index corresponding to frequencies ω and ω_g.

Received signal upper sideband

$$\phi_{i+r} = \theta + \pi + \pi \left[\frac{\omega + \omega_g}{\omega_o} - (i+r) \right] \qquad (3.3.5$$

50

Received signal lower sideband

$$\phi_{i-r} = -\theta + \pi \left[\frac{\omega - \omega_g}{\omega_o} - (i-r) \right]$$ (3.3.6

Phase reference

$$\phi_{2r} = \pi + \pi \left[\frac{2\omega_g}{\omega_o} - 2r \right]$$ (3.3.7

Equation 3.3.8 shows how these may be processed to determine θ.

$$2\theta = \phi_{i+r} - \phi_{i-r} - \phi_{2r}$$ (3.3.8

The phase reference may be dispensed with if it is arranged that the position of the time window relative to the goniometer rotation is known, but then the frequency dependant terms on the RHS of equations 3.3.5 to 3.3.7 do not cancel out so must be allowed for when calculating θ.

A complex quantity P_i of phase 2θ and magnitude proportional to the product of the amplitudes of the two components is defined by equation 3.3.9, where A_i is the complex amplitude of spectrum point i (* denotes complex conjugate).

$$P_i = A_{i+r} \, A^*_{i-r} \, A^*_{2r}$$ (3.3.9

In the simple case where one plane vertically polarised wave is received, from equation 3.3.3, the amplitudes of the two components are equal and proportional to the amplitude of the wave, hence $|A_{i+r}|=|A_{i-r}| \propto B_0$. From equation 3.3.9 then $|P_i^{1/2}| \propto B_0$, also the phase of $P_i^{1/2}$ is θ and so the quantity $P_i^{1/2}$ represents the amplitude and bearing of the received signal.

In practice other signals may be present, resulting in the amplitudes being contributed to by more than one wave. Then the product P_i is the sum of the desired signal and an interfering signal. However, if the products from N spectra are added (equation 3.3.10), the desired signals add coherently while the interfering signals add incoherently, resulting in a $N^{1/2}$ enhancement of the desired signals.

$$R_i = \sum_k P_{ik} \qquad\qquad (3.3.10$$

(The subscript k denotes results from successive spectra.)

The magnitude and phase of the quantity R_i yields amplitude and bearing spectra of the received waves.

The method could be applied to variable frequency signals by averaging products at different frequencies in successive spectra. The bearing of a signal with a bandwidth several times Δf such as a whistler could be averaged over a number of adjacent points in one spectrum.

52

3.4 Future Whistler Analysis System

A digital whistler analysis system could be constructed using a fast fourier transform analyser to produce a series of complex spectra which are stored in a large array of memory (64K bytes would be required for 2.5 seconds of VLF data). The data would most conveniently be stored as magnitude and phase, with the magnitude scaled logarithmically. The magnitude data could then be written directly to an imaging display with the spectral amplitudes represented by different shades of grey or as different colours. The required event (such as a whistler) would be selected by marking a few points on it using the display cursor, then the computer would identify the whole of the event either by fitting a whistler dispersion curve to the marked points or by following the peaks in spectral amplitude between the logged points. The latter has the advantage that it may be used for signals other than whistlers. Once the event is identified the bearing may be determined using the complex spectral amplitudes stored in memory. The quantity P_i given by equation 3.3.9 would be determined for all spectral points within the trace of the event and then all these values would be summed to give the quantity R_i, the phase of which gives the bearing of the received waves.

This approach to VLF analysis has many advantages over the present method of storing the time series in analogue form on a rotating tape loop and using a programmable filter to track the event of interest. Firstly

53

the quality of the data is not degraded by recording it on tape for a second time. Perhaps most importantly all the spectral data of the event is immediately accessible to computer programs. Such programs could be used for accurately determining the frequency time profiles, and amplitudes of whistlers and other VLF emissions using the methods described in section 3.2. Amplitude measurements in particular are difficult to do accurately with the present system for any variable frequency signal.

Bearing measurements also should be more accurate since the area in the frequency-time space over which the bearing is calculated can be accurately matched to that of the signal. Also the bearing of a nose whistler could be measured in one go; this cannot be done with the present system since the tracking filter cannot follow the whistler above and below the nose simultaneously. Finally the display of the spectral data can be on a normal television monitor which provides a flicker free picture that can be viewed in normal lighting conditions. The amplitude at each frequency-time coordinate would most easily be represented by a grey scale as in a standard spectrogram, but with the addition of a little extra circuitry and a colour monitor, colour spectrograms could be produced.

An Advanced VLF Data Analysis System (ADVAS) using some of the methods mentioned above is currently being developed and will be deployed at Halley in 1983.

The prototype imaging display (monochrome) for the ADVAS was used to produce colour spectrograms. A microcomputer was programmed to generate monochrome displays representing intensities of the three primary colours which make up a colour picture. These were photographed one at a time through the corresponding colour filter onto the same piece of colour film to produce colour spectrograms such as the one in figure 3.3.

Chapter 4 Power Line Radiation in Newfoundland

4.1 Introduction

An assessment of the possibility that line radiation events observed at Halley may be due to magnetospheric amplification (linear or non-linear) of power line harmonics radiated in the conjugate region requires an estimate of the radiated power of those harmonics. To obtain data from which to obtain an estimate, a series of measurements were made in Newfoundland, the conjugate region to Halley, in June/July 1980. Two mobile VLF receiving stations were available and these were used to record, on magnetic tape, the electric and magnetic ELF/VLF field components at several distances from certain power lines.

The tapes were later analysed to determine the strengths at each harmonic frequency of each field component. These were then used to estimate the current in the line and the skin depth in the ground as a function of frequency, from which the radiated power at each harmonic could be estimated for a particular power line.

Detailed measurements were made on two power transmission lines, one a 230 kV line between Stoneybrook (near Grand Falls) and Buchans, the other a 138 kV line on the Baie Verte peninsula. These will subsequently be referred to as the Buchans and Baie Verte lines respectively. Some measurements were also made on the 230 kV line supplying the Erco phosphorous plant at Long Harbour and on a 7.2 kV local distribution line at Cooks Harbour near St. Anthony.

The power line measurement areas are shown in the maps in figures 4.1, 4.8, 4.9 and 4.10.

4.2 Theory of Radiation from Power Lines

4.2.1 A Power Line as a Transmitting Aerial

A schematic diagram of a section of power transmission line between two terminal stations (using Y connected transformers) is shown in figure 4.2. Only the high voltage windings on the transformers are shown; power enters or leaves the transmission line via other windings. If the system were perfectly balanced, the currents in the three wires would sum to zero and no current would flow through the earth connections. In practice, however, even if the system were perfectly balanced at the fundamental it would not be at the higher harmonics, and since most power lines in Newfoundland do not have earth wires except for within 1 km of the terminal stations, all the unbalanced current returns through the ground. The current is distributed through the ground to a depth of the order of the skin depth, δ, which is typically between 100 m and 1 km at VLF. T.R. Kaiser (private communication) has shown (by considering the power line as a transmission line) that for the purpose of estimating the radiated power, the ground current may be represented by a line image at a depth of $\delta 2^{\frac{1}{2}}$. We can therefore calculate the radiated power from a section of line by using the formula for magnetic dipole radiation with a dipole moment of $Il\delta 2^{\frac{1}{2}}$, where I is the
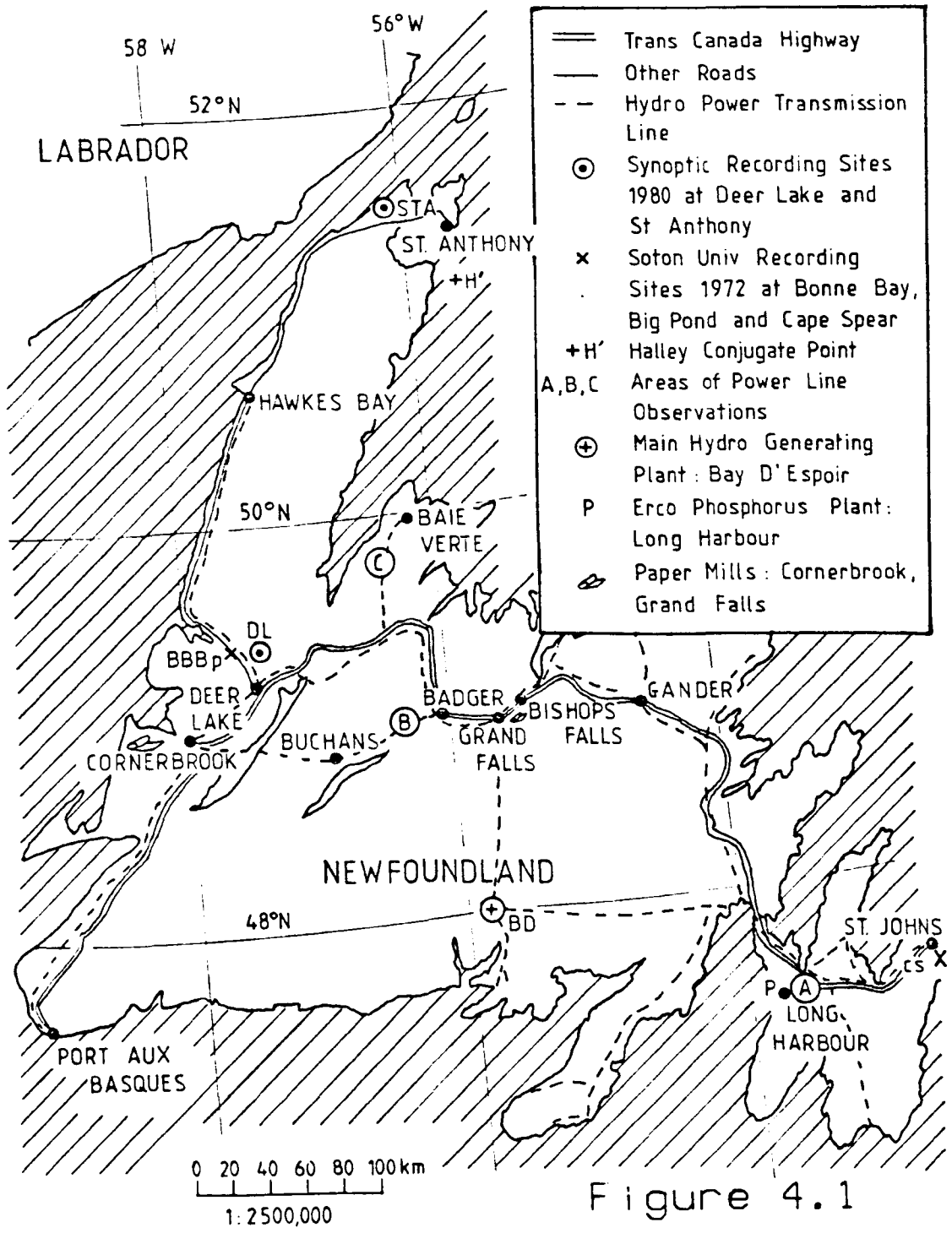
Figure 4.1

3 PHASE TRANSFORMER
(Only high voltage
windings shown)
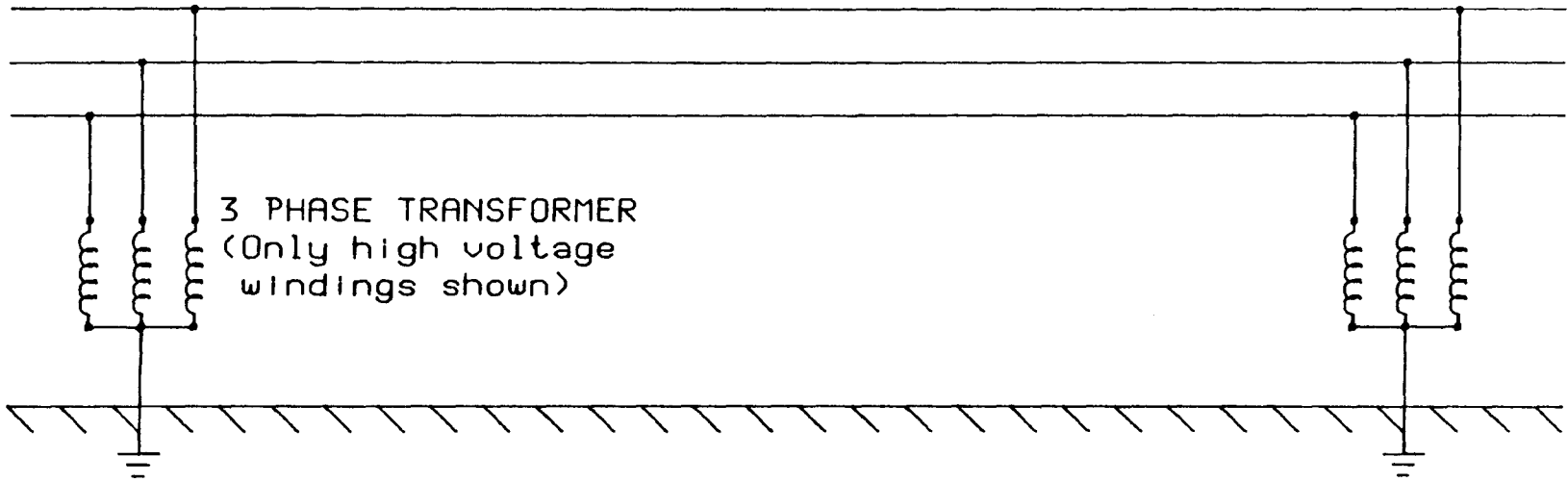
Figure 4.2 . Schematic Diagram of a Section of 3 Phase
Power Line Between 2 Terminal Stations.

unbalanced current in the line and l is the length of the line.

Inactive power lines have been used as VLF transmitting aerials (Dazey 1980, Garnier et. al 1981) by connecting the transmitter at one end of the line between an earth connection and the three conductors. The far end of the line may either be connected to earth or left open circuit. A capacitor or inductor was usually also connected in the circuit for tuning the line to resonance. The current in the line was measured directly and the skin depth was determined by measuring the impedance of the line as a function of frequency with the far end both open and short circuited. However, this method of determining the skin depth does require the power line to be taken out of service and so its application is rather limited.

A description of how the unbalanced current and the skin depth can be determined from measurements of the magnetic field components (due to the normal operating currents in the line) close to the ground at several distances from the power line follows in section 4.2.3. It is also shown that measurements of the electric field at the surface of the ground provide a check on these values. It is convenient to use a coordinate system in which the z axis points in the direction of the power line, since there is a degree of cylindrical symmetry about this axis. The y axis is vertical and the x axis is perpendicular to the other two as shown in figure 4.3.

58

4.2.2 The Effect of an Earth Wire

Some power lines (such as the Cooks Harbour line), have in addition to the main conductors, an earth conductor. To estimate the effect of the earth conductor on the radiation efficiency of the power line, the proportion of the unbalanced current which returns through the earth wire (and thus not contributing to the radiation) is determined by consideration of the mutual impedance of the main conductors and the earth conductor. For simplicity we assume that the line consists of just two conductors, spaced vertically by a distance s, one carrying the net unbalanced current and the other the earth return current. The EMF induced in the circuit consisting of the earth wire and ground return may be expressed as

$$V = I_1 z_1 + I_2 z_{12} \qquad (4.2.1$$

where I_1 and I_2 are the currents flowing in the earth and main conductors respectively, Z_1 is the self impedance of the ground circuit and Z_{12} is the mutual impedance of the ground circuit and of the circuit consisting of the main conductor with ground return. Since the former is a closed loop with no sources we set V=0 in 4.2.1 . The ratio of I_1 to I_2 which indicates the proportion of the unbalanced current which returns through the earth wire is given by

$$\frac{I_1}{I_2} = - \frac{z_{12}}{z_1} \qquad (4.2.2$$

Carson (1926) gives expressions for the self (Z_1) and mutual (Z_{12}) impedance per unit length of overhead wire circuits with ground return. Since, in this case, the separation of the wires and the height above ground is small compared to the skin depth, only the first term in the expression for the effect of the ground on the impedances has to be included.

$$z_1 = R + \frac{i\mu_o \omega}{2\pi} \ln\left[\frac{2h_e}{a}\right] + \frac{\mu_o \omega J}{\pi} \qquad (4.2.3$$

$$z_{12} = \frac{i\mu_o \omega}{2\pi} \ln\left[\frac{h_m + h_e}{s}\right] + \frac{\mu_o \omega J}{\pi} \qquad (4.2.4$$

In the above equation a is the radius of the conductor, s is the separation of the conductors, h_m and h_e are the heights of the main and earth conductors, δ is the skin depth, ω is the angular frequency, and R the series resistance per unit length of the earth conductor. The quantity J in 4.2.3 and 4.2.4 is defined in 4.2.10 where in this case $\theta = \pi/2$ and $r = 2h_e$ in 4.2.3 and $r = h_m + h_e$ in 4.2.4 . Assuming that h_m and h_e are small compared to δ 4.2.3 and 4.2.4 may be rewritten as follows.

$$z_1 = R + \frac{\mu_o \omega}{8} + i\frac{\mu_o \omega}{2\pi} \ln\left[\frac{\delta \sqrt{2}}{a}\right] \qquad (4.2.5$$

60

$$z_{12} = \frac{\mu_o \omega}{8} + i \frac{\mu_o \omega}{2\pi} \ln \left[\frac{\delta \sqrt{2}}{s} \right] \qquad (4.2.6$$

Provided the line is sufficiently long so that the earth terminal resistances do not contribute significantly to the impedances of the circuits, the values yielded by 4.2.5 and 4.2.6 may be placed in 4.2.2 since the length of the line will cancel out. Taking typical values of $\omega = 2\times10^4$ rads^{-1}, $a = 0.01$m, $s = 5$ m, $R = 10^{-4}\Omega$m^{-1} and $\delta = 500$m we have,

$$z_1 = (3.2 + 44.7i)\times10^{-3} \; \Omega \; m^{-1}$$

$$z_{12} = (3.14 + 19.8i)\times10^{-3} \; \Omega \; m^{-1}$$

For a power line several kilometers long or more, the impedances will be of the order of 100 Ω which should be much larger than the earth terminal resistance, therefore I_1/I_2 may be taken as $-Z_{12}/Z_1 = -0.44$. In this case then, approximately half the return current flows in the wire, and so the efficiency of the power line as a transmitting aerial has been halved. The value of R used above is that for a copper conductor of radius about 1 cm; if the earth wire was made of a lower conductivity material the reduction in radiated power would be less.

4.2.3 Determination of Skin Depth and Current

The skin depth in the ground and the unbalanced current flowing in the power line can be determined from measurements of the electric and magnetic field components at a number of distances from the line.

This is done by using a model which allows the E and B field components to be calculated as a function of distance, skin depth, and current. For the purposes of calculating the field associated with an unbalanced current in a power line it is assumed for simplicity the current flows in a single wire with the return current distributed in the ground. This is a problem which has been considered by Carson (1926) and more recently by Wedepohl and Efthymiadis (1978), although at VLF Carson's theory is quite valid. He gives the following expressions for the magnetic field at the surface of the ground and perpendicular distance x from a wire carrying a current I at a height h above the ground of conductivity σ. They are valid for the simplifying assumptions of a flat ground of uniform conductivity and infinite length of line. It is also assumed that the field point is within the induction zone (i.e. $x << \lambda$). The co-ordinate system is shown in figure 4.3 together with the dimensions x and h. δ is the skin depth in the ground at angular frequency ω.

$$B_x = \frac{\mu_o I}{2\pi} \left[\frac{h}{h^2 + x^2} + \int_0^\infty \phi(\mu) \cos x\mu \; d\mu \right] \qquad (4.2.7a$$
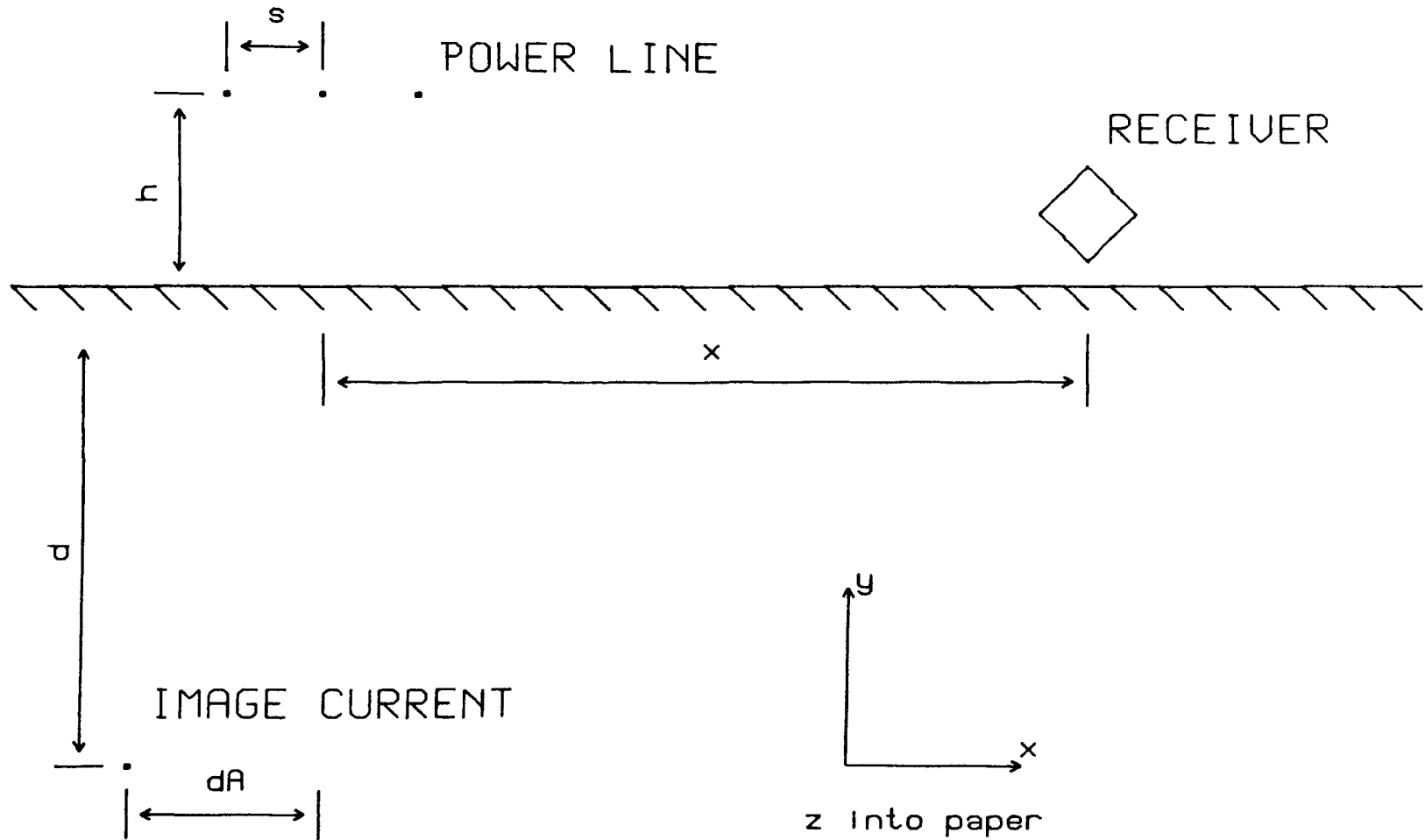
Figure 4.3 . Diagram Showing a Power Line, the Position of
the Equivalent Image Current and the VLF Receiver used to
Measure the Electric and Magnetic Fields. The Co-ordinate
System used in the Text is also Shown.

$$B_y = \frac{\mu_o I}{2\pi} \left[\frac{x}{h^2 + x^2} + \int_0^\infty \phi(\mu) \sin x\mu \; d\mu \right] \qquad (4.2.7b$$

$$B_z = 0 \qquad (4.2.7c$$

where

$$\phi(\mu) = \frac{(\mu^2 + i\alpha)^{1/2} - \mu}{(\mu^2 + i\alpha)^{1/2} + \mu} e^{-h\mu}$$

and

$$\alpha \equiv \omega\mu_o\sigma = \frac{2}{\delta^2}$$

The electric field above the ground is given by the following expression.

$$E_z = -\frac{\mu_o \omega I}{2\pi} \left[2J + i\frac{1}{2}\ln\left[\frac{(h+y)^2 + x^2}{(h-y)^2 + x^2} \right] \right] - \frac{\partial V}{\partial z} \qquad (4.2.8$$

where

$$J = \int_0^\infty ((\mu^2 + i)^{1/2} - \mu) e^{-\alpha^{1/2}(h+y)\mu} \cos(\alpha^{1/2} x\mu) d\mu \qquad (4.2.9$$

The last term in the expression for E_z represents the field due to charges on the wire. There will also be x and y

63

components of E due to charges but these are not relevant to the present problem. Carson does not evaluate the integrals in 4.2.7a and 4.2.7b but he does evaluate the integral in 4.2.9 (for E_z) in terms of two infinite series. These series converge sufficient rapidly in the extreme cases of x << δ and x >> δ that only the first few terms need be considered. For x << δ the integral in 4.2.9 is given by

$$J = \frac{\pi}{8} - \frac{r \sin \theta}{3\delta} + i\left[-0.0386 + \frac{1}{2}\ln(\frac{\delta\sqrt{2}}{r}) + \frac{r \sin \theta}{3\delta}\right] \qquad (4.2.10$$

and for x >> δ by

$$J = \frac{(1+i)\delta \sin \theta}{2r} - \frac{\delta^2 \cos 2\theta}{2r^2} \qquad (4.2.11$$

where r and θ are the conventional cylindrical polar co-ordinates (x = r cosθ , y = r sinθ). This differs slightly from the notation used by Carson.

For the electric field measurements made close to the line (x<<δ, y=0) following expression for E_z may be obtained from 4.2.8 and 4.2.10 . The last term in 4.2.8 may be neglected since there will be no contribution to E_z at the surface of the ground due to charges on the wire.

$$E_z = - \frac{\mu_0 \omega I}{8}\left[1 + i\frac{4}{\pi}\ln(\frac{\delta\sqrt{2}}{x})\right] \qquad (4.2.12$$

This equation can be used to give an estimate of the unbalanced current in the line once an approximate value for δ is known.

While equations 4.2.7a and 4.2.7b could be solved numerically, a simple analytic expression for B_x and B_y is more convenient when analysing the experimental results. For points close to the line ($x \ll \delta$) the only significant field is that due to the current in the line (ie the field due to ground currents may be neglected), while for $x \gg \delta$ it is only the magnetic moment of the currents that is important and not the actual distribution of currents that cause it, and so in this region the ground currents may be represented by a line image. In fact the image current model may be used over the entire range of x to give B_x and B_y to an acceptable degree of accuracy for this work, as will be shown by comparing the fields given by the image current approximation with a numerical solution of equations 4.2.7a and 4.2.7b in the intermediate range $x \sim \delta$.

To verify the relation between the depth of the image current (d) required to represent the dipole moment of the current distribution in the ground and the skin depth in the ground, the magnetic field in the region $x \gg \delta$ was calculated using Carson's expression for E_z and relating $\underline{E}$ to $\underline{B}$ with Maxwell's equations.

$$\frac{\partial \underline{B}}{\partial t} = - \text{curl } \underline{E} \qquad (4.2.13$$

Since all fields are assumed to have an $e^{-i\omega t}$ dependence we may use 4.2.13 to obtain B_x and B_y at the surface of the ground as follows.

65

$$B_x = \frac{i}{\omega} \frac{\partial E_z}{\partial y}\bigg|_{y=0} = \frac{i}{\omega r} \frac{\partial E_z}{\partial \theta}\bigg|_{\theta=0} \qquad (4.2.14a$$

$$B_y = -\frac{i}{\omega} \frac{\partial E_z}{\partial x}\bigg|_{y=0} = \frac{i}{\omega} \frac{\partial E_z}{\partial r}\bigg|_{\theta=0} \qquad (4.2.14b$$

Using 4.2.9 and 4.2.11 to substitute for E_z in 4.2.14 the following expressions for B_x and B_y are obtained.

$$B_x = \frac{\mu_o I \delta (1-i)}{2\pi x^2} \qquad (4.2.15a$$

$$B_y = \frac{\mu_o I \delta^2 i}{\pi x^3} \qquad (4.2.15b$$

The field components may be calculated for the image current approximation by using Ampere's law. For an image current $-I$ flowing at a depth d directly below the wire the fields are given by the equations below where it is assumed that the height of the wire is small compared to x .

$$B_x = \frac{\mu_o I d}{2\pi (x^2 + d^2)} \qquad (4.2.16a$$

$$B_y = \frac{\mu_o I d^2}{2\pi x (x^2 + d^2)} \qquad (4.2.16b$$

Comparing 4.2.15 and 4.2.16 it is observed that they give the same magnitudes for the field components at $x \gg \delta$ if we set $d = 2^{1/2} \delta$. This agrees with the calculation of T.R. Kaiser (private communication) used to estimate the radiated power.

The phases of the field components given by 4.2.15 and 4.2.16 differ, but this does not matter in this work since only the magnitudes of the fields were measured. In the rest of this chapter equations 4.2.16a and 4.2.16b are considered to represent only the magnitude of the field components.

Quantities B and θ (not to be confused with the polar co-ordinate θ used above) which will be used in the analysis of the results are defined below.

$$B \equiv (B_x^2 + B_y^2)^{1/2} = \frac{\mu_o I d}{2 \pi x (x^2 + d^2)^{1/2}}$$
(4.2.17

$$\tan\theta \equiv \frac{B_y}{B_x} = \frac{d}{x}$$
(4.2.18

Equation 4.2.17 may be used to determine the unbalanced current from measurements close to the line and the image depth from simultaneous measurements at greater distances. Equation 4.2.18 may be used to determine the image depth from single measurements at $x \sim \delta$.

To test the validity of the image current approximation in the range x~δ Carson's expressions for the magnetic field components (equations 4.2.7a and 4.2.7b) were solved numerically using typical values of 10 m for the height of the power line, 0.447 km for δ (giving α=10) and a series of values for x. Firstly 4096 values of $\phi(\mu)$ were calculated for $\mu = 0\rightarrow204.75$ and then the integrals were performed using the Fast Fourier transform algorithm (the limit of μ=204.75 was chosen so that the calculation would yield values of B at ~30m intervals). The first 400 points were used to give values of B_x and B_y up to 12 km. These were compared with those predicted by the image current method. There was a good agreement between the B_y/B_x ratios obtained from both methods.

Figure 4.4 shows the variation of B_y/B_x with distance calculated using the image current approximation (broken line) and Carson's theory (solid line). The large deviation at small distances is because the image current model used assumes that the height of the power line is zero. This could be taken into account, but since the height of the line is comparable with the uneveness of the ground surface, which cannot in practice be allowed for, there is no point in allowing for the former.

Five values of B_y/B_x taken from the numerical solution at distances corresponding to those used for the measurements on the Buchans line were put into the program to calculate image depths using equation 4.2.18. The value returned agreed with that used in the program to generate
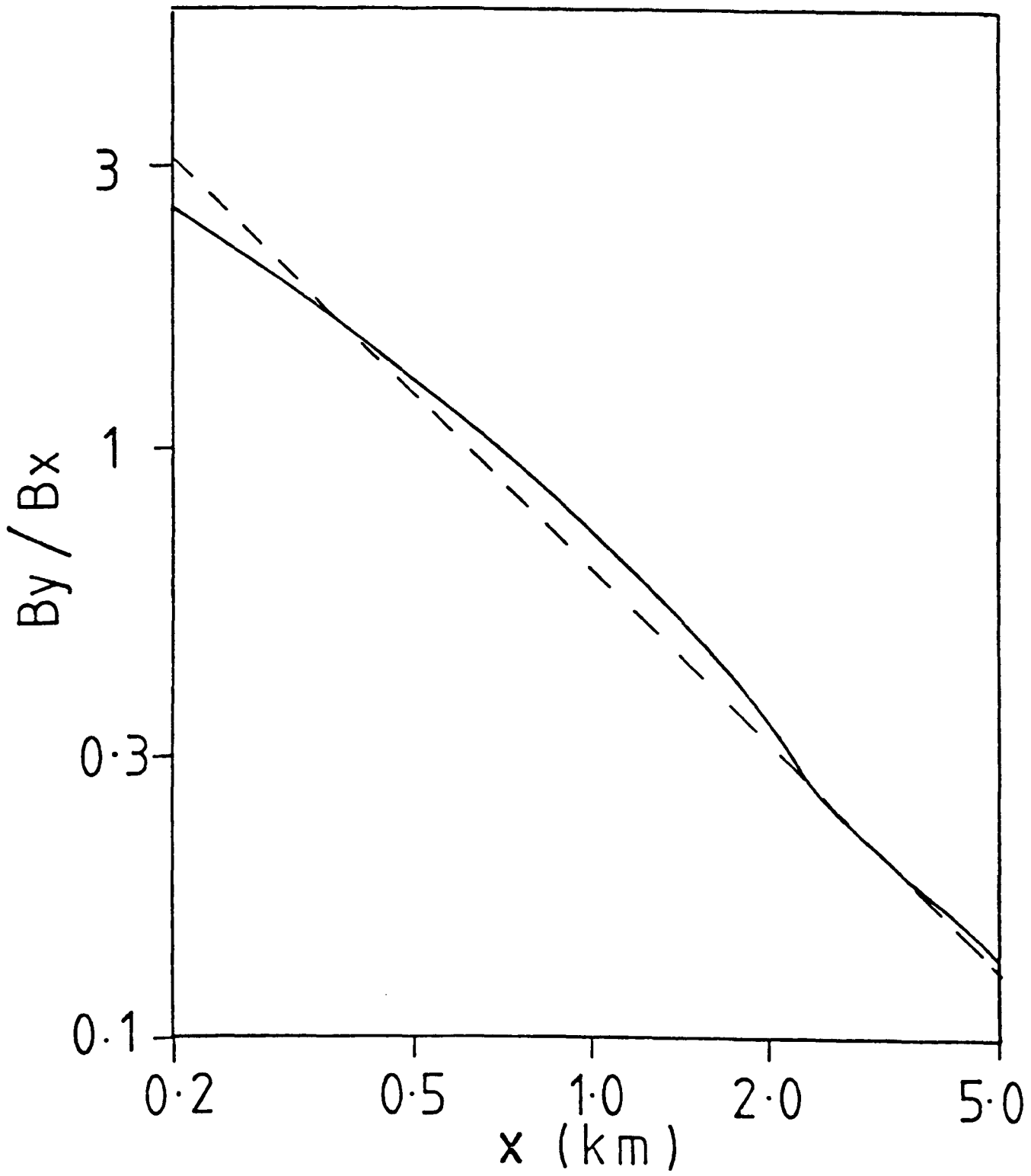
Figure 4.4 . Comparison of ratio of y to x components of B calculated using the image current approximation (broken line) and Carson's theory (solid line) for h=10m and d=633m .

the data to within 2%.

The difference between the values of B calculated numerically and using the image current approximation were larger than for B_y/B_x , but it is the latter which is important since that quantity was used in the analysis of the results.

4.2.4 The Effect of Balanced Currents

We have assumed that the net unbalanced current in the power line can be represented by that current flowing in a single wire. While this is a valid representation of the unbalanced current it does not take into account the effect of the balanced currents in the line, which at the fundamental frequency, are much stronger than the unbalanced currents. The actual situation is rather complicated since the power lines are three phase, but a rough estimate of the field (B_x' and B_y') due to the balanced currents may be obtained by considering two wires spaced 2s apart carrying equal and opposite currents I'. The resultant field is simply the vector sum of the fields due to the individual currents and can be calculated using Ampere's law.

$$B_x' = \frac{\mu_o I' 2hs}{2\pi \ x^3} \qquad\qquad (4.2.19a$$

$$B_y' = \frac{\mu_o I' s}{2\pi \ x^2} \qquad\qquad (4.2.19b$$

Since x>>h the vertical term B_y' is dominant and so we

consider this term. Comparing equation 4.2.19b with equation 4.2.16b we get (for x<<d)

$$\frac{B_y{'}}{B_y} = \frac{I'}{I} \times \frac{s}{x}$$

(4.2.20

Equation 4.2.20 shows that the effect of balanced currents decreases as x increases, so measurements made close to the line are more likely to be affected by balanced currents than those made further away. We can determine whether measurements are affected by balanced currents by examining the variation of B_y with distance close to the line; if the variation follows a 1/x law then there is no effect from balanced current, whereas if the variations follow a $1/x^2$ law, then unbalanced currents do have significant effect, as might be expected very close to the line.

   To estimate the effect of balanced currents on the electric field measurements we use a similar approach in which the electric fields due to currents +I' and -I' flowing in two wires are summed. Taking only the imaginary term from equation 4.2.12 (the real term is assumed constant and so will give rise to equal and opposite fields due to the two currents +I' and -I') we can derive equation 4.2.21 (for s<<x<<δ).

$$\frac{E_z{'}}{E_z} = \frac{I'}{I} \times \frac{s}{x \; \ln(x/\delta\sqrt{2})}$$

(4.2.21

By comparing equations 4.2.20 and 4.2.21 we see that

70

balanced currents have a proportionally less effect on E_z measurements by the factor $\ln(x/2\ \delta)^{1/2}$. This factor would typically have a value of -2.7 for $x=0.1\delta$.

4.2.5 Effect of Conductivity Asymmetries

The effect of an asymmetry in the conductivity of the ground can be modelled using a horizontally displaced image current. In this case 4.2.17 and 4.2.18 can be modified as follows.

$$B = \frac{\mu_o Id}{2\pi x}\left[\frac{1+A^2}{(1+A^2)d^2+x^2-2xdA}\right]^{1/2} \qquad (4.2.22$$

$$\tan\theta = \frac{d}{x}(1+A^2)-A \qquad (4.2.23$$

A is the ratio of the horizontal displacement of the image current to its depth d, and is positive for a displacement in the direction of x. The behaviour of equation 4.2.22 as $x \to \infty$ is the same as equation 4.2.17 with d replaced by $d(1+A^2)^{1/2}$ which represents the separation of the line and the image current. Therefore if asymmetries are present, values of d calculated from 4.2.17 represent distance of the image current from the power line, rather than from the surface of the ground. The value of A cannot be estimated from 4.2.22 since it is only significant when x is of the same order as d, and then the image current approximation is not valid. However, the effect of A on values of d calculated from field directions is rather more severe as

can be seen in equation 4.2.23 . Firstly, d is multiplied by $1+A^2$ rather than $(1+A^2)^{1/2}$ and secondly, A appears as a constant term also. The latter can be turned to advantage though, as it provides a means of estimating the value of A since as $x \to \infty$ $\tan\theta \to -A$.

4.3 Measurement Procedure in the Field

4.3.1 Equipment

The equipment used was essentially the portable VLF recording station shown in figure 4.5, with the following changes and additions. The tape recorder CH1 input was connected to the goniometer A channel output and the CH2 input was normally connected to the B channel output, to record the field components directly rather than with goniometer processing. The programmer and power supply (described in appendix A) used for the mobile station was modified so that the 7 kHz calibration tone was permanently on. For measurements close to the line a stronger calibration tone than normal (1 pT) was required and this was done by connecting the calibration coil to the direct calibration output via external resistors chosen to give a suitable current in the coil. For measurements of the electric field in the ground the standard preamplifier was substituted by a low noise, high impedance, differential amplifier (see section 2.5) which was connected to two copper rods placed in the ground several metres apart. The electric field measurements were calibrated by connecting the amplifier to a 7 kHz sine wave signal generator instead of to the copper rods.

Measurements were made using a fixed station set up close to the power line (see figure 4.7) with a single loop to record B_x and a mobile station to record the five components B_x, B_y, B_z, E_x and E_z at several of distances
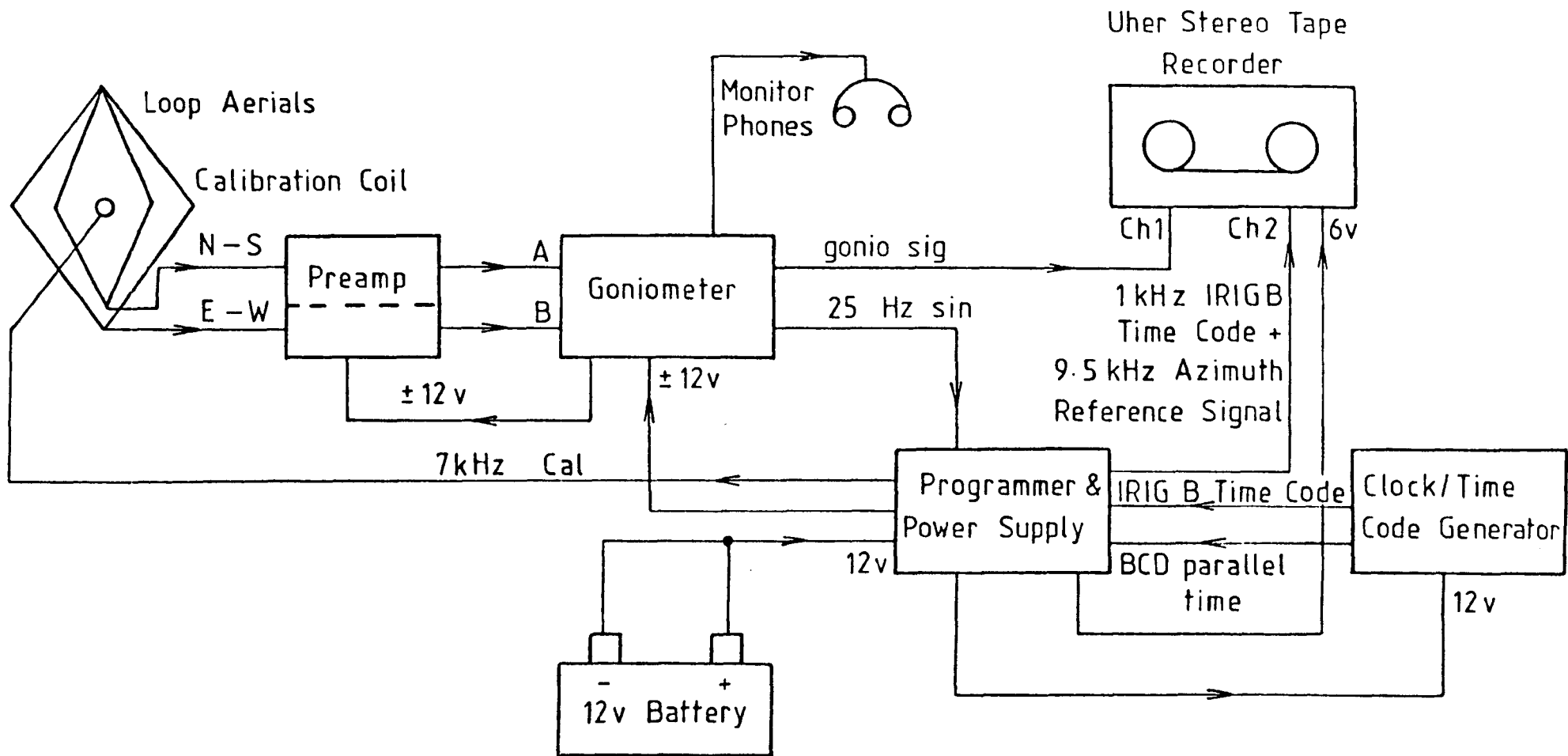
Figure 4.5

PORTABLE VLF GONIOMETER RECORDING STATION AS USED IN NEWFOUNDLAND
JUNE / JULY 1980
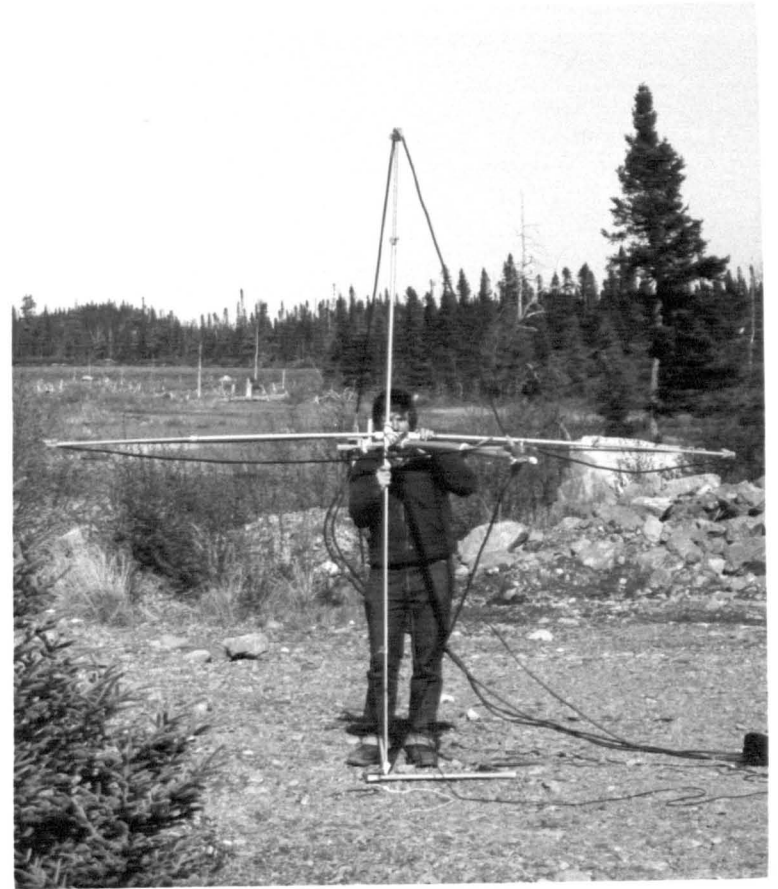
Figure 4.6 . Photographs showing the positions of the loop aerials used for recording the x and z components of B (left) and the x and y components of B (right).

Figure 4.7 . Photograph of the Buchans power line with the loop aerial used at the fixed station.

from each power line studied. Since only two components could be recorded at once on the two track tape recorder, they were recorded in four sets of pairs with B_x on channel 1 and the other components in turn on channel 2.

The magnetic field measurements at the mobile station were done by holding the loop aerials in the position in figure 4.6(left) when recording B_x and B_z, and in the position in figure 4.6(right) when recording B_x and B_y.

The calibration coil for the magnetic field measurements was fixed at $45°$ to the two loops of the mobile station and parallel to the single loop of the fixed station. Time code (IRIG B) was recorded at both fixed and mobile stations to allow identification of simultaneous recordings during analysis. The time code was recorded continuously on channel 2 at the fixed station, but at the mobile station, since both channels were required for data, a 10 second section of time code was recorded on channel 2 at the start of each recording. To compare the two time code generators they were connected to the two channels of the same recorder at the begining and end of each day's measurements, and a short recording made.

4.3.2 Measurements on the Long Harbour Power Line

These were done on the 230 kV line supplying the ERCO phosphorous plant at Long Harbour, mainly as an exercise for field testing the equipment and procedures. The site was also near a low voltage line to Long Harbour

74

village, but was the only suitable one that could be found (see map figure 4.1).

Recordings were made at sites 120 m and 460 m from the line. The distance of the first site relative to the line was determined by theodolite readings an two nearby pylons, using a 100 m base line, while the second site position was determined by taking compass bearings on the same pylons. From the theodolite measurements it was determined that the pylons were 364 m apart and 22 m high, and the three conductors were separated from each other by 7 m. The measurements made are summarised as follows:

Long Harbour 7 June 80

Station	Site	Dist. (x)	CH 1	CH 2	Time UT
Fixed	2	120m	B_x	IRIG B	as mobile
Mobile	2	120m	B_x	B_z	1741-1743
			B_x	B_y	1745-1747
			B_x	E_z	1753-1755
			B_x	E_x	1807-1809
	3	460m	B_x	B_z	1900-1902
			B_x	B_y	1904-1906

4.3.3 Measurements on the Buchans Power Line

For detailed measurements on a 230 kV power line a section of the Stoneybrook to Buchans line (hereafter referred to as the Buchans line) was chosen. The measurements were made in the area 15 km south-west of Badger(see map figure 4.8) where the line was virtually straight and remote from other power lines and settlements. The Badger to Buchans road, which carried very little traffic, crossed the power line at an angle of 30°, and since both the road and power line were straight, sites for the mobile station were located 100 m, 200 m and 500 m from the line by measuring 200 m, 400 m and 1 km along the road from the intersection point. Other sites were located by map reading using the vehicle odometer as a guide.

The fixed station was located on a forest track 86 m from the power line, near where it crossed the road.

The recording sites were surveyed and marked on the 9th of June and recordings made the following day, as shown in the table on the following page.
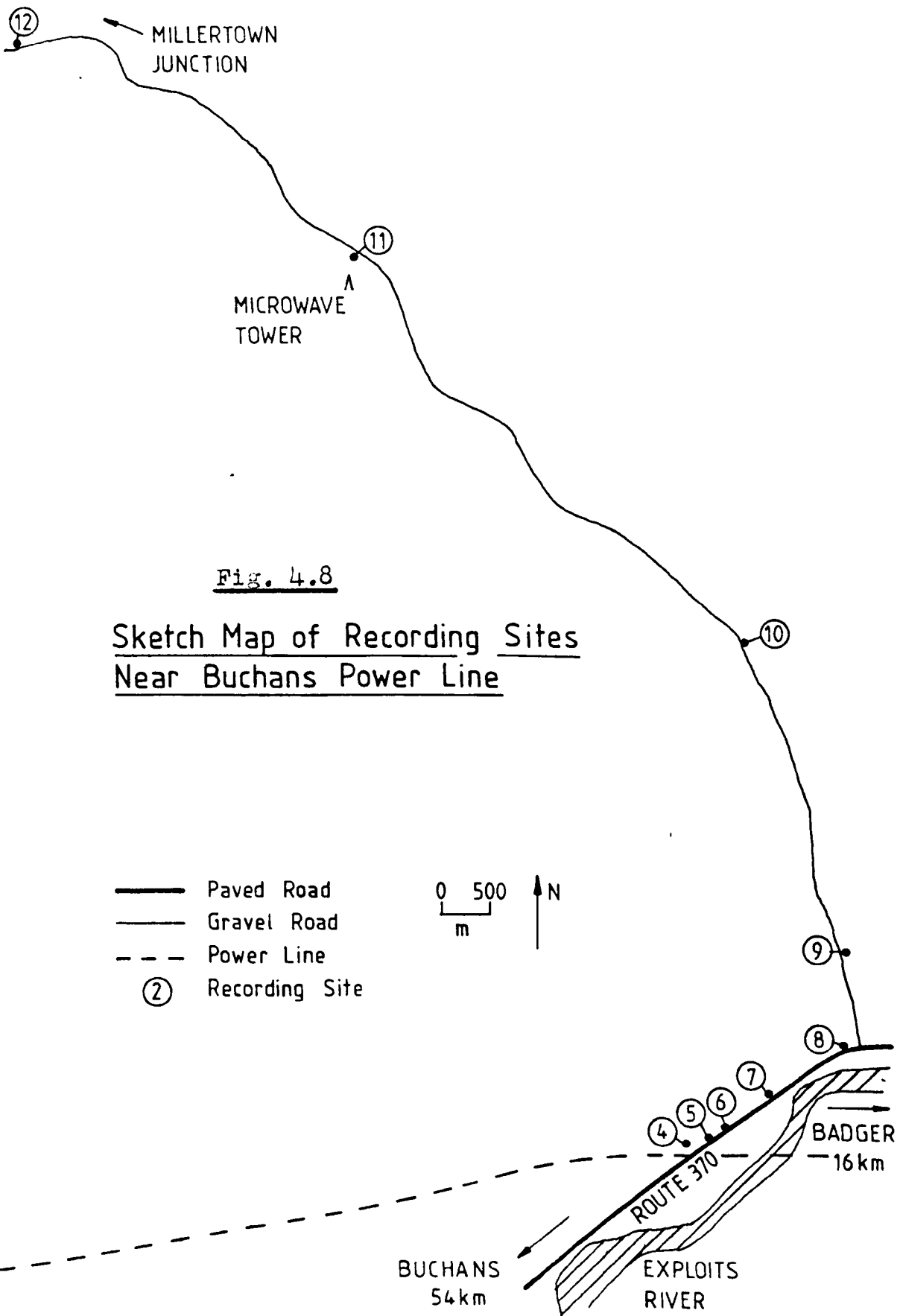
Fig. 4.8

Sketch Map of Recording Sites
Near Buchans Power Line

MILLERTOWN
JUNCTION

MICROWAVE
TOWER

⎯⎯⎯ Paved Road
⎯⎯⎯ Gravel Road
⎯ ⎯ ⎯ Power Line
② Recording Site

0 500
⎯⎯⎯
m

N

BADGER
16 km

ROUTE 370

BUCHANS
54 km

EXPLOITS
RIVER

Buchans 10 June 80

Station	Site	Dist. (x)	CH 1	CH 2	Time UT
Fixed	4	86m	B_x	IRIG B	as mobile
Mobile	5	100m	B_x	B_z	1440-1442
			B_x	B_y	1443-1445
			B_x	E_z	1454-1456
			B_x	E_x	1508-1510
	6	200m	B_x	B_z	1553-1555
			B_x	B_y	1557-1559
			B_x	E_z	1603-1605
			B_x	E_x	1615-1617
	7	400m	B_x	B_z	1705-1707
			B_x	B_y	1710-1712
			B_x	E_z	1715-1717
			B_x	E_x	1720-1722
	8	950m	B_x	B_z	1800-1802
			B_x	B_y	1805-1807
			B_x	E_z	1810-1812
			B_x	E_x	1815-1817
	9	2.0km	B_x	B_z	1905-1907
			B_x	B_y	1910-1912
	10	5.3km	B_x	B_z	2010-2011
			B_x	B_y	2015-2016
	11	10.0km	B_x	B_z	2045-2046
			B_x	B_y	2050-2051
	12	12.9km	B_x	B_z	2110-2111
			B_x	B_y	2115-2116

Site 11 was 120 m from a microwave repeater which was powered by a generator but no interference was detected. At site 12, 12.9 km from the line the level of harmonics was very low.

The following information on the Buchans line was obtained from the Newfoundland and Labrador Hydro office at Bishops Falls.

A typical current would be 225 A, giving at 230 kV, a power transmission of about 90 MW. A random check for a summer day (11 June 1980) showed a minimum load of 52 MW at 0400 LT and a maximum of 93 MW at 1200 LT. On a Sunday (8 June 1980) the minimum was 50 MW and maximum 81 MW.

The conductors are 26 strand aluminium and 7 strand steel core with an overall diameter of 25 mm. They are supported on towers typically 20 m high and 300 m apart.

4.3.4 Measurements on the Baie Verte Line

For measurements on a 138 kV line, the line from Indian River to Baie Verte was chosen, since this ran through reasonably remote country around Wild Cove Pond (see map figure 4.9). The situation was not ideal for the following reasons; the main road was quite busy (car interference was heard on some recordings), the line was not straight and there was access to sites only up to 4 km distant from the line (and that on a rather poor gravel road).

The sites were surveyed and marked on 11 June 1980 and recordings were made on the following day. While surveying the recording sites the following typical dimensions were determined:

Distance between pylons 150 m

Separation between conductors 3.8 m

Height of conductors 11 m

The same recoding methods were used as for the Buchans line, and the following recordings were made.

Fig. 4.9

Sketch Map of Area Around
Baie Verte Line Recording Site

TRAP
POND

⑲
⑱
⑰
⑳ KIDNEY
POND

BAIE VERTE
32 km

69 kV

ROUTE 410

⑯

SLINK POND

WILD
COVE
POND

⑮

N

0   1km

⑭

Paved Road
Gravel Road
Power Line
⑯ Recording Site

LOGGING
CAMP ◉

MICMAC
LAKE

TRANS CANADA HIGHWAY 20km
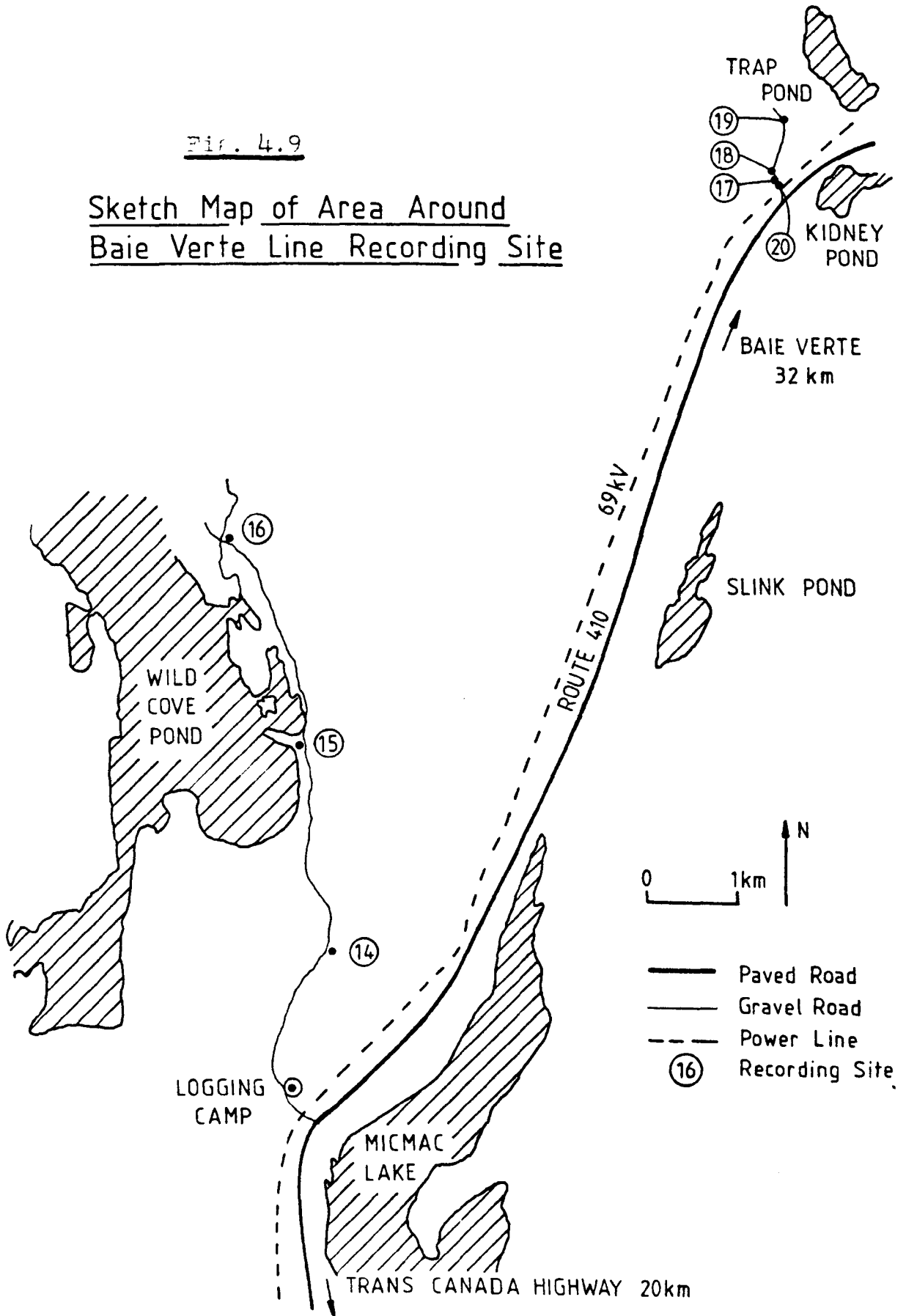
Baie Verte 12 June 80

Station	Site	Dist. (x)	CH 1	CH 2	Time UT
Fixed	17	104m	B_x	IRIG B	as mobile
Mobile	17	104m	B_x	B_z	1324-1326
			B_x	B_y	1327-1329
			B_x	E_z	1332-1334
			B_x	E_x	1348-1350
	18	198m	B_x	B_z	1434-1436
			B_x	B_y	1441-1443
			B_x	E_z	1445-1447
			B_x	E_x	1452-1454
	19	526m	B_x	B_z	1523-1525
			B_x	B_y	1527-1529
			B_x	E_z	1533-1535
			B_x	E_x	1540-1542
	14	1.0km	B_x	B_z	2000-2001
			B_x	B_y	2005-2006
	15	2.3km	B_x	B_z	1930-1931
			B_x	B_y	1935-1936
	16	3.8km	B_x	B_z	1900-1901
			B_x	B_y	1905-1906

4.3.5 Measurements on the Cooks Harbour Line

This was a 7.2 kV line running from Cooks harbour to the airport, and was the nearest line to the St. Anthony recording site. The following measurements were made using just the mobile station at two sites near Cooks Harbour Junction (see map figure 4.10), on 13 June 1980.

Cooks Harbour 15 June 80

Site	Dist. (x)	CH 1	CH 2	Time UT
24	500m	B_x	B_z	2108:00-2110:00
		B_x	B_y	2110:30-2112:30
25	1.0km	B_x	B_z	2125:00-2127:00
		B_x	B_y	2127:30-2129:30

Fig. 4.10 St. Anthony Area, Newfoundland

Legend:
— Paved Road
— Gravel Road
© Cabin
·········· Telephone Line
— — — 7.2 kv Power Line
• Settlement
⊕ Generating Plant
ψ LORAN Radio Transmitter
⊗ IGS Magnetometer Site

BELLE ISLE STRAIT

ST. ANTHONY RECORDING SITE
JUNE / JULY 1980

CAPE NORMAN
COOKS HARBOUR
SHIP COVE
L'ANSE AUX MEADOWS
QUIRPON
BOAT HARBOUR
RALEIGH
FILLING STATION
PISTOLET BAY
GRIQUET
ST. LUNAIRE
BIG BROOK
Route 437
VIKING MOTEL
AIRPORT
Route 436
GT BREHAT
Route 430
DEER LAKE
ST. ANTHONY BIGHT
ST. ANTHONY
GOOSE COVE
HARE BAY
MAIN BROOK
BURNT VILLAGE
FISCHOT ISLANDS
CROQUE

N

Approximate Conjugate Point to Halley.

0   5km

4.4 Method of Analysis

The first stage of the analysis was to make film spectrograms of the recordings to determine the best period during each recording to measure the signal amplitude. Ideally the recordings at both fixed and mobile stations should be free of local interference and the power line harmonic amplitude should be constant over the time of measurement.

The measurements were made as follows. The data tape was replayed with tape recorder channel 2 output feeding a time code reader, and either channel 1 or channel 2 feeding the Unigon fast fourier transform spectrum analyser. The latter produced spectra covering a range of 0 to 5120 Hz with a resolution of 10 Hz. For each measurement 64 spectra, calculated from adjacent (non-overlapping) 100 ms time samples, were averaged. Each averaged spectrum was then read into the memory of the M6800 microprocessor using the interface and control program described in appendix B. The BASIC program for measuring amplitude and frequency of spectral peaks described in section 3.2 was used to measure the frequency and amplitude of all peaks between 50 Hz and 4500 Hz. The upper limit was chosen to be less than 5120 Hz to reduce the possibility that a peak in the spectrum may be the alias of a frequency above 5120 Hz. The output from this program was sent, via a terminal line at the Sheffield workstation, to the IBM 370 computer at Daresbury. There, the uncorrected frequency and amplitude data were placed in disk files, one for the fixed station

measurements and one each for each channel of the mobile station measurements. Auxiliary data describing the amplitude of the 7kHz calibration tone, the type and site number of the measurements, and the frequency response of the recording system were typed into additional files.

The FORTRAN program PLRANL was then used to correct the amplitude measurements using the calibration tone and frequency response data and to interpret the frequencies in terms of harmonic number. The fundamental frequency was found by dividing the 7th harmonic frequency by 7. The latter generally had the largest (apparent) amplitude in the spectrum and was easily identified near 420 Hz. This procedure gave the fundamental frequency to sufficient accuracy to determine the harmonic numbers up to the upper frequency limit. The output from the program was a table of dB amplitudes (relative to 1 pT RMS) for each numbered site and for harmonic numbers from 1 to 75 (60 to 4500 Hz). One such table was produced for each type of recording, and for each channel at the fixed and mobile sites. The program PLRRAT was then used to compute the ratios between measurements made at the same time on each of the recording channels.

Two methods were used to estimate the unbalanced currents in the Buchans and Baie Verte lines. The first used the vertical magnetic field measured close to the line with 4.2.16b and the second the parallel electric field with 4.2.12 . Neither method could be used for the Cooks Harbour line since the closest measurement was made 500 m from the

line which is not small compared with the skin depth. In this case equation 4.2.18 was used to give an estimate of the skin depth which was then substituted into equation 4.2.17 to give the following expression for the current.

$$I = \frac{2\pi x (B_x^2 + B_y^2)}{\mu_o B_y}$$
(4.4.1

Two methods were also used to estimate the skin depth, firstly using the variation of field direction with distance, and secondly using the variation of field magnitude.

The first method used equation 4.2.18. A linear regression of the field ratio, $\tan \theta$, against $1/x$ is used to estimate d. A weighting factor of $\cos^2\theta$ was applied to each point since for $\theta \sim 90^o$ a small angular error, $\delta\theta$ such as may be due to antenna misalignment, gives rise to large variations in the field ratio. For example, when $\theta = 45^o$ a 1° error in θ gives a 4% error in $\tan \theta$, but when $\theta = 85^o$ a 1° error in θ gives a 25% error in $\tan \theta$.

This method was later refined by using equation 4.2.23 to estimate values of d and A when the variation of B with distance showed that significant asymmetry was present.

In the second method to estimate d and also I from the variation of field magnitude with distance from the line, equation 4.2.17 was rewritten as below.

$$B^2 x^2 = \frac{B^2 x^4}{-d^2} + \left[\frac{\mu_o I}{2\pi}\right]^2$$
(4.4.2

85

Using measurements at different distances from the line to give a series of B,x values equation 4.4.2 was solved using the standard least squares method to give values for d and I.

4.5 Results

4.5.1 Unbalanced Currents

The unbalanced currents in the Buchans and Baie Verte lines were estimated using measurements of the vertical magnetic field (B_y) and the parallel electric field (E_z) at about 100 m and 200 m distant from the lines. There was good agreement between the currents determined from magnetic and electric fields for the Buchans power line, although measurements made at 100 m gave larger (5 dB on average) currents than those made at 200 m. This may indicate that balanced currents make a significant contribution to the fields measured at 100 m, but if this were so then we would expect a disagreement between the magnetic and electric field measurements. At the high frequency end of the range 200 m is becoming comparable with the skin depth and so ground currents would significantly reduce the field measured at 200 m.

For the Baie Verte line, however, the situation is reversed. We have good agreement between the measurements at 104 m and 198 m, but the electric field measurements give currents typically 2 to 3 times those determined from the magnetic fields. It is unlikely that the difference could be due to balanced currents since the measurements at 104 m and 198 m agree. One possibility is that local variations in surface conductivity result in a higher than average electric field in the area where the measurements were made.

One exception to the above was the 2nd harmonic, 120 Hz, for which the electric field gave a current larger than the magnetic field by a factor of 8 for Buchans and 20 for Baie Verte. The other low order even harmonics showed the same effect to a lesser extent. The two histograms in figure 4.11 show the unbalanced currents at each harmonic frequency for the Buchans and Baie Verte lines. The data presented are derived from B_y measured at 100 m from the line. Data recorded at 100 m were chosen since $x << \delta$ for the whole frequency range, and because a greater number of lines were present in the spectrum than in data recorded at 200 m. Magnetic rather than electric field measurements were used since the former are not subject to error due to variations in ground conductivities.

Figure 4.12 shows the out of balance currents for Long Harbour and Cooks Harbour. The data for the former were determined from the vertical magnetic field at 120 m from the line and that for the latter from both magnetic field components at 500 m from the line (using equation 4.4.1).

4.5.2 Variation of Field Magnitude and Direction

Figures 4.13 to 4.16 show the variation of the B field magnitude and the ratio of B_y/B_x with distance from the line for the Buchans and Baie Verte data. Both axes are logarithmic in each figure so that variations predicted by the image current theory appear as straight lines. In figures 4.15 and 4.16 there are additional Y axes to show the direction of the magnetic field although the sign of the
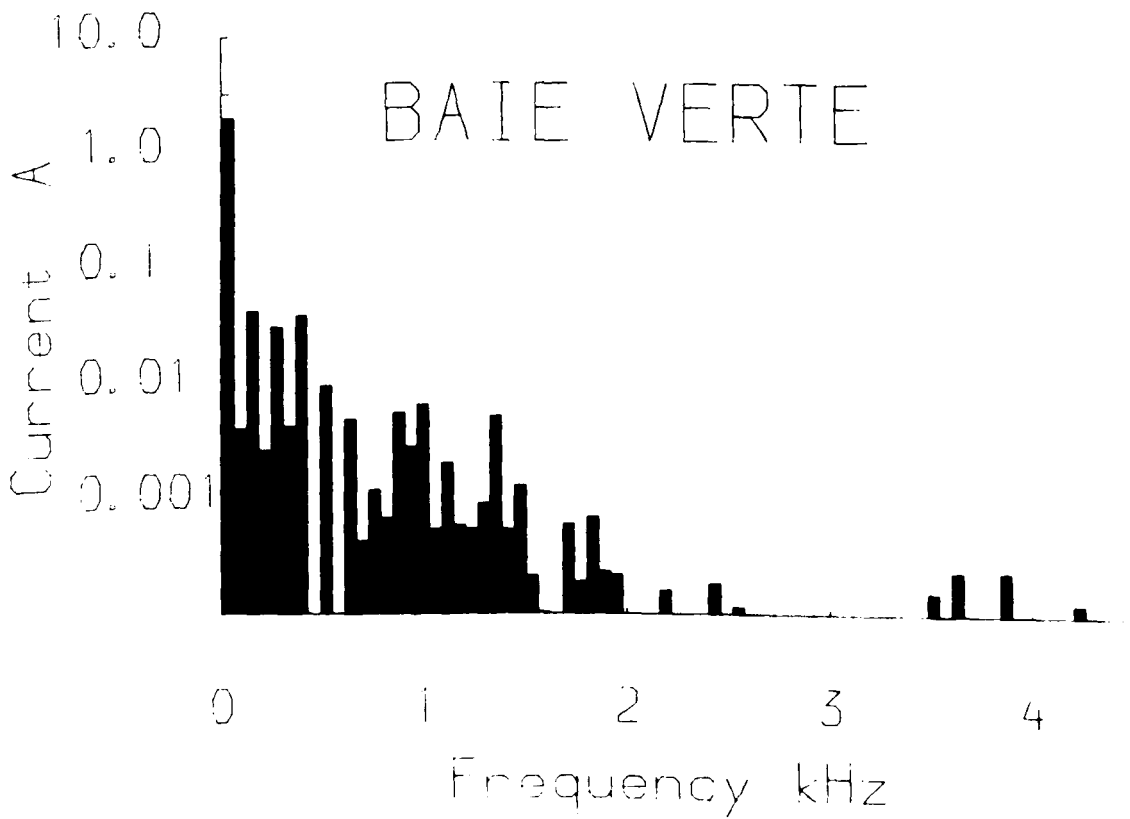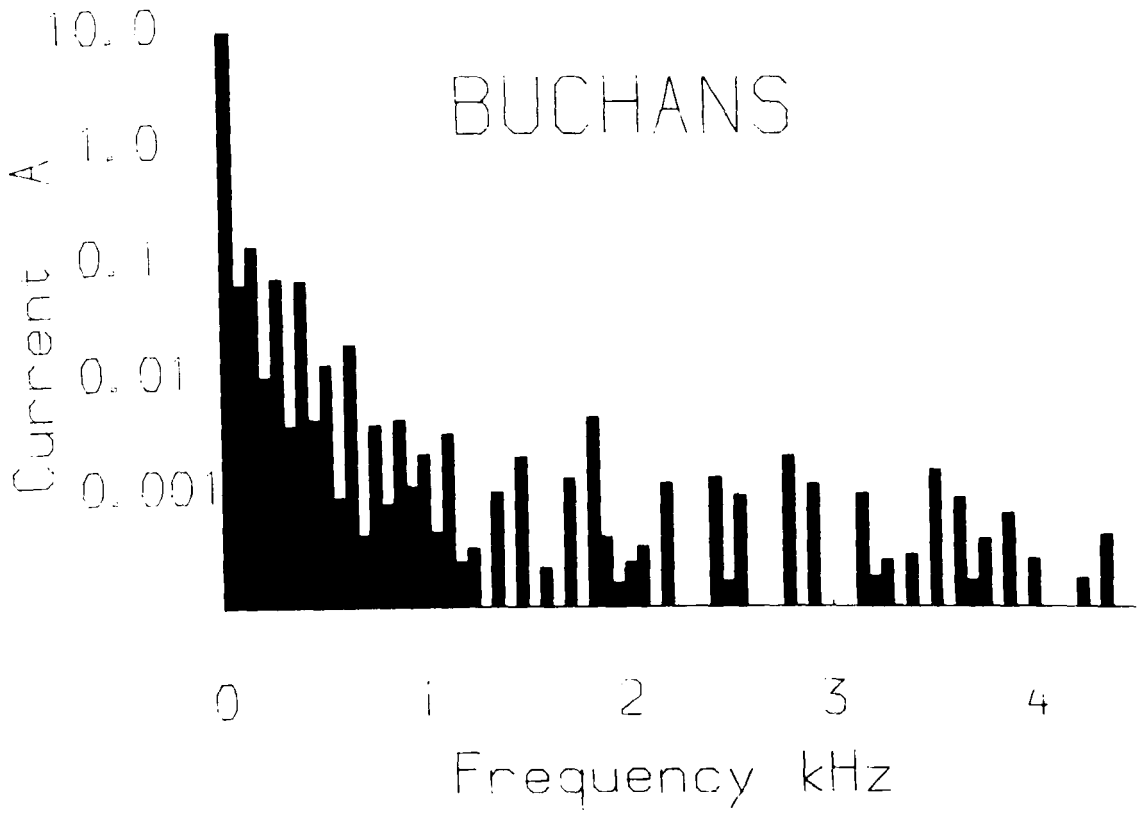
Figure 4.11 . Histograms of the unbalanced currents,
at each harmonic, measured for the Buchans and
Baie Verte power lines.
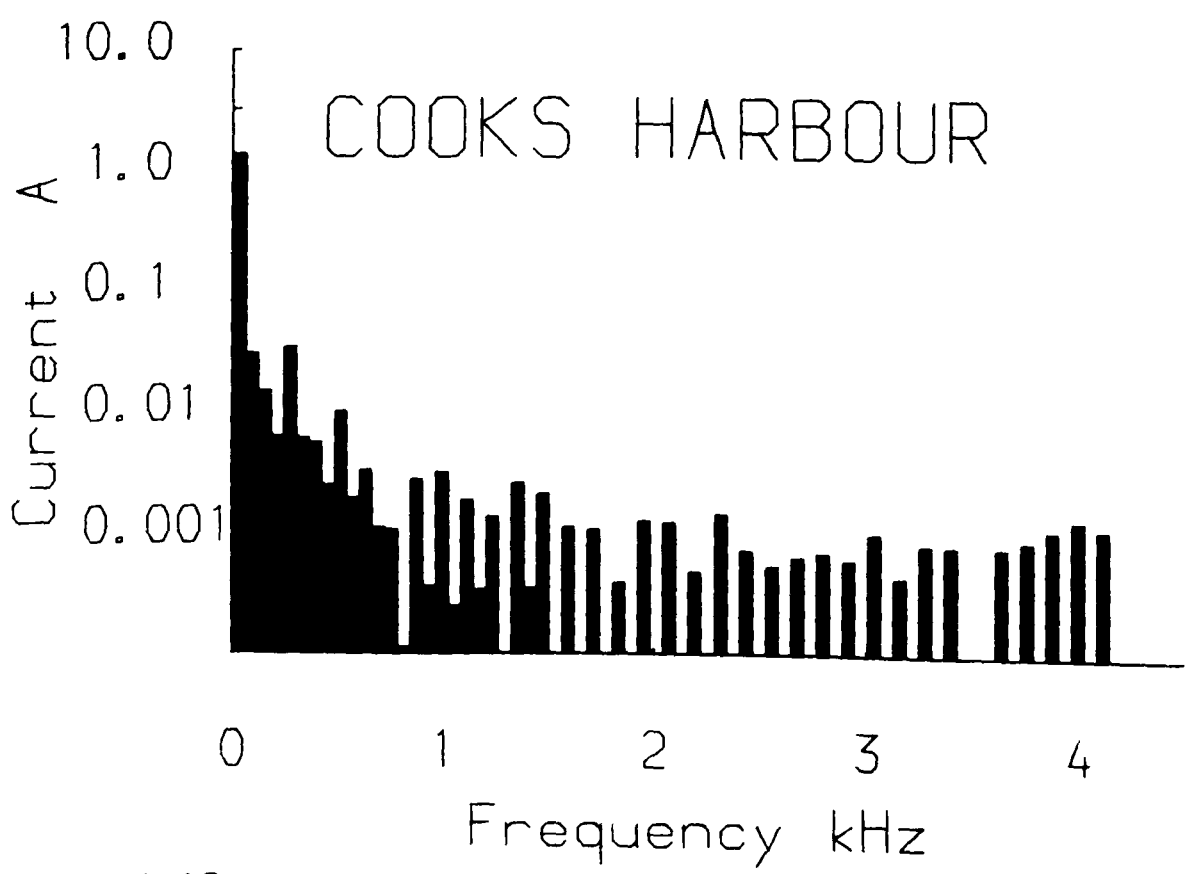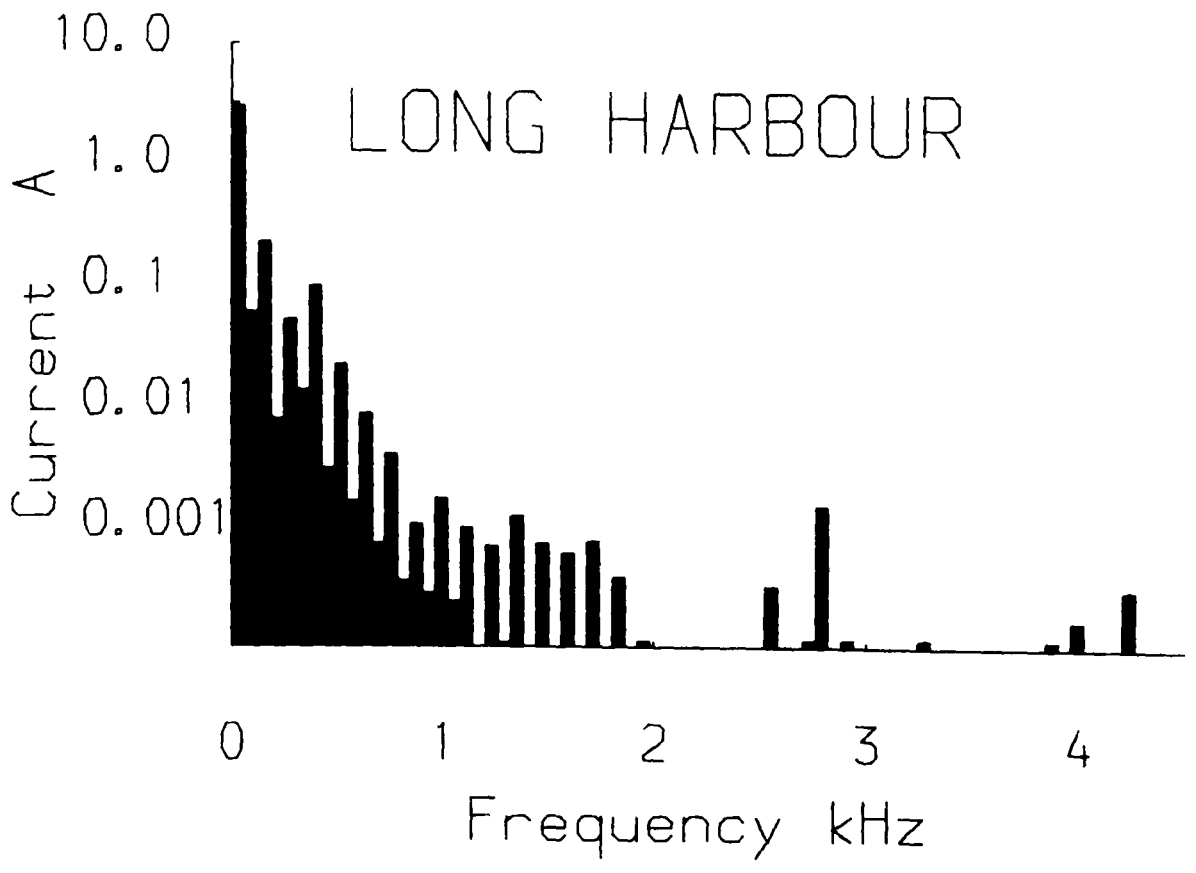
Figure 4.12 . Histograms of the unbalanced currents, at each harmonic, measured for the Long Harbour and Cooks Harbour power lines.
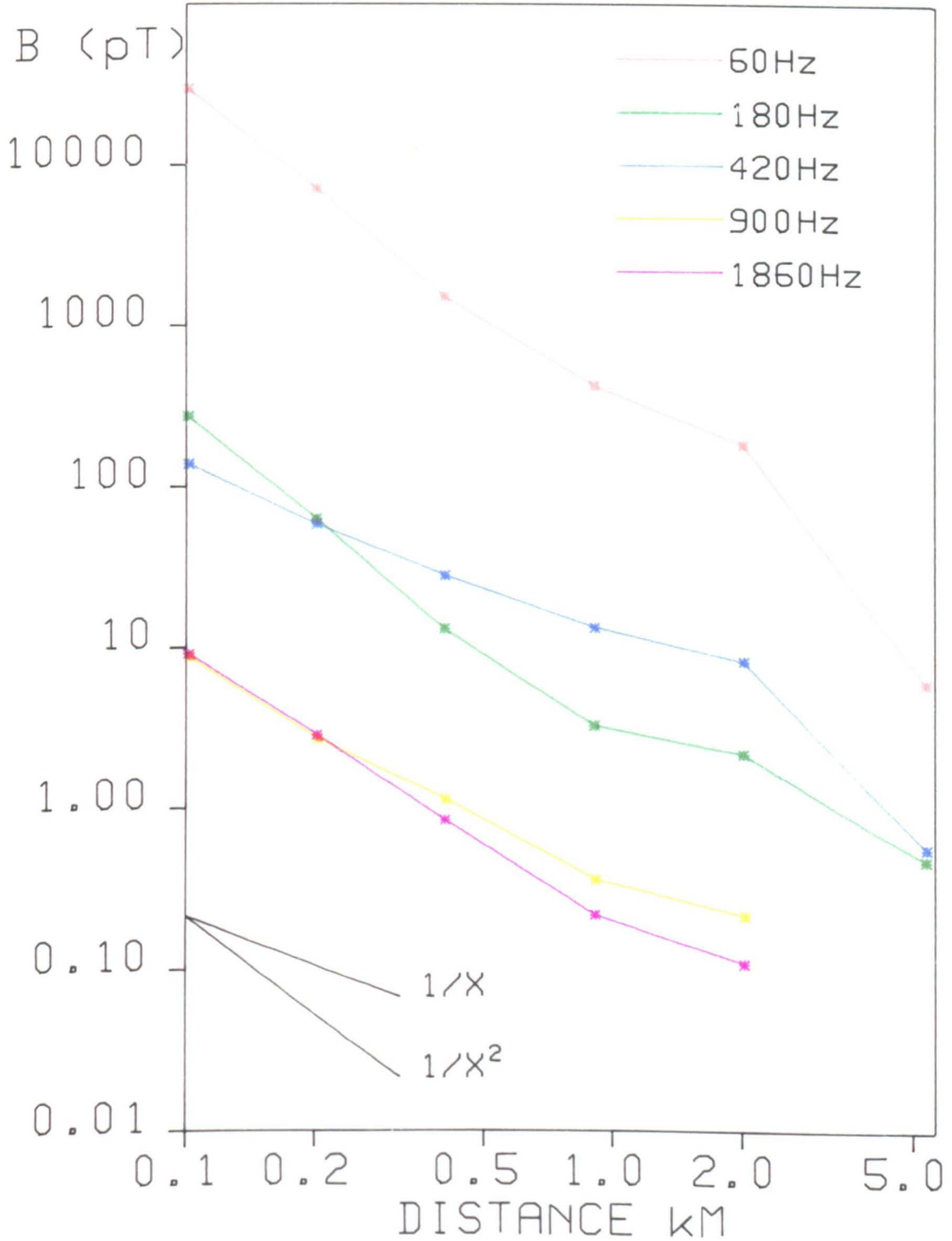
Fig. 4.13

Magnetic field magnitude as a function of distance
from the Buchans power line.

Fig. 4.14

Magnetic field magnitude as a function of distance
from the Baie Verte power line.
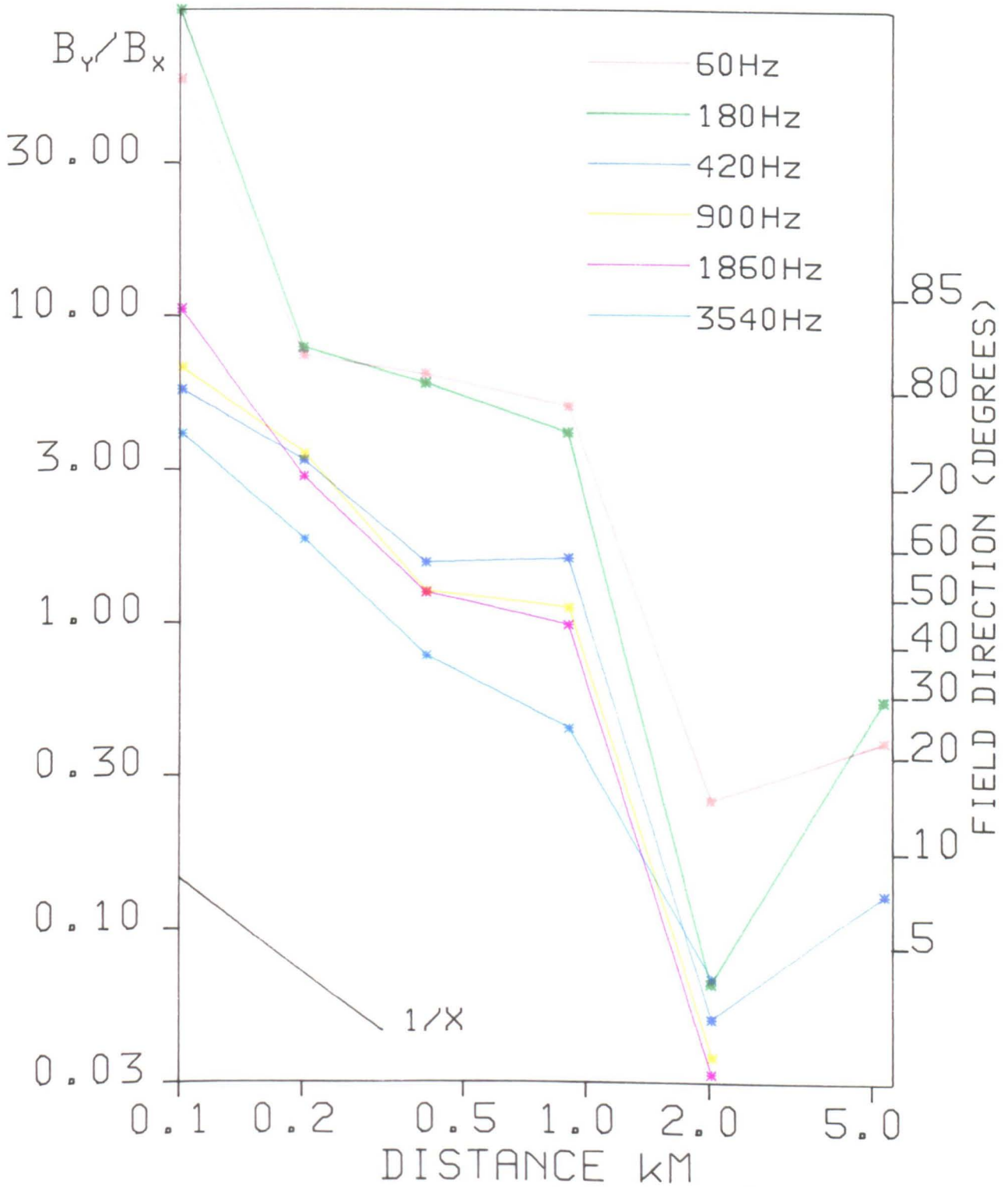
Fig. 4.15

Ratio of vertical to horizontal magnetic field as a
function of distance from the Buchans power line.

BAIE VERTE
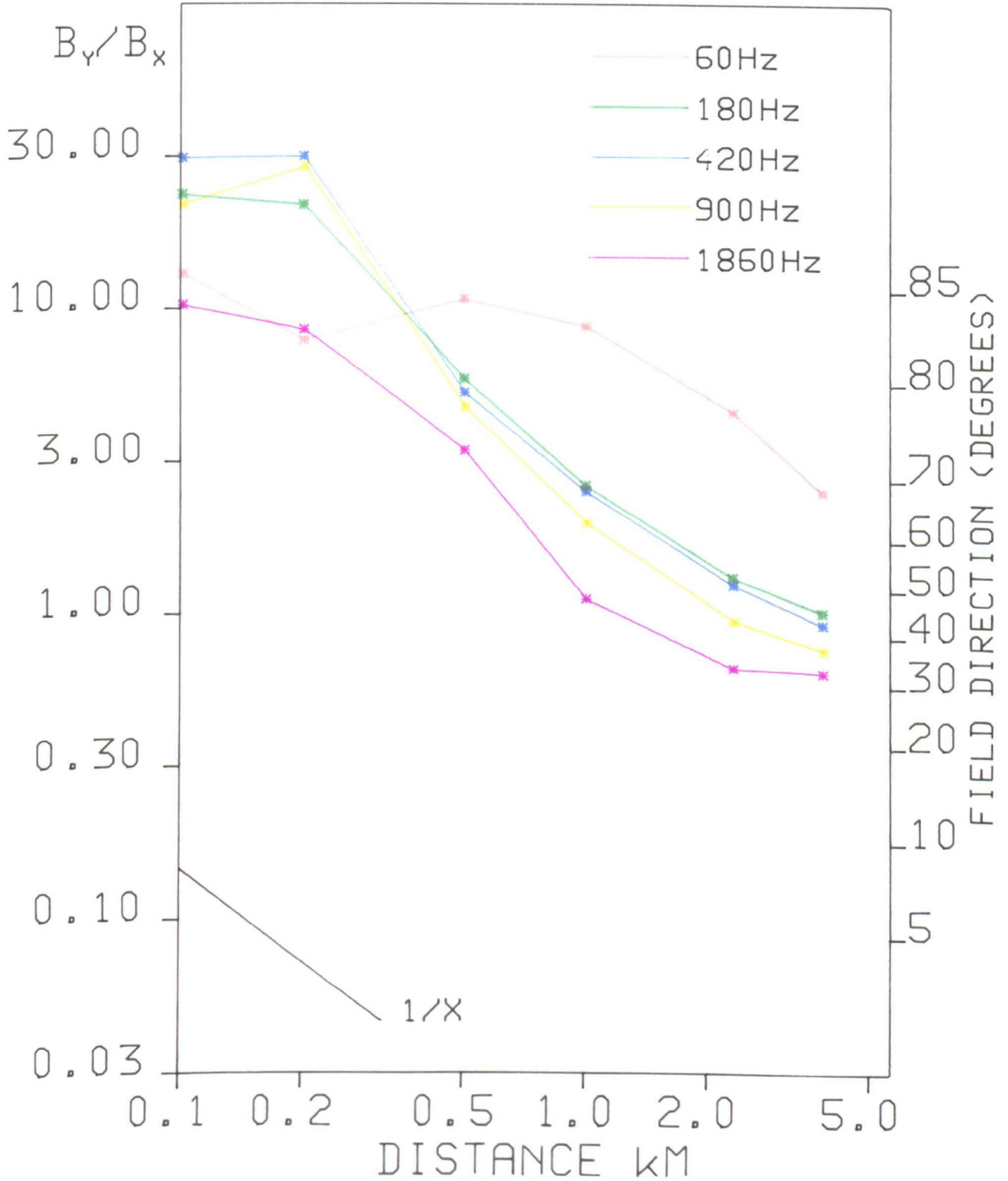
Fig. 4.16

Ratio of vertical to horizontal magnetic field as a
function of distance from the Baie Verte power line.

direction is not known since the phases of the field components were not measured.

It is apparent that there are some large deviations from the predicted variations, but most of these can be explained. Firstly, there is a large scatter in the field ratios measured close to the line, but, in fact, these correspond to changes in direction of only a few degrees. The reason for this is discussed in section 4.4 .

Secondly, the field ratio data for Buchans (figure 4.15) reach a minimum at 2 km and increase with further distance from the line. This can be explained by assuming that the ratio changes sign (only the magnitude of the ratio was measured) near x=2 km, which from section 4.2.5 means that the ground return current is biased towards the side of the line on which measurements were made. Since the line was fairly straight near the measurement sites the asymmetry is probably due to conductivity asymmetry in the ground.

The Baie Verte data, however, show a variation in field direction which indicates that the return current flows on the side opposite to the measurement sites.

4.5.3 Determination of Skin Depth and Conductivity

To calculate the skin depth both methods described in section 4.4 were tried. It was found that the results determined from the field magnitudes were far less consistent than the results from the field directions, and so the latter are presented in figures 4.17 and 4.18. The
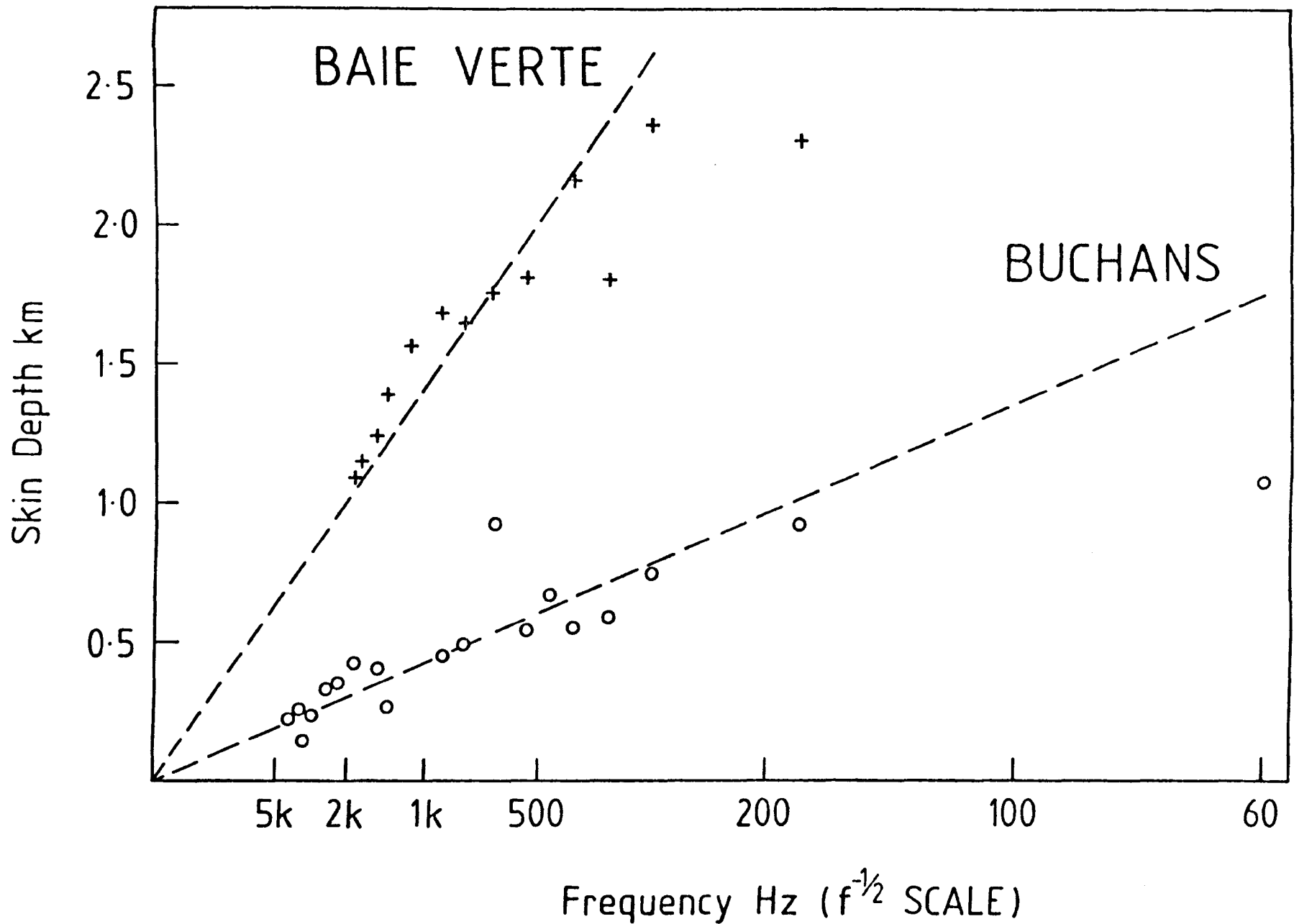
Figure 4.17 . Skin depth as a function of frequency for the Baie Verte and Buchans lines. Best fit straight lines through the points are shown dashed.
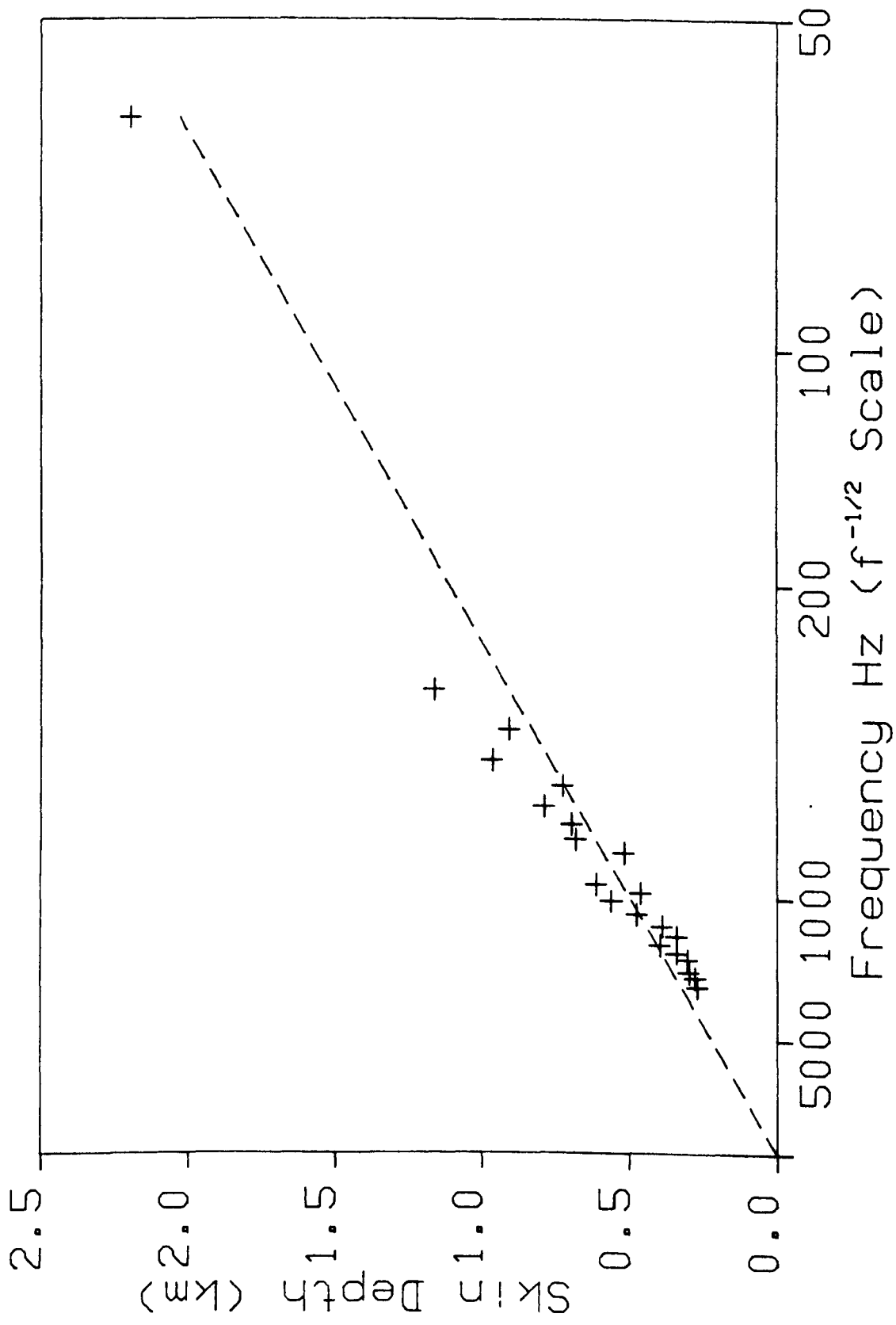
Figure 4.18 . Graph of skin depth against frequency for the Cooks Harbour power line.

reason for the poor quality of the results from field magnitudes is probably that the measurements at different distances were done at different times, between which the unbalanced currents flowing in the power line changed. Although an attempt was made to allow for changes when comparing field magnitudes, it turned out that the fixed station, used to monitor the unbalanced current was positioned rather too close to the line. Therefore the measurement was influenced by balanced currents which may not have the same time dependence as the unbalanced currents, and so the latter were not properly allowed for.

Each point on the graphs in figures 4.17 and 4.18 represents the frequency and skin depth of a particular harmonic. The frequency is plotted on an inverse square root scale so that the theoretical variation of skin depth with frequency for a constant conductivity ground is a straight line through the origin. It is observed that as well as some scatter due to random errors there are significant systematic departures from the best fit straight lines drawn through the points. This is to be expected since the conductivity of the rock will certainly vary with depth.

Average conductivities for the three sites determined from the slope of the best fit straight lines are given in the following table.

Buchans 1.4×10^{-3} S m^{-1}

Baie Verte 1.2×10^{-4} S m^{-1}

Cooks Harbour 1.0×10^{-3} S m^{-1}

These values are typical of those determined by geologists using audio-frequency magneto-tellurics (Koziar and Strangway 1978).

4.5.4 <u>Estimate of Radiated Power</u>

A rough estimate of the average radiation field at the ionosphere due to PLHR can be obtained by calculating the radiation field at 100 km altitude above one power line, since the spacing between large power lines in Newfoundland is of the order of 100 km. Tatnall (1978) gives an expression for the radiation field at 100 km altitude above a power line assuming it behaves as a magnetic dipole radiator and $l \ll \lambda$.

$$B_{100} = 55.8 \times \frac{Il\delta}{\lambda^2} \times 10^{-12} \qquad (4.5.1$$

The RMS currents and skin depths for the frequency range 2.7 to 3.7 kHz are as follows.

Power line	Current(mA)	Skin depth(m)
Buchans	3.2	240
Baie Verte	0.31	800
Cooks Harbour	3.0	278

The frequency range is chosen to be compatible with the Ariel 3 & 4 satellite VLF receivers and the observed frequency of MLR. We take an average value for the wavelength of $\lambda = 10^5$ m. The Buchans power line is 100 km

'ong between terminal stations; since this is comparable with the wavelength, the radiation from different parts of the line will not be in phase. Therefore we take an effective length of $l = \lambda/2 = 5 \times 10^4$ m. For the Baie Verte and Cooks Harbour lines lengths of 5×10^4 and 1.4×10^4 were used. The latter is the point to point distance between the generator and the end of the three phase portion of the line, in fact the line is curved.

The following values for the field at 100 km altitude were determined from equation 4.5.1 .

Buchans $\quad\quad$ 2.2×10^{-16} T

Baie Verte $\quad\quad$ 6.9×10^{-17} T

Cooks Harbour $\quad\quad$ 6.6×10^{-17} T

To estimate the radiated power the standard formula for magnetic dipole radiation is used, where the various symbols have their usual meanings.

$$W = \frac{c \mu_o M_o^2}{12 \pi \lambda^4} \tag{4.5.2}$$

Substituting $M_o = 2 I l \delta$ and evaluating the constants gives the equation below where W is the power radiated into the upper hemisphere and I is the RMS current.

$$W = 3.2 \times 10^4 \, \frac{I^2 l^2 \delta^2}{\lambda^4} \tag{4.5.3}$$

Using the values obtained for I,l and δ for the three lines we get the following powers for a 1 kHz bandwidth centered on 3.2 kHz

Buchans   470 nW

Baie Verte   49 nW

Cooks Harbour   45 nW

The typical powers per individual harmonic are about one tenth of those given above.

4.6 Discussion

The level of PLHR input to the magnetosphere required to trigger observable effects, will depend on the energetic particle population which interact with the waves. A typical estimate of the power required can be obtained by looking at the results of active experiments in which VLF transmitters have been used to stimulate a magnetospheric response. Park and Chang (1978) used an estimated radiated power of 0.5 W for one harmonic to obtain a magnetospheric response when radiating simulated PLHR from the Siple transmitter. Helliwell et al. (1980), again using the Siple transmitter, quote a threshold of 1 W radiated power for wave growth and triggering.

The estimates of radiated power from the three lines studied in Newfoundland, are less than 1 microwatt, so it is unlikely that these sources cause a significant magnetospheric effect. However, it is possible that much larger powers are radiated from power lines further west. Helliwell et al. (1975) quote a harmonic amplitude at 1500 Hz of 0.22% of the fundamental amplitude for a power line supplying an aluminium smelting plant at Arvida near Roberval, Quebec. Typical harmonic amplitudes for the Newfoundland lines were 5×10^{-5} of the fundamental. The high harmonic content near Roberval is most likely due to the rectifiers used to produce the direct current required for the electrolytic reduction of the aluminium ore. The phosphorous plant at Long Harbour uses AC electric arcs which generate a fairly low harmonic content according to

the measurements made there (section 4.3.2 and figure 4.12).

During magnetospheric disturbances, harmonic currents, and hence radiated power may be considerably increased due to geomagnetically induced currents causing saturation of transformers (Albertson et al. 1973). However, magnetic conditions were fairly disturbed (Kp=4-5) during the measurements in Newfoundland whereas MLR events, which may be related to PLHR, tend to occur in quiet to moderate conditions. Therefore the PLHR input to the magnetosphere during MLR events is unlikely to be higher than normal.

It had previously been thought that only power lines without earth wires made a major contribution to PLHR, since if the line had an earth wire the unbalanced current would return through the wire rather than through the ground, resulting in a current loop of much smaller area. However, it is shown in section 4.2.2 that about 50% of the unbalanced current will still return through the ground even if the line has an earth wire. This means that low voltage distribution lines may be significant PLHR sources, since they carry a considerable unbalanced current (due to the single phase loads which are connected to them), a large proportion of which will return through the ground. The results from the Cooks Harbour line showed quite large unbalanced currents (only the proportion of the current returning through the ground is measured). The low voltage lines are rather shorter than the high voltage ones which results in a lower radiated power per line but they are more numerous.

Apart from the possibility of much stronger harmonics than those in Newfoundland, the greater density of power lines in the more populated parts of eastern Canada and USA, will result in a greater radiated power per unit area. This is consistent with the results of Bullough and Kaiser (1979) from Ariel 4 measurements in which they find a permanent emission zone at 3.2 kHz over NE USA, but not over Newfoundland. The Ariel 4 receiver sensitivity was 4.8×10^{-16} $Wm^{-2}Hz^{-1}$, which for the 1 kHz bandwidth used corresponds to a free space equivalent field strength of 3×10^{-2} pT. This may be compared to the PLHR field strengths estimated for 100 km altitude if it is assumed that the energy propagates vertically upward without attenuation to the satellite height of 550 km. The largest field strength $(2.2 \times 10^{-4}$ pT) estimated (for 100 km over the Buchans power line) is 40 dB below the Ariel 4 receiver sensitivity.

To obtain a direct estimate of the strength of PLHR in eastern Canada and NE USA a series of further measurement on individual lines should be made. For measurements made in Newfoundland the most useful results were obtained from the magnetic field measurements made at the mobile station. In a future expedition, much time could be saved if the magnetic fields only were measured using only one station; this would then allow measurements to be made on a greater number of lines. However, for easy interpretation of results, the method is restricted to isolated lines. A useful development would be a theory for interpreting measurements made on non-isolated lines.

Finally it is worth while to compare the method described here for determining the conductivity of the ground with the audio frequency magnetotelluric method used by geophysicists. This method was first described by Cagniard (1953), and two examples of its use are Koziar and Strangway (1978) and Hutton et al. (1980). The method consists of the measurement of the ratio of the horizontal electric field to the perpendicular horizontal magnetic field (at the surface of the ground) as a function of frequency. The energy source normally used is the sferic background in the earth-ionosphere wave guide. The ratio of the electric to magnetic field is used to calculate the apparent resistivity as a function of frequency, and then a model of ground conductivity is constructed that is compatible with the apparent resistivity measurements. A disadvantage of the magnetotelluric method is that the electric field measurements are subject to some scatter due to surface ground conductivity irregularities. By measuring magnetic fields only this problem is removed and so the method described here could provide better results than the magnetotelluric method if the errors in measurement of field magnitudes and directions could be reduced. The error would be reduced by measuring the amplitudes of the field components on site (by an on site micro-computer) rather than from a tape recording thus eliminating the distortions of the measured field components caused by the tape recorder.

Chapter 5   Magnetospheric VLF Line Radiation

5.1 Description of events

5.1.1 General characteristics of MLR events

Magnetospheric VLF line radiation is a fairly rare occurrence at Halley longitudes. As stated in chapter 1 the events are broad band VLF emissions exhibiting line structure in their spectra. An emission is only classed as an MLR event if at least two lines are present which are clearly of magnetospheric origin (Matthews 1980, Matthews and Yearby 1981). Magnetospheric lines always have a bandwidth of about 30 Hz or greater, which clearly distinguishes them from induction lines from local power systems which have extremely narrow bandwidths, much less than the resolution of the spectrum analysers used (10 Hz for the Unigon 4512 on the 5 kHz range). Also most line events exhibit echoing or triggering behaviour.

In order to observe the line structure in an MLR event it is necessary to average the spectra calculated from several adjacent time samples. This may be done by photographic means as in a compressed time scale spectrogram (see section 3.2 for more details) such as figure 5.1 which shows the 27 June 1980 MLR event, or by electronic means, as in figure 5.2, which shows three spectra each averaged over successive one second intervals from the same event. In this case a microprocessor was used to average the digital output of a real time spectrum analyser.

98
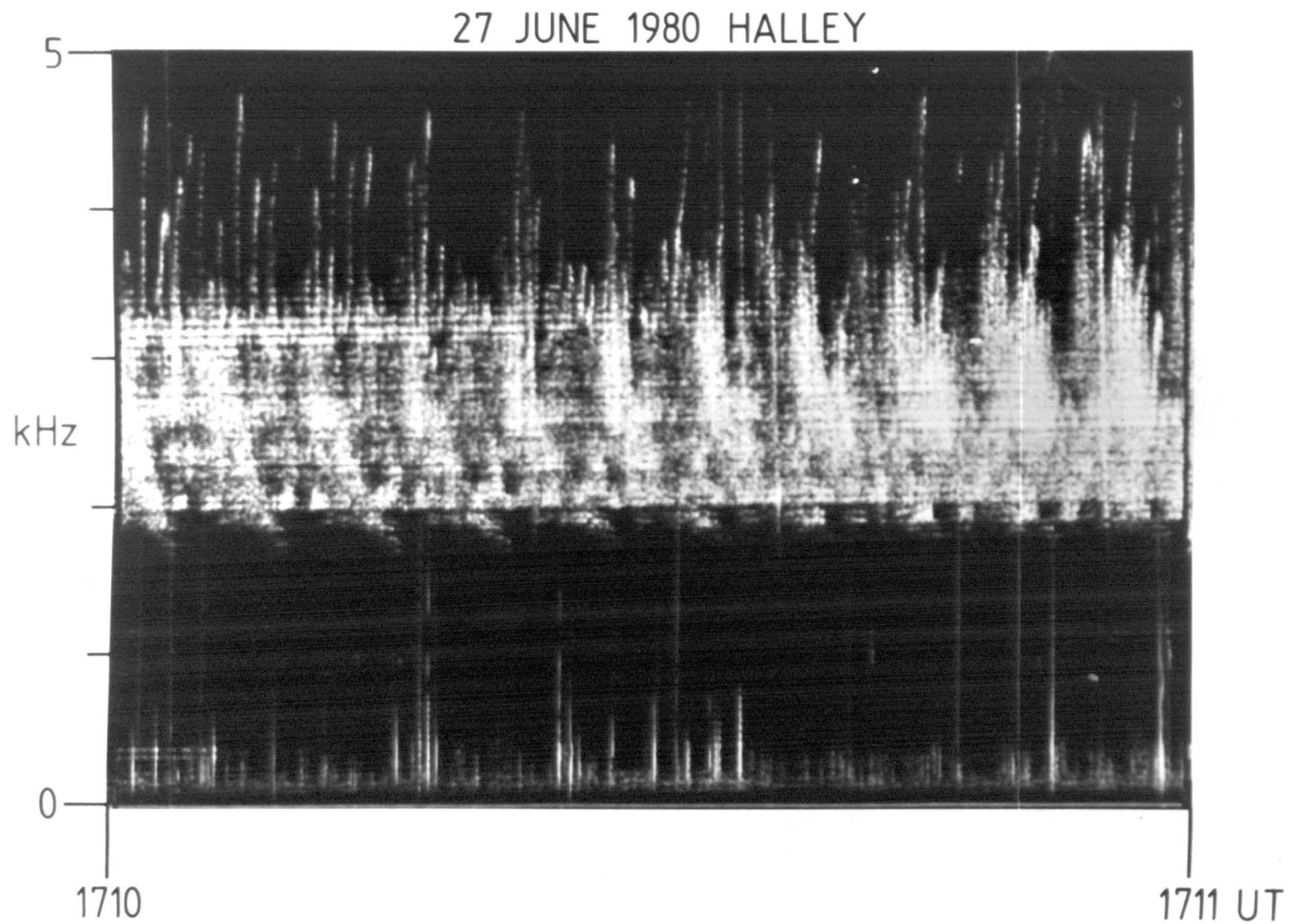
Figure 5.1 . A spectrogram of an MLR event received at Halley
on 27 June 1980 .

HALLEY 27 JUNE 1980

1710:03 UT

1710:04 UT

1710:05 UT
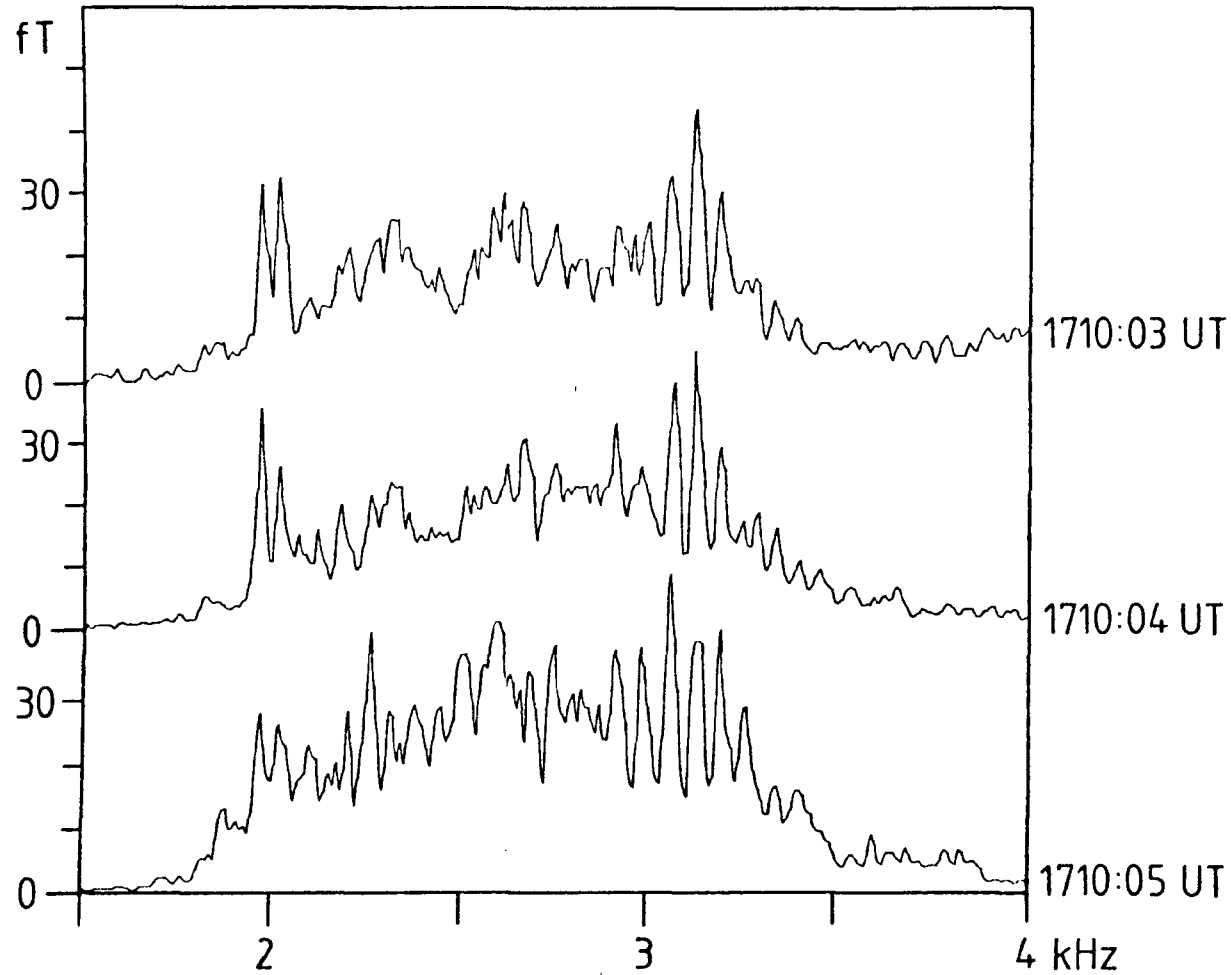
Figure 5.2 . Amplitude (in a 10 Hz bandwidth) against frequency spectra averaged over three successive one second intervals from the 27 June 1980 MLR event.

Within the basic criterion defining an event there is a considerable variation in the characteristics of the MLR events seen at Halley. For example, on the 24th of June 1977 there was a period of VLF activity lasting several hours during which several periods of line structured emissions were received. A spectrogram taken from one of these periods is shown in figure 5.3 . Associated with the line structure are many triggered emissions.

By contrast the event received at Halley and Newfoundland on the 27th of June 1980 (figure 5.1) appears to be a hiss band that has pronounced line structuring at the beginning of the event (1710 - 1711 UT) which gradually dies out as time progresses.

Another hiss like event was received at Halley on 12 July 1977 . Figure 5.4 shows this event which at the time shown consists of two separate bands of hiss each with line structure.

On the 15th of July 1977 the MLR event shown in figure 5.5 was received at Halley. The part of the event before 1655 was not recorded because the recording was made in the one minute in five mode. This is a fairly weak structured hiss event which fades out after 1655.20 to be replaced by some triggered emissions.

Underlying the variability of MLR events are some common characteristics. These were mentioned by Matthews and Yearby (1981) and were present in all the events presented in that paper (all from 1977 Halley data) and also in most of the events presented here. Principally, the frequency of
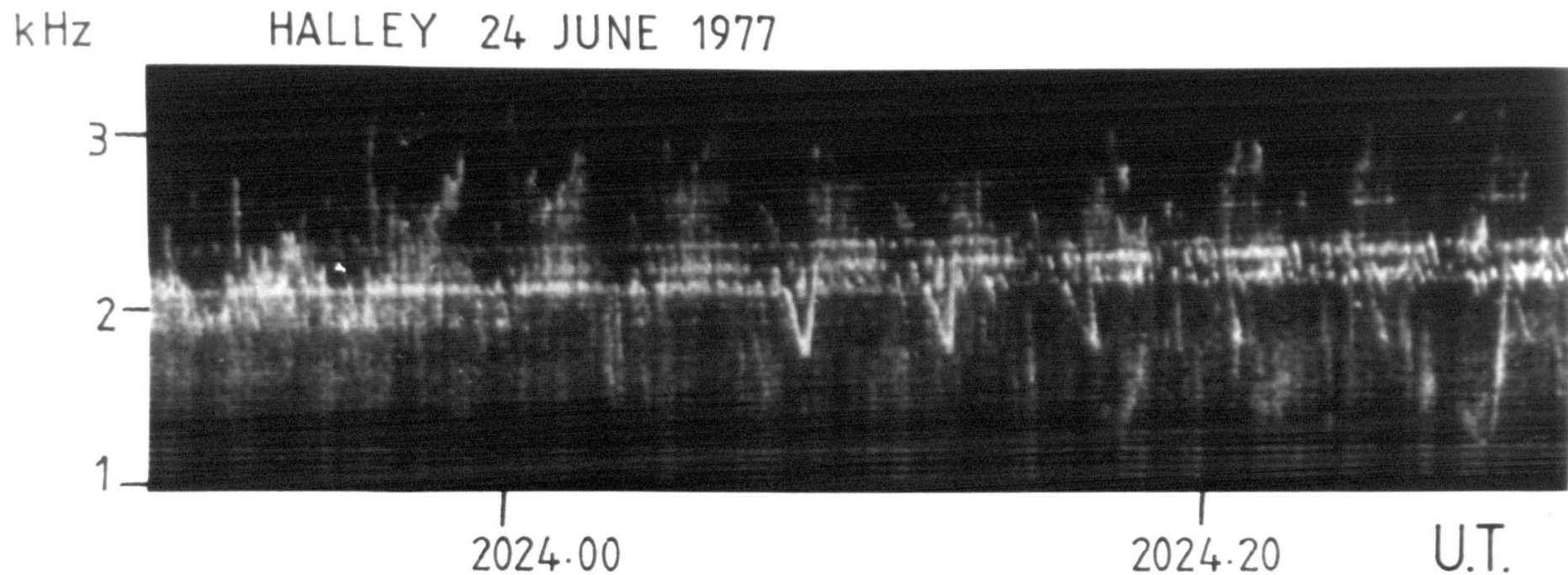
Figure 5.3 . A spectrogram of an MLR event received at Halley
on 24 June 1977 .
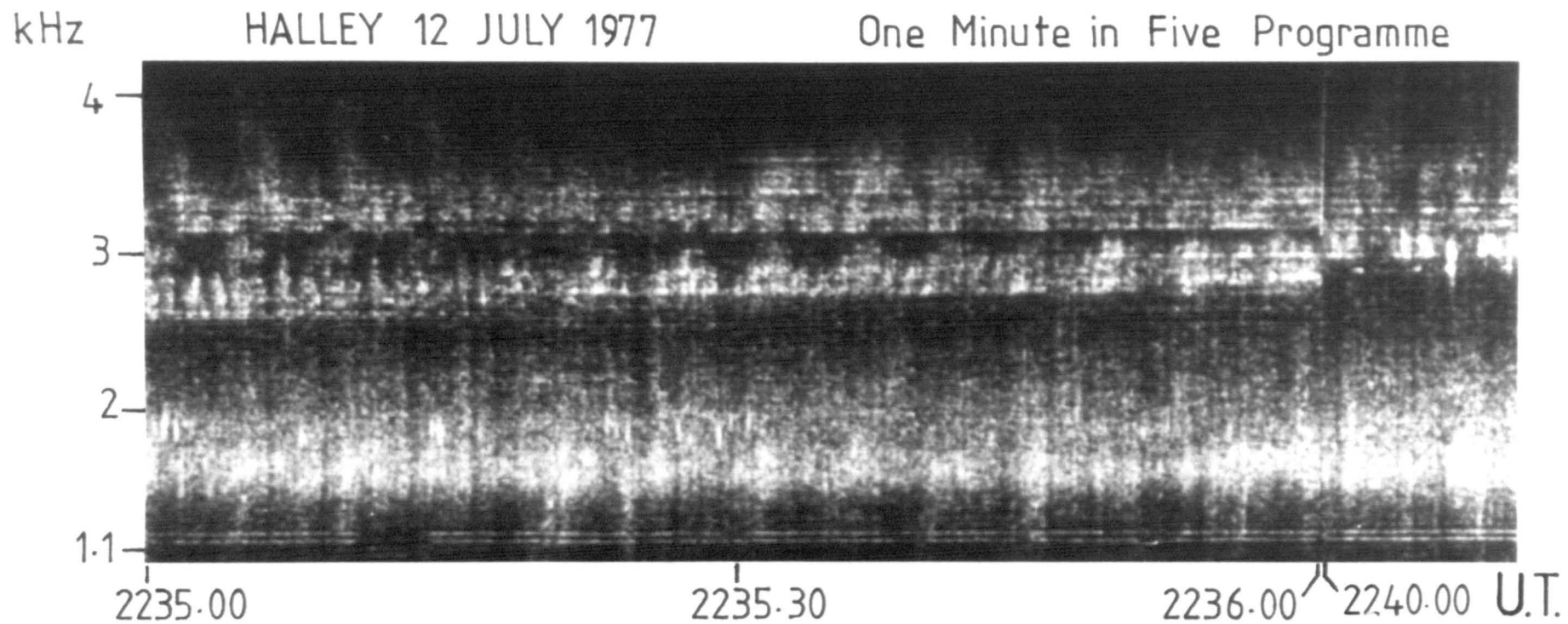
Figure 5.4 . A spectrogram of an MLR event received at Halley
on 12 July 1977 .
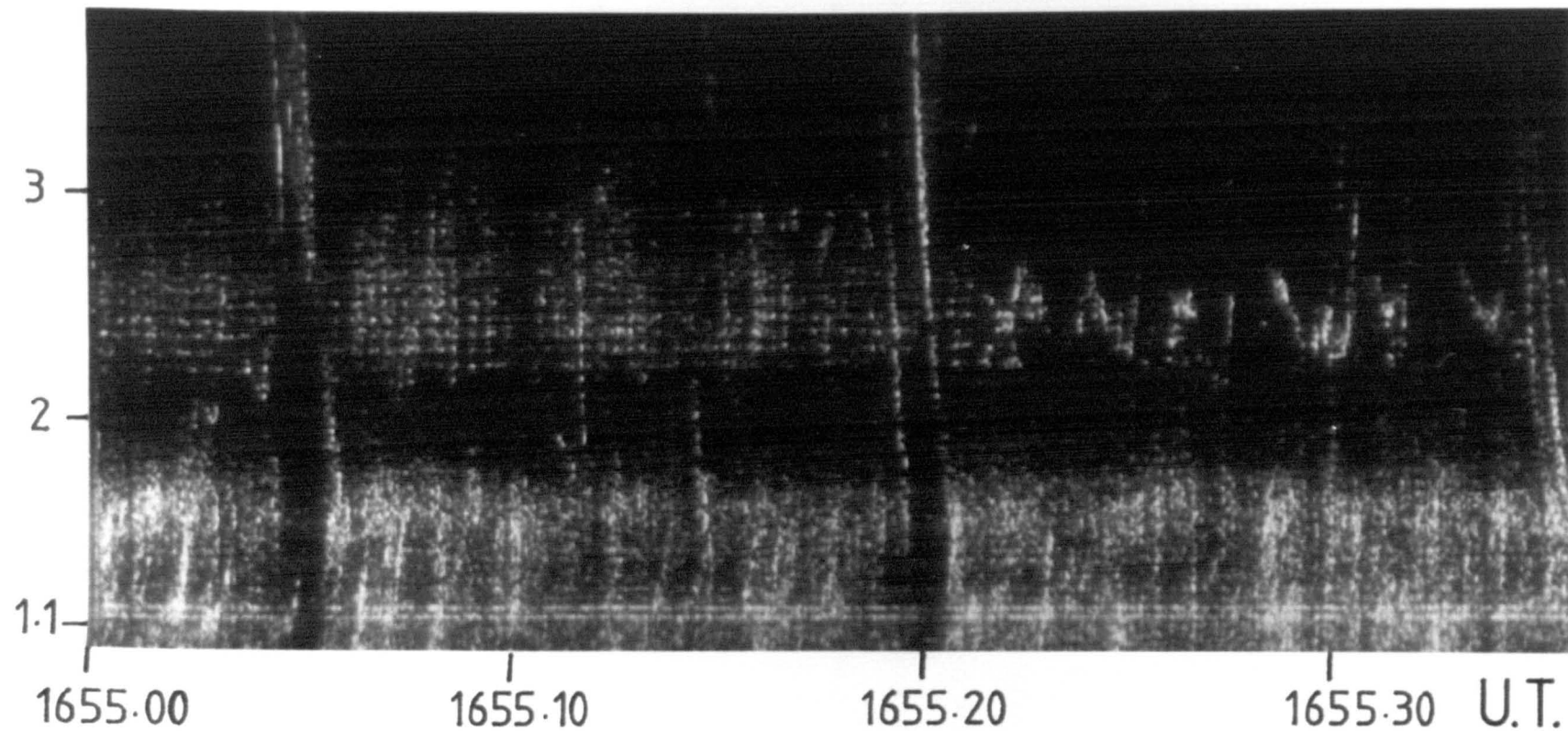
Figure 5.5 . A spectrogram of an MLR event received at Halley on 15 July 1977. After 1655.25 the event fades out to be replaced by some triggered emissions.

the lines is very stable, compared with most natural VLF emissions. Line frequency drifts up to a maximum of 120 Hz per minute have been observed, almost always upwards. This is in sharp contrast to VLF emissions such as chorus elements which have drifts of the order of 1 kHz per second. A summary of the line drifts observed is shown in figure 5.6 (from A.J.Smith private communication) . Frequency drifts are measured from averaged spectra such as those shown in figure 5.2 using two computer programs. In the first, the peak finding program described in section 3.2 is used to measure the frequency of all significant peaks in the spectra and then the second program traces the lines from one spectrum to the next and calculates the average drift. It is evident from the figure that negative drifts are quite rare.

The spacing in frequency between the lines in an array varies between 50 Hz and 150 Hz with a typical value of about 80 Hz. The similarity of this spacing to the 60 or 120 Hz spacing between the harmonics of a 60 Hz power system is one reason for considering power line harmonic radiation (PLHR) as a possible origin of MLR.

The dependence on local time and magnetic activity of the MLR events so far identified on Halley records, are shown in the histograms of figures 5.7a and 5.7b . In figure 5.7b the values of Kp at the time of the event and the maximum value during the previous 24 hours are shown. Figure 5.7b shows that MLR events tend to occur during quiet to moderate magnetic conditions following a more active period.
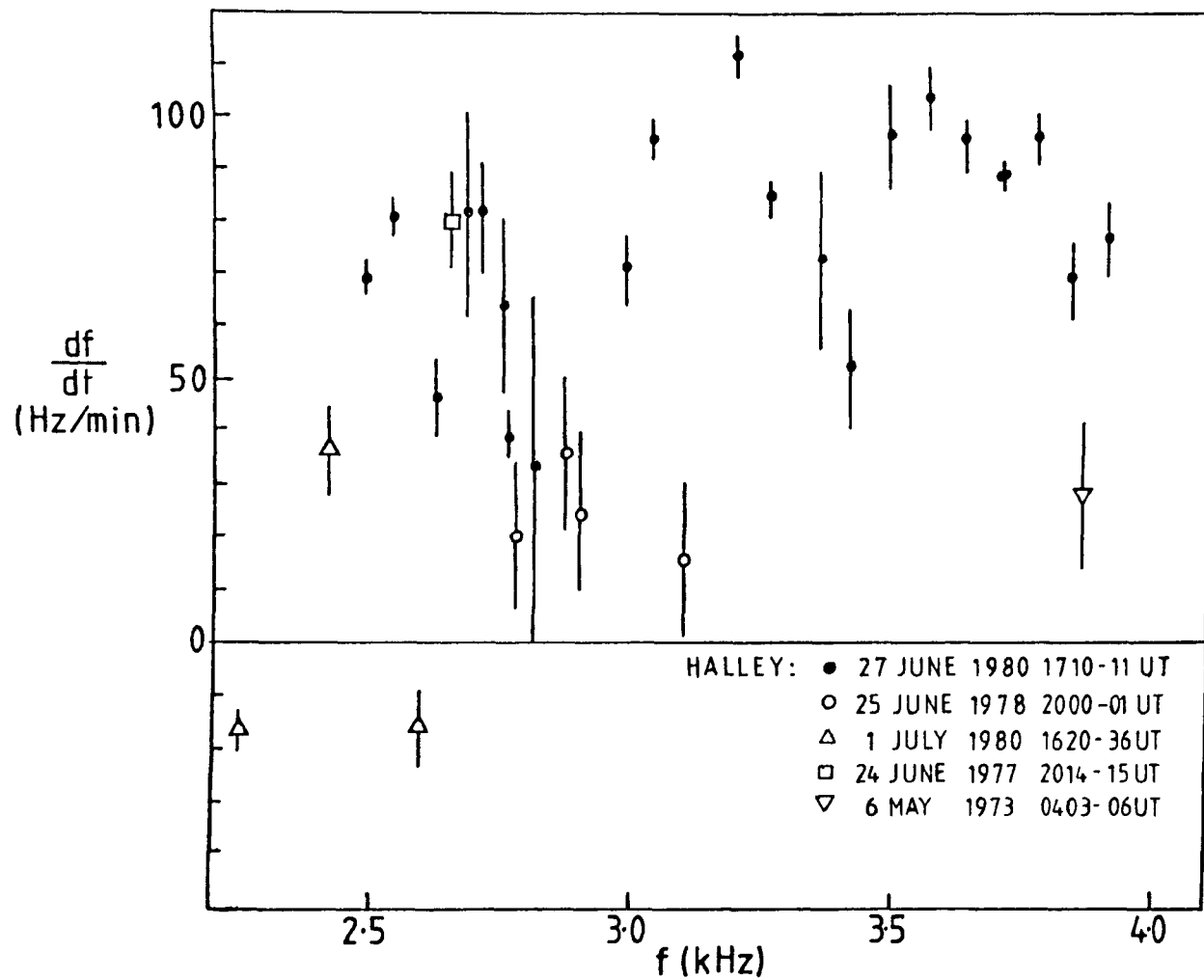
Figure 5.6 . Line frequency drifts observed for five Halley MLR events shown plotted against the frequency of the lines (A.J. Smith private communication).
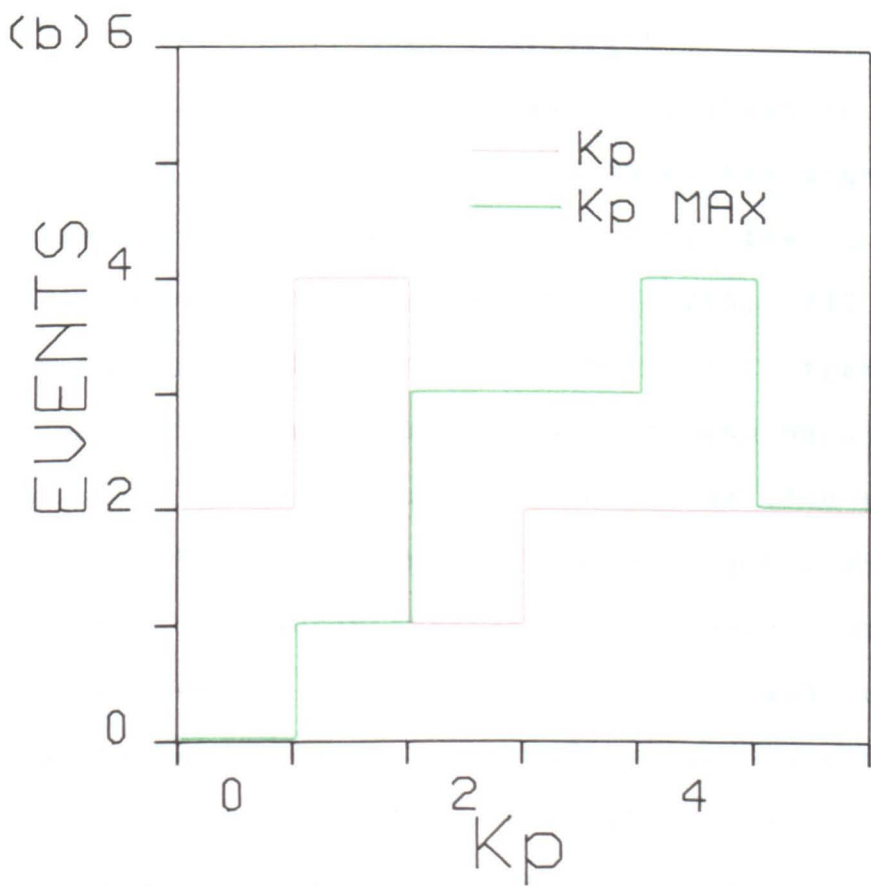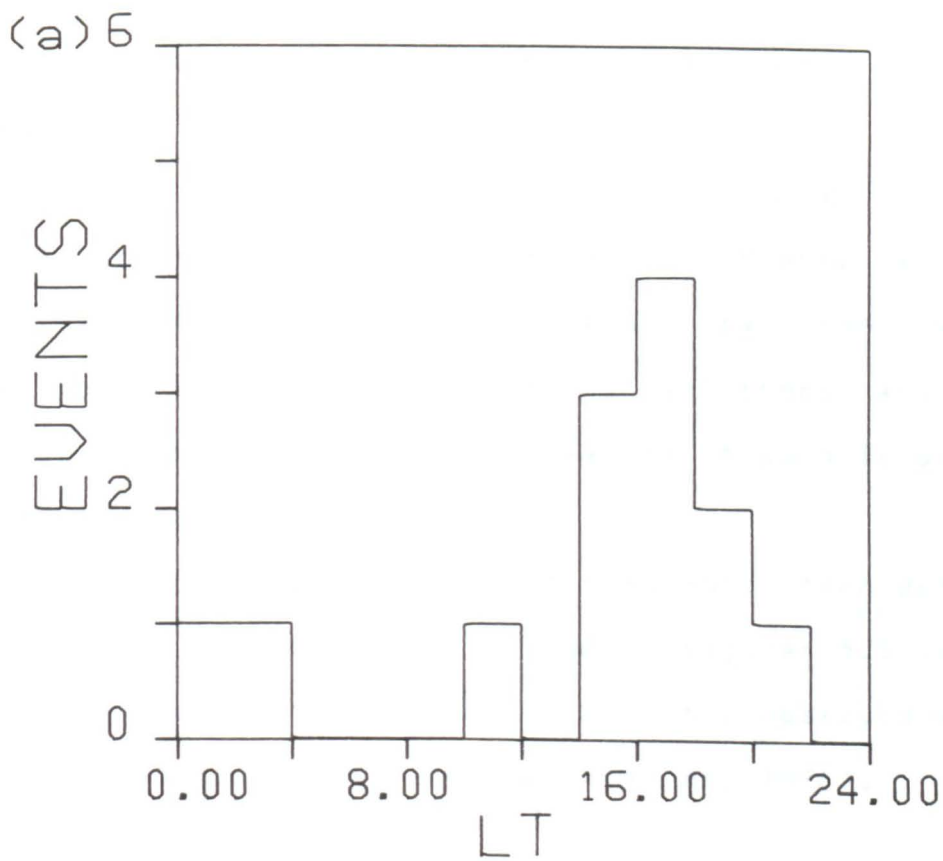
Figure 5.7 . Histograms showing the number of
Halley MLR events that have occurred in each
two hour segment of local time (a) and in each
interval of Kp (b). Kp MAX refers to the
maximum value of Kp in the 24 hours preceding
the event.

A list of MLR events identified on Halley recordings is given in table 5.1 .

All MLR events so far observed at Halley have occurred at times of good echoing conditions. The lines themselves frequently show visible two hop amplitude modulation, and multi-hop echoing whistlers are often observed at the same time as MLR events. A good illustration of this is figure 5.8 .

Triggering behaviour is frequently seen during MLR events; some examples are shown in figures 5.3 and 5.5 . Triggering and echoing are also frequently observed with MLR events received at Siple (Helliwell et al. 1975).

5.1.2 The 27 June 1980 event

The 27 June 1980 MLR event is shown in figures 5.1 and 5.8 . The former is a spectrogram of the signal received at Halley between 1710 and 1711 UT, while the latter shows the one minute periods commencing at 1705, 1710 and 1715 UT at both Halley and St. Anthony. The first frame shows a multi-hop echoing whistler train, and echoing behaviour can also be seen in the subsequent frames. The line structure is clearly visible in the centre frame and just visible in the last frame. An auto-correlation technique was used to measure the degree of line structuring and the average spacing between lines. Firstly 60 averaged spectra like the three shown in figure 5.2 were calculated for each one minute segment of the event. The auto correlation functions of the spectra were calculated and summed over each one

HALLEY MLR EVENTS

TABLE 5.1

DATE	TIME	K_p	K_p (max)	f_{LOW}	f_{HIGH}
	UT			±200 Hz	±200 Hz
6 MAY 73	0400	1	2+	2800	3800
24 JUNE 77	2014	2	3-	1900	2800
12 JULY 77	1820	0+	2+	2800	3500
12 JULY 77	2235	1+	2+	2600	3600
15 JULY 77	1655	3-	3	2200	2900
21 JUNE 78	1810	5	5+	1100	2200
25 JUNE 78	2000	4+	4+	1600	2500
26 JUNE 78	0310	5+	5+	2100	2700
6 JULY 78	1655	4-	4-	1800	2200
7 JULY 78	1232	3+	4-	1100	3300
27 JUNE 80	1710	0+	4+	1800	3500
28 JUNE 80	1800	1	1+	1500	3300
1 JULY 80	1835	1	3-	1800	2700
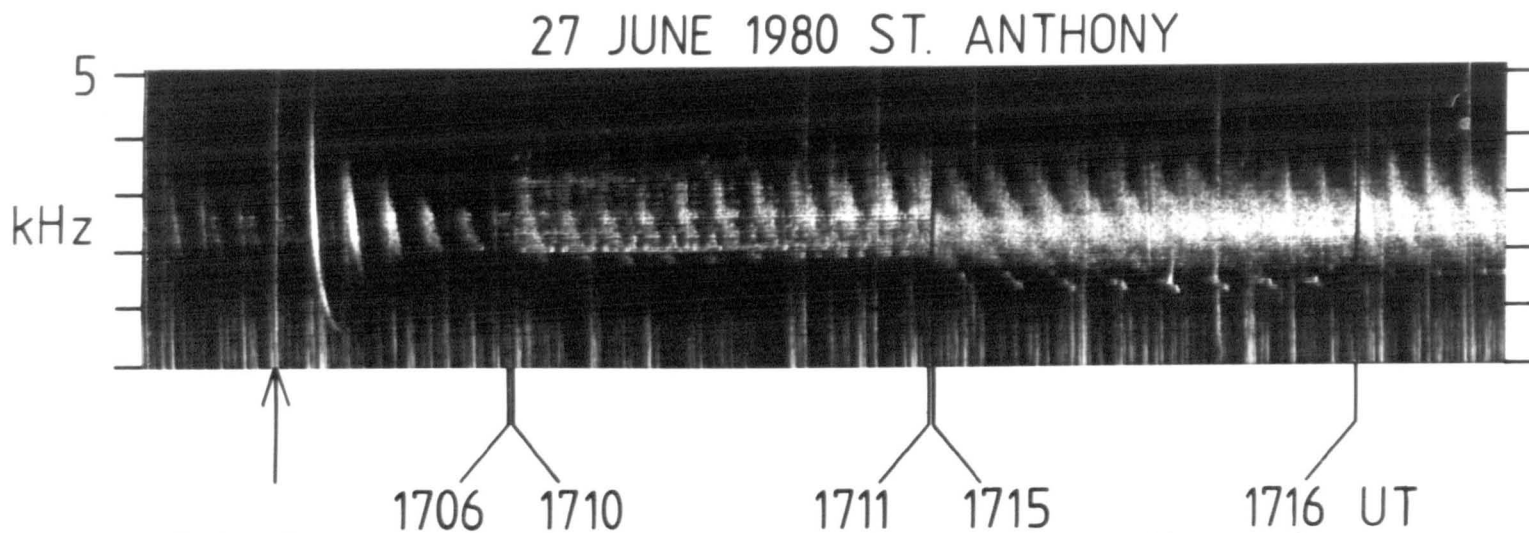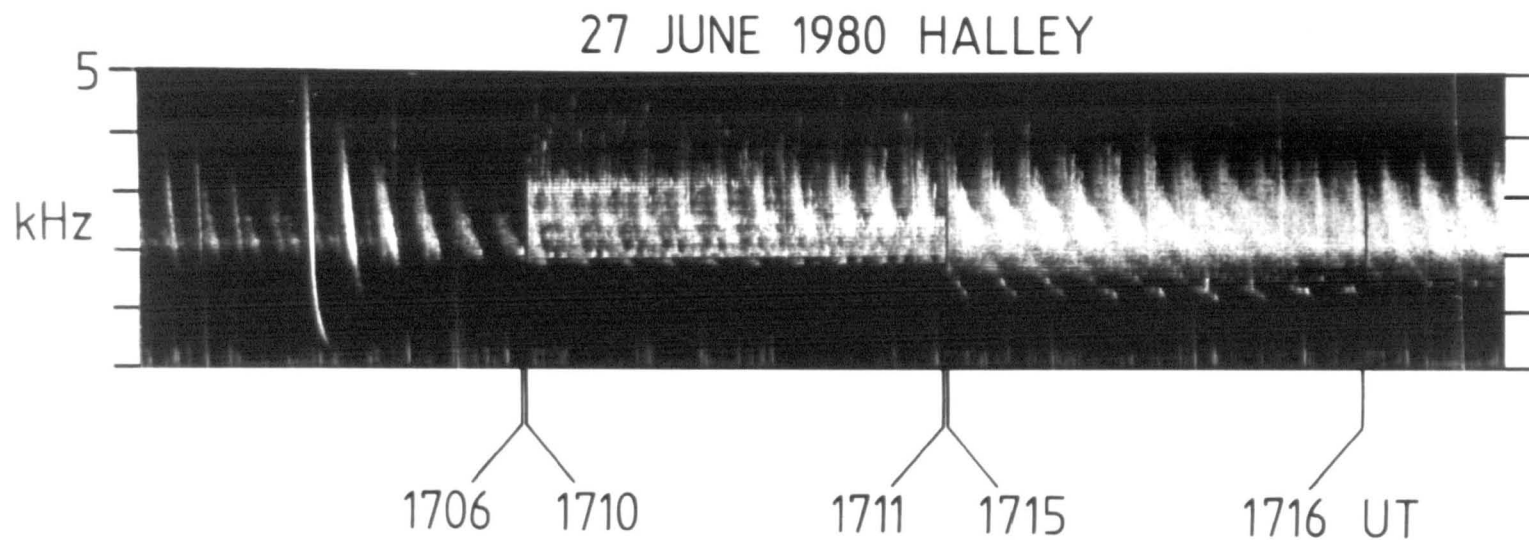
Figure 5.8 . Spectrograms showing an MLR event received simultaneously at Halley and St. Anthony (Newfoundland).The arrow on the lower frame marks the causative sferic of the multi-hop echoing whistler.

minute interval. The results are shown for four periods within this event in figure 5.9 . The position of the second peak in the correlation function indicates the average frequency spacing, while the vertical separation between the peaks and adjacent troughs indicates the degree of line structuring. Figure 5.10 (from A.J.Smith private communication) shows auto-correlation and cross-correlations of the time variation of the amplitude of the 2560 Hz line in the 27 June 1980 MLR event observed at Halley and at St. Anthony and Deer Lake in Newfoundland. The auto-correlations for the three stations show that strong amplitude modulation with a period of about 5.5 seconds is present in each case, confirming the visual impression from figure 5.8 . The Halley/St. Anthony cross-correlation shows that the amplitude modulation is out of phase in the two hemispheres thus verifying that the modulation is the result of two hop whistler mode echoing. A St. Anthony/Deer Lake cross-correlation is also shown which confirms that the amplitude modulation is in phase at the two Newfoundland stations.

It is useful to determine the L value and equatorial electron density (n_{eq}) of the path on which an MLR event occurs, since these may be used to estimate the energy of the resonant electrons. The values of L and n_{eq} were estimated in two ways. Firstly if the event showed definite two hop amplitude modulation over a range of frequencies it was possible to measure the two hop echo period as a function of frequency. By halving the two hop

HALLEY 27 JUNE 1980
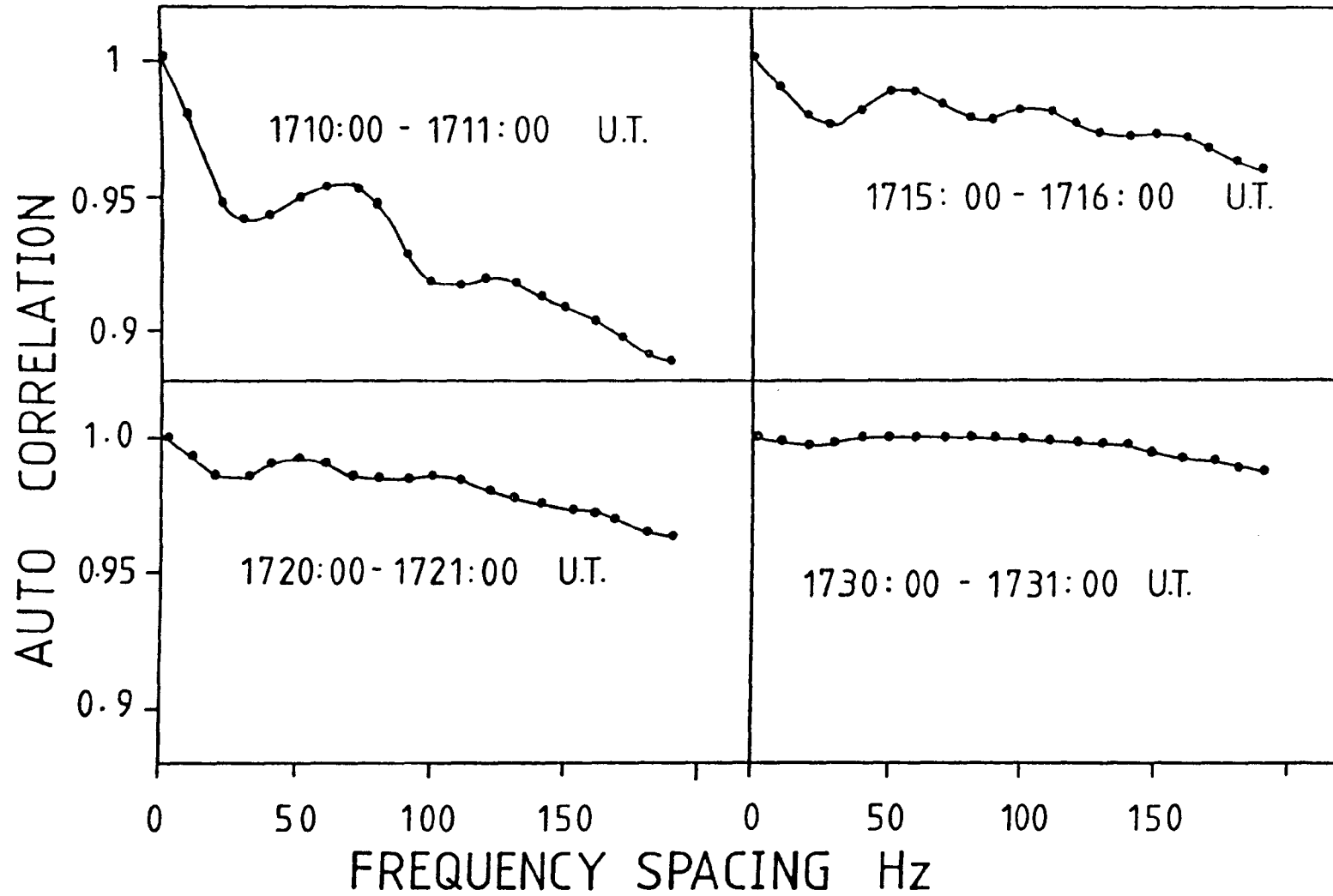
Figure 5.9 . Normalised auto-correlations of the amplitude-frequency spectra of four one minute periods from the 27 June 1980 MLR event.
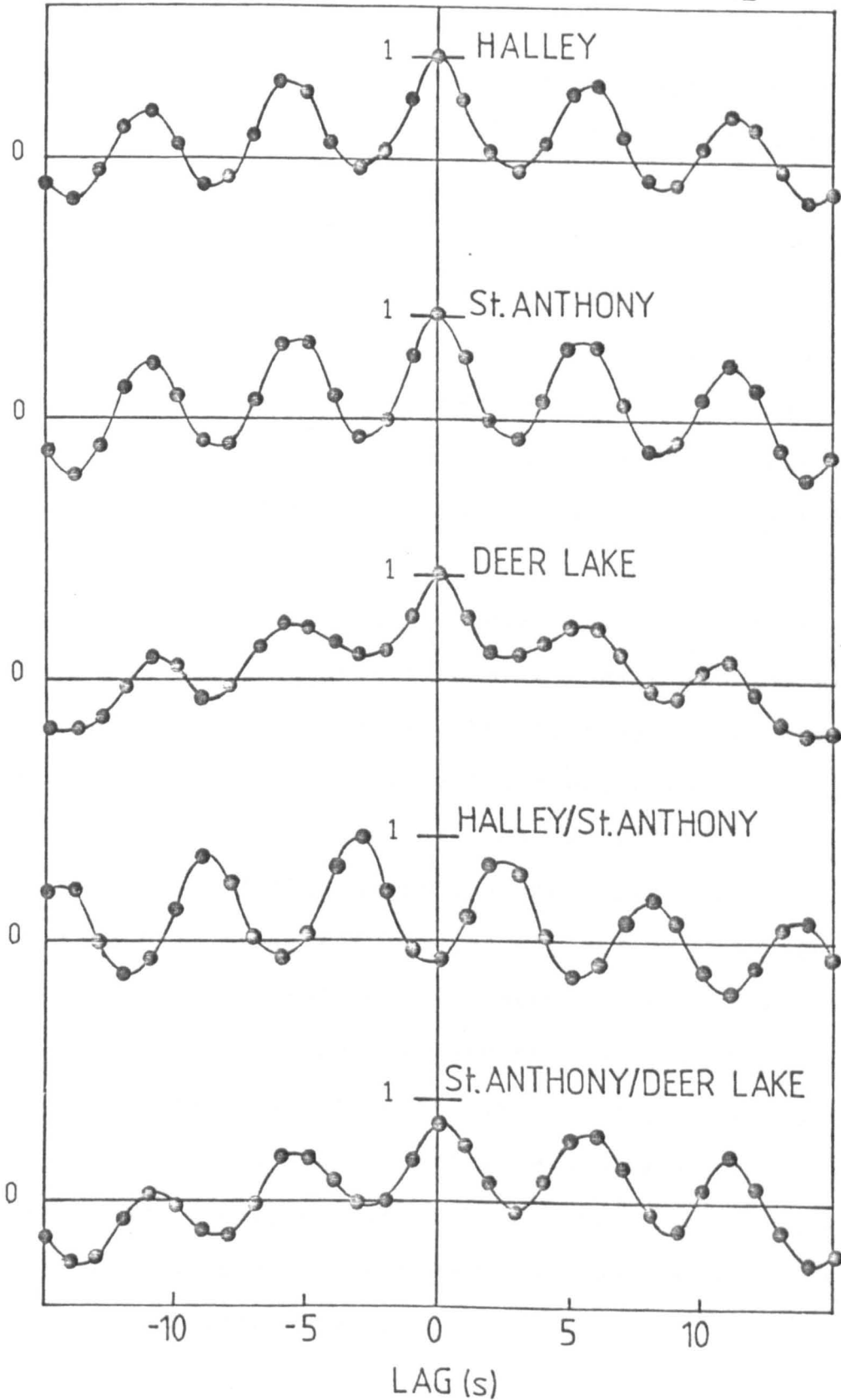
Figure 5.10 . Normalised auto-correlations (Halley, St. Anthony, Deer Lake) and cross-correlations (Halley/St. Anthony, St. Anthony/Deer Lake) of the time variation of the amplitude of the 2560 Hz magnetospheric line received at the three stations (A.J. Smith private communication).

time the dispersion curve equivalent to a one hop whistler with known sferic could be constructed. The method of Bernard (1973) was then used to estimate the nose frequency and time, and hence L and n_{eq} using a diffusive equilibrium model (Park 1972).

Alternatively, the dispersion of a whistler component occurring during or shortly before or after the MLR event was measured. In this case it was necessary to assume that the MLR event propagated on the same duct as the chosen whistler component. The bearings of the MLR event and the whistler components may be compared to select a suitable component.

The signal bearings of MLR events and whistlers were measured using the semi-automated whistler analyser described by Smith et al. (1979). The bearings of whistlers were measured in the normal way by programming the tracking filter to follow the trace of the whistler and then measuring the phase of the modulation envelope. However, an MLR event is a very different type of signal; in particular, the bandwidth and duration are much larger than for whistlers, while the frequency is almost constant. A filter was used at several fixed frequencies in turn, covering the bandwidth of the event, the bearing measurement at each frequency being averaged over the duration of the event. Finally, by averaging over frequency a mean bearing was calculated for the whole event.

To estimate the parallel electron energy required for transverse cyclotron resonance ($W_{\parallel}$) for a given L and n_{eq} the relations given in Rycroft (1976) were used.

For the 27 June 1980 MLR event both methods were used to determine L and n_{eq}. Using the dispersion of the two hop echoing of the MLR event at Halley the values of L=4.8+0.15 and n_{eq}=190+40 cm^{-3} were estimated. Alternatively using the whistler at 1705:30 UT (figure 5.8) the values of L=4.16+0.1 and n_{eq}=350+30 cm^{-3} were obtained.

This would suggest that the whistler and the MLR event travelled in separate ducts, although in this case the bearings of the MLR event (142+10°) and the chosen component of the whistler (152+10°) were similar.

In the northern hemisphere the two hop whistler had no distinguishable duct structure and so it was not possible to identify any individual components. However, since two direction finding VLF receivers were operating in the conjugate region at this time it was possible to determine the exit point by triangulation. At the St. Anthony receiver (51.55 N, 56.06 W) there was no bearing information in the signal of the whistler which indicated that the exit point was very close by. At Deer Lake (49.36 N, 57.35 W) a well defined bearing was measured in the direction of St. Anthony, which confirmed an exit point near the St. Anthony receiver. For the MLR event, bearings could be measured at both receivers and these indicated an exit point 150 km north-east of St. Anthony, thus confirming that in this case the MLR event propagated in a different

duct from the majority of the whistler energy.

Two values for $W_{\parallel}$ were determined for the MLR event, the first (0.55 keV) using the values of L and n_{eq} derived from the observed dispersion of the MLR event itself and the second (2.3 keV) using values of L and n_{eq} derived from the dispersion of the whistler. In each case an average frequency of 3kHz for the MLR event was used.

5.1.3 The 26 June 1978 event

On the 26th of June 1978 an MLR event was received at Halley which differed in some ways from most Halley events. The characteristics of the event are summarised in table 5.2 . The values of L, n_{eq} and $W_{\parallel}$ were estimated using measurements made on the whistler at 0315.55 UT (figure 5.11). The estimate of $W_{\parallel}$ is higher than the two values determined for the 27 June 1980 Halley MLR event although it is within the range of values measured by Helliwell et al. (1975) for Siple MLR events. However, the values of Kp and the local time in particular differ from those typical for Halley MLR events (figures 5.7a and 5.7b). Further differences can be seen in the spectrogram in figure 5.11 which shows six adjacent time segments from a one minute in five recording. From 0320 UT to 0336 UT horizontal line structure is clearly visible. The lower four lines visible during the minutes starting at 0320 UT and 0325 UT show a regular spacing of 121$\pm$3 Hz with very small upward drifts of less than 10 Hz per minute. This drift may be due to tape speed variations within each one minute recording since some

MLR Event Halley 26 June 1978   Table 5.2

Frequency	2100 - 2700	Hz
Frequency Spacings	120 - 150	Hz
B_w at receiver	10^{-14}	T
Kp (during event)	5+	
Kp (max)	5+	
MLT	0015 - 0040	
Bearing	19 ± 5	degrees
L value	3.75 ± 0.2	
N_{eq}	335 ± 15	cm^{-3}
$W_{\parallel}$ (for gyro-resonance)	16 ± 4	keV
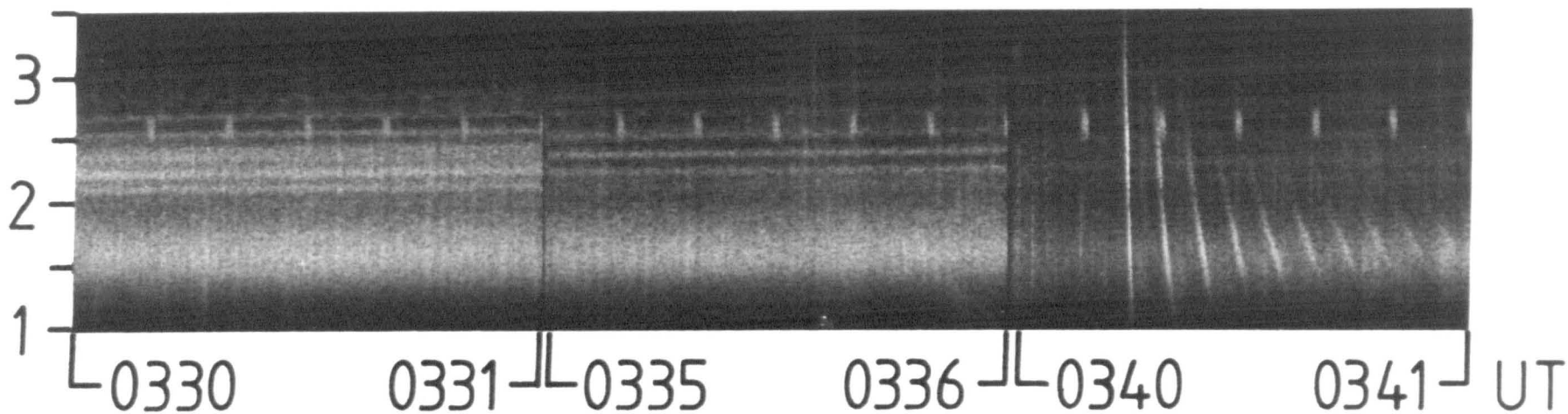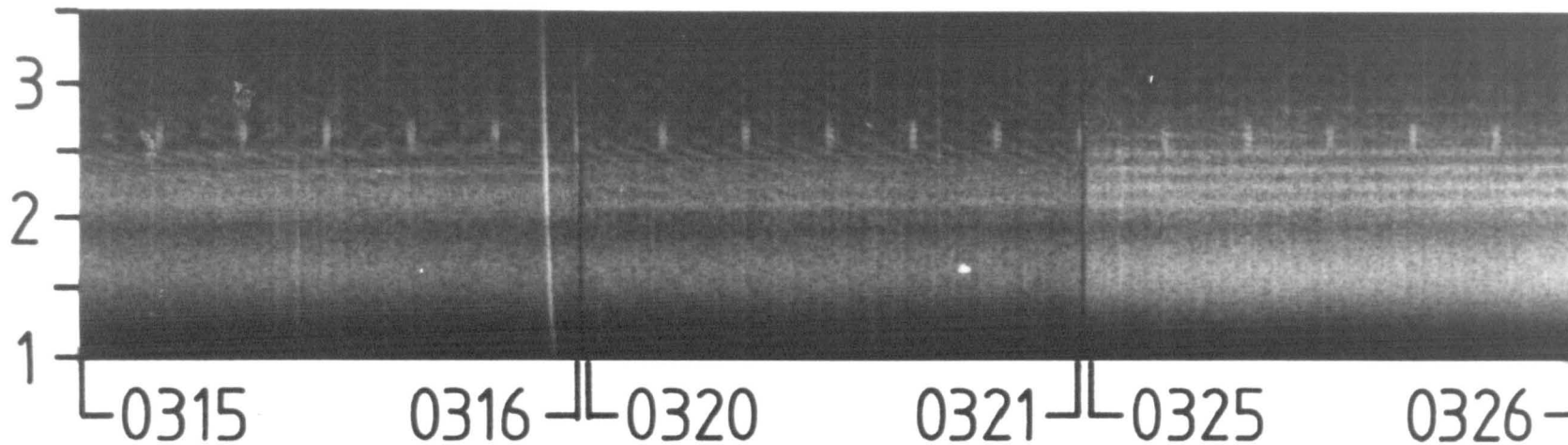
Figure 5.11 . Spectrograms of six one minute segments showing the
26 June 1978 MLR event.

of the lines revert to their original frequencies at the start of the next minute. The line of frequency 2250 Hz could be traced over three adjacent one minute segments and showed an average drift of less than 1 Hz per minute.

The highest frequency line (2625 Hz) in the segments commencing 0320 UT and 0325 UT is about 135 Hz above the next lower line, which is a deviation of 15 Hz from a regular 120 Hz line array. In the following segment (beginning 0330 UT) the line frequencies have changed, the upper two lines being separated by about 135 Hz with upward drifts of around 30 Hz per minute.

Another unusual characteristic of this event which is visible in the figure is that the lines show negligible two hop amplitude modulation in spite of the fact that good echoing conditions are present as demonstrated by the echoing whistler train in the segment commencing 0340 UT.

The lack of amplitude modulation, together with the regular line spacing of approximately 120 Hz suggest that the lines are strongly controlled by power line harmonics. The fact that some of the high frequency lines show spacings greater than 120 Hz may be due to sideband generation. Park (1981) reports sidebands generated by nonlinear interactions of the one hop signal from the Siple transmitter with energetic particles. Sideband separations up to 100 Hz have been observed with amplitudes sometimes greater than the parent wave. The amplitudes of the sidebands may be symmetrical or asymmetrical about the parent wave but in the asymmetrical case it is usually the

upper sidebands which are stronger.

An example of sideband generation observed at Halley is shown in figure 5.12 . This is an amplitude (in a 4 Hz band width) against frequency spectrum of a two hop magnetospheric echo of a constant frequency (3750 Hz) pulse transmitted by the Siple VLF transmitter. The line labelled E_1 is at the frequency of the transmitted signal and the line labelled E_2 is an upper sideband at 30 Hz above the transmitted signal. Both lines are split into doublets by the action of the goniometer. There is probably also another sideband between E_1 and E_2. In this case only upper sidebands are visible and their amplitudes are about half that of the parent wave.

The magnetospheric lines observed during the 26 June 1978 event do not show any obvious sideband structure but they are fairly broad lines (~50 Hz) which could be the result of a sideband structure which has been smeared out. Park and Helliwell (1981) observed magnetospheric line radiation which showed a positive frequency offset of 20 to 30 Hz from the nearest PLHR induction lines. In this case, using a receiver at Roberval, Quebec, they were able to observe the two hop magnetospheric lines together with the induction lines.

There is a degree of uncertainty in the frequency of the magnetospheric lines seen at Halley, which results from the action of the goniometer. As discussed in section 3.2 the goniometer splits any line in the spectrum into two components at 25 Hz above and below the original frequency.

HALLEY   16 JUNE 1977   1036·45 UT
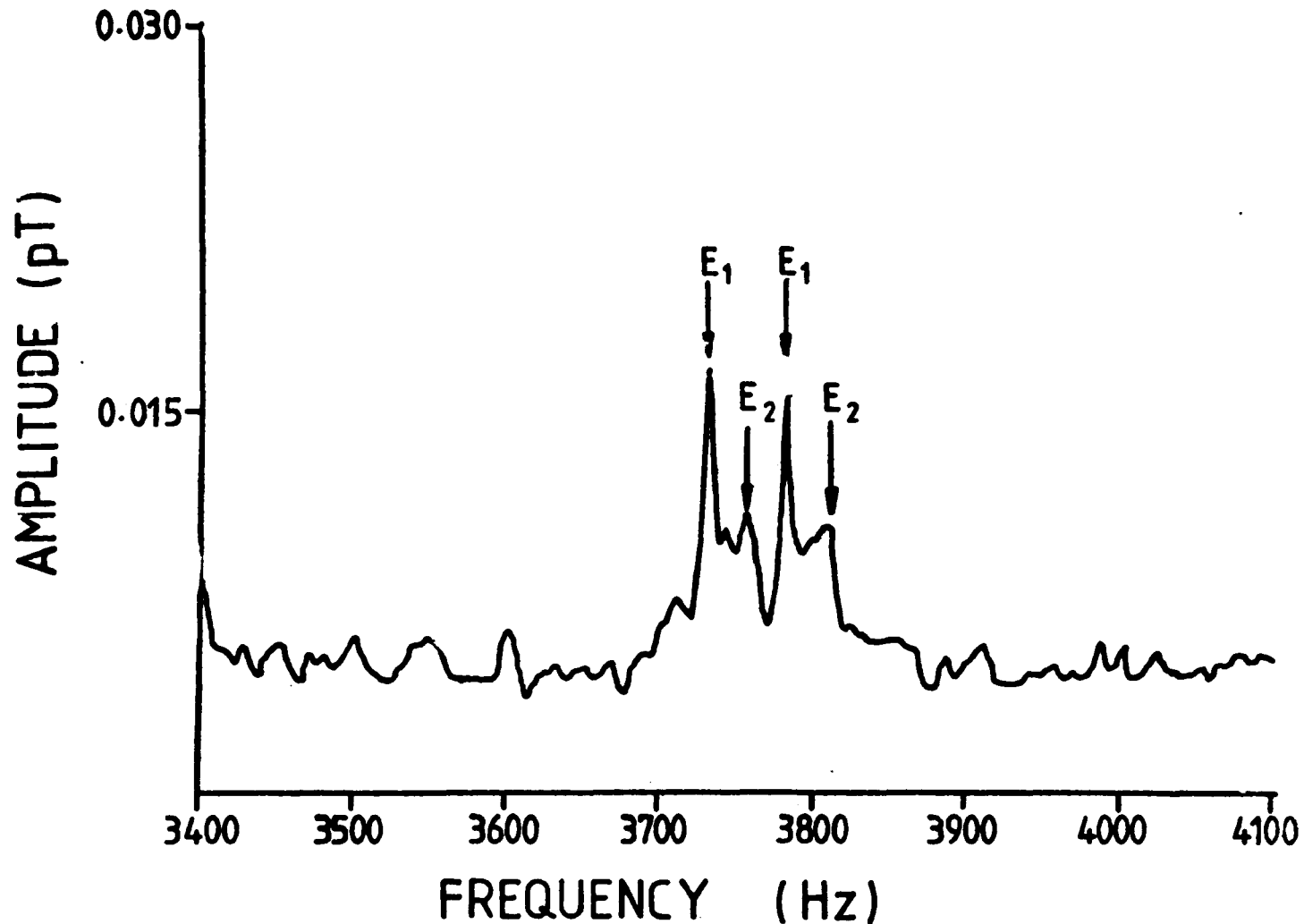
Figure 5.12 . An example of upper sideband generation (E_2) observed
at Halley on th two hop echo of the Siple transmitter (E_1). Both
lines are split into doublets by the action of the goniometer.

Since, in this case, the lines have a bandwidth of the order of 50 Hz the two components merge into one, the frequency of which depends on the relative amplitudes of the two components. The relative amplitudes in turn depend on the polarisation of the signal which depends on the distance from the ionospheric exit point of the signal to the receiver and the frequency of the signal. Therefore the apparent frequency of the lines will be shifted by an amount of the order of 25 Hz which depends on frequency in an unpredictable way. In this way an array of lines which in fact have a regular 120 Hz spacing may appear to have a slightly irregular spacing with an average value of approximately 120 Hz.

The exact frequency of the power system in the northern conjugate region at the time of the event is unknown, but if it is assumed that the power line fundamental frequency was exactly 60 Hz, the lines observed during the minutes commencing 0320 UT and 0325 UT show positive offsets of 28 to 45 Hz from odd power line harmonics. Odd harmonics are usually radiated much stronger than even harmonics (see figure 4.12) due to the characteristics of the power system components which cause them. In the following two minute segments it is difficult to see any relation between the frequencies of the higher magnetospheric lines and of power line harmonics, so these lines perhaps were originally locked to power line harmonics but have since become free and drifted up in frequency.

Following the method of Helliwell (1965) we can derive a rough estimate of the strength of PLHR required in the northern hemisphere to explain the observed MLR in terms of a PLHR source. Initially we assume the magnetospheric lines result from one hop propagation of a PLHR source. In fact the observed lines are probably the sum of many successive odd hops.

The first step is to calculate the strength of the wave field at the lower boundary of the ionosphere for a certain radiated power. Unlike the vertical wire antenna considered by Helliwell a power line source has the peak of its polar diagram in the vertical direction. The power flux in this direction is given by equation 5.1.1 where W is the radiated power and r the distance from the source. This is derived by equating the radiated power to the power flux (which has a $\sin^2\theta$ dependance) integrated over all directions.

$$P = \frac{3W}{8\pi r^2} \qquad (5.1.1$$

The electric field is given by 5.1.2 , where z_o is the impedance of free space.

$$E_i = \sqrt{Pz_o} = \frac{1}{r}\sqrt{\frac{3Wz_o}{8\pi}} \qquad (5.1.2$$

We now estimate the electric field E_o at the exit point of the duct. From the presence of the multi-hop echoing whistler at 0340.15 UT, it is evident in this case

that sufficient amplification occurs as the wave travels through the magnetosphere to almost equal the losses occurring in ducted propagation, in propagation through the ionosphere to the point of reflection, and in reflection. If we assume that the point of reflection is at the boundary of the lower ionosphere then the amplification will approximately cancel out the ionospheric attenuation and duct losses experienced by a one hop signal. Therefore we can allow for the duct amplification by using Helliwell's calculation with a duct transmission efficiency (T_d) of 1 and no ionospheric losses. Using Helliwell's equation 3.67 reproduced here as 5.1.3 we have the electric field at the output of the duct (E_o).

$$E_o = \frac{E_i}{\mu} \sqrt{\frac{T_d A_d}{2\pi \times 10^6 (1-\cos\theta_T)}} \qquad (5.1.3$$

In the above equation A_d is the effective cross sectional area of the duct and θ_T is the trapping angle.

Finally using Helliwell's figure 3.39 we estimate the field strength at a receiver close to the exit point of the duct, E_r, to be 0.05 E_o. After evaluating the constants in equations 5.1.2 and 5.1.3, the latter using Helliwell's values of $A_d = 5 \times 10^7$, $\mu = 2.3$ and $\theta_T = 25^\circ$, we have a value for E_r in terms of the radiated power.

$$E_r = 1.34 \frac{\sqrt{W}}{r} \qquad (5.1.4$$

Using a value for r , the height of the lower ionosphere boundary of 100 km and the measured field strength of 10^{-14} T we require a radiated power of 50 mW. This figure is much less than the power of 0.5 W used by Park and Chang (1978) when radiating simulated PLHR from the Siple transmitter since the latter figure was that required for triggering effects which are not observed during the 26 June 1978 event. Also the magnetospheric amplification was probably higher during the 26 June 1978 event than during Park and Chang's experiment.

To get this radiated power from the Buchans line (see chapter 4) would require an unbalanced current of about 1.3 A per harmonic at 2.5 kHz, while for the Baie Verte line 500 mA would be enough. Lower radiated powers would be required if the observed lines are the sum of several successive hops but the decrease would be less than an order of magnitude.

These currents, while much greater than those measured for Newfoundland power lines in chapter 4 are not impossibly high being only a few parts per thousand of the typical fundamental currents (200 A) for high voltage transmission lines. Geomagnetically induced currents could result in transformer saturation and hence greater harmonic currents (Albertson et al. 1973) than those measured. Magnetic activity was fairly high at the the time of the event.

5.2 Comparison of MLR at Halley and Siple

Magnetospheric line radiation is frequently observed at Siple (Helliwell et al. 1975; Park and Helliwell 1978). To compare the relative frequency of occurrence of MLR at Siple and Halley the number of events occurring in continuously surveyed periods of time were examined. The activity at Siple during the months of June and July 1977 was surveyed by Sonwalkar (private communication). In this period 29 separate MLR events with an average duration of 50 minutes were identified. An event was only counted as separate if it was separated from other line activity by an interval of at least an hour.

Continuous data were not available for this period at Halley so the period from 19th June to 16th July 1978 was surveyed by Strangeways (private communication). In this period there were ten MLR events with an average duration of about 20 minutes. At both Halley and Siple the actual duration of the MLR events vary between extremes of a few minutes to a few hours.

There is a problem deciding whether or not a particular section of VLF activity qualifies as an MLR event as there is no universally agreed definition. The ten events identified at Halley include several border-line cases, but all these were of quite short duration. Therefore the total length of time when MLR activity is present will be less sensitive to the subjective decisions of the observer, than will the number of individual events.

Comparing the total time during which MLR activity is seen (as a proportion of the time surveyed) at Halley (42 minutes in 27 days) and Siple (286 minutes in 61 days) we find that MLR is 3 times more common at Siple. In making this comparison it must be noted that the magnetic activity was higher on average during the survey of Halley data than during the survey of Siple data. This may bias the measurements in either direction since the higher magnetic activity will correspond with greater fluxes of energetic particles to take part in wave particle interactions and may also increase the level of PLHR sources as a result of geomagnetically induced currents in power systems, but at the same time VLF propagation conditions will be poorer due to increased ionospheric absorption.

No event has yet been observed simultaneously at Halley and Siple although line activity was observed at Siple just prior to the 27 June 1980 MLR event shown in figures 5.1 and 5.8 .

The character of MLR activity at Halley is different from that at Siple. Out of the total of about 15 well defined MLR events seen at Halley only one (see section 5.1.3) shows line frequencies that can be related to 60 Hz power line harmonics, whereas most of the Siple MLR events detailed in publications by the Stanford group (Helliwell et al., 1975; Park, 1977; Park and Helliwell, 1981) can be related to a power line source.

The average frequency of an MLR event (average of the highest and lowest frequency lines of each event) is quite similar at Halley and Siple. During the two periods compared above, the average frequency for Halley events was 2600 Hz, while that for Siple was 2300 Hz.

Park and Helliwell (1978) show histograms of the number of MLR events occuring as a function of local time, magnetic activity, and resonant electron energy. The local time dependence at Siple shows a sharp increase at 0600 LT and a steady decrease throughout the afternoon, which is quite different from the Halley local time dependence shown in figure 5.7a .

The dependence of MLR activity on magnetic activity is quite similar for Halley (see figure 5.7b) and Siple. Park and Helliwell (1978) explain this dependence as due to the combination of good propagation conditions existing during quiet magnetic conditions with the enhanced electron fluxes needed for strong wave particle interactions which remain for a few days after a magnetic disturbance.

Measurements of resonant electron energies have only been made on two Halley events, but both are within the spread of values observed for Siple events.

The differences between Halley and Siple MLR activity, in terms of frequency of occurrence and character of the emissions, can largely be explained in terms of the much greater intensity of PLHR in the Roberval (Siple conjugate) area than in Newfoundland. Data provided by the Newfoundland Hydro show an average total load of 450 MW

during the summer, the largest single load being the ERCO phosphorus plant at 120 MW. The largest harmonic currents measured on the line feeding this plant (see section 4.5.1) at frequencies above 1kHz were a few mA (figure 4.13). This is about 5×10^{-6} of the fundamental current corresponding to 120 MW in a 230 kV line. Park and Miller (1979) present some curves of weekly variations in load on Hydro-Quebec. The mean load is about 10 GW, about 22 times the total mean load for Newfoundland. A large consumer of power in the Roberval area is the Alcan refinery at Arvida, which uses 12-phase rectifiers to produce the direct current required for the electrolytic reduction of aluminium. The use of rectifiers is well known to result in injection of harmonics into the power system (Pileggi et al 1981).

Helliwell et al (1975) quote a harmonic content of 0.22% of the fundamental at 1500 Hz for a power line in this area. This would correspond to several amps of harmonic current in the lines supplying the Alcan refinery, which carry 1000 MW. Radiated powers of the order of the estimated 50 mW required to observe the one hop signal in the southern hemisphere (see section 5.1.3), and even the 0.5 W per harmonic required for non-linear and triggering effects (Park and Chang 1978) would be possible with this magnitude of harmonic current.

5.3 Discussion

It is clear that Halley MLR events (with the exception of the 26 June 1978 event) are not simply the result of linear magnetospheric amplification of PLHR. The line frequencies are not usually related to power line harmonic frequencies, and it was determined by the measurements in chapter 4 that at least at the time the measurements were made, the intensity of PLHR in the conjugate region was far too small to cause any strong magnetospheric effects. Also, individual magnetospheric lines are often observed to drift as much as 100 Hz in one minute, which means a line could not be controlled by any one power line harmonic.

The drift of the lines in an MLR event may be related to the upper sideband generation that is often observed with magnetospheric signals (Park 1981). The example in figure 5.12 shows a two hop magnetospheric echo which has an upper sideband about 30 Hz above, and half the amplitude of, the parent wave. The increase in average frequency resulting from the two passes through the magnetosphere of this signal is about 6 Hz, which for a signal echoing repeatedly through the magnetosphere with a typical two hop echo time of 6 seconds would correspond to an average increase in frequency of about 60 Hz per minute. This is typical of the drift rates observed for MLR events.

More generally, it is shown in figure 5.6 that the line drifts in MLR events are nearly always upward, which is consistent with the observation of Park (1981) that when asymmetrical sideband generation occurs it is usually the upper sideband that is stronger. Although a sideband structure has not been observed within the lines of an MLR event, the large bandwidth of the lines (~30 Hz) would prevent individual sidebands from being distinguished.

One possible mechanism suggested to explain the MLR events received at Halley is that the resonant amplification of PLHR which occurs at Siple longitudes imposes a fine structure on the electron energy distribution. These electrons then drift to Halley longitudes where the fine structure causes preferential amplification at the frequencies observed in the MLR event. For a mechanism of this type to be possible the electron would have to drift from Siple to Halley longitudes in sufficiently short a time for the fine structure to remain stable. Halley line events have an average duration of 20 minutes and so the fine structure might be expected to remain stable for this length of time. The drift time of the non-relativistic electrons for one complete revolution round the earth is given by Hargreaves (1979)

$$T_r = \frac{733}{E\,R_o} \times \frac{G}{F} \qquad\qquad (5.3.1$$

where T_r is in hours, E is the energy of the electrons in keV, R_o (~L) is the equatorial crossing radius of the

electrons in earth radii, and G/F is a factor equal to 1 for an electron mirroring at the equator and 1.5 for a particle mirroring at the poles.

In section 5.2.1 the resonant electron energy for the 27 June 1980 MLR event was estimated to be 0.55 keV, and the L value 4.8 . Using these values a drift time of 20 hours is obtained for the 24° of magnetic longitude separating Siple and Halley. It is unlikely then, that any fine structure imposed on the electron distribution at Siple longitudes, would survive until the electrons reached Halley, so a mechanism of this type is not a likely cause of MLR .

Dowden et al (1978) suggest that a relatively weak coherent signal such as a power line harmonic can generate an 'embryo emission' under favourable conditions, which may be up to 40 dB stronger than the input signal. The emission will be controlled by the input wave so long as the difference in frequency is less than a quantity termed the control frequency which may be about 100 Hz even for weak signals such as PLHR . However the embryo emission events observed by Dowden et al. last only between one and three seconds and usually transform into a free emission. Although MLR events observed at Halley are sometimes associated with triggered emissions, it is unlikely that the lines are embryo emissions since it is difficult to explain the slow, steady frequency drifts observed.

It has been shown by Lashinsky et al (1980) that the principal features of MLR as observed by Helliwell et al (1975) and other workers can be explained as a van der Pol oscillation subject to incomplete entrainment by a power line harmonic. This mechanism results in a main emission with a small frequency offset from the power line harmonic and a series of weaker side bands at multiples of the basic frequency offset. Since the frequency offset can vary from one line to the next a series of lines with irregular spacings distributed about a mean close to 120 Hz can arise. If certain even harmonics were able to entrain emissions as well as the odd harmonics then the irregular spacings with a mean of about 80 Hz observed at Halley may arise. However, it would be difficult to explain the observed frequency drifts by this mechanism.

It was suggested by Matthews and Yearby (1981) that if the particle distribution function had several sharp local gradients then using linear theory wave growth would be largest at discrete frequencies. Using the treatment of Coroniti et al (1971) they showed that the time required for quasi-linear particle diffusion to smooth out such pitch angle gradients was of the same order as the duration of MLR events.

From the study by Ashour-Abdalla (1972) on the effect of low amplitude whistler mode signals on the electron distribution function, it was shown that the frequency of maximum growth would drift upwards at a rate of the order of 10 Hz per minute. This is in rough agreement

with the observations of MLR line drifts.

The above mechanism could give rise to selective amplification of certain frequencies within magnetospheric hiss resulting in line structure. The 27 June 1980 MLR event in particular may be caused in this way since it commences suddenly (in less than four minutes) and then gradually evolves into an unstructured hiss band over a period of 30 minutes (see figures 5.8 and 5.9).

Matthews (1982) has suggested that successive quiet band generation could give rise to the array of lines observed in an MLR event. The quiet band phenomenon is described more generally by Matthews et al. (1982) and the first observation of the quiet band is reported by Raghuram et al. (1977). In this mechanism a weak monochromatic whistler mode wave, such as a power line harmonic, modifies the distribution of the energetic electrons by a particle trapping process. This is illustrated in figure 5.13 . The initially negative gradient in the electron flux with respect to $v_\parallel$ (positive with respect to the corresponding gyro resonant frequency shown in the figure) is that required for wave growth (Dowden 1981). As the electron distribution is modified as illustrated by the solid line in the figure, the gradient just below f is reversed, suppressing wave growth, and resulting in the quiet band which is observed if hiss is initially present.

More important to the current problem are the increases in gradient which occur below and just above f . The corresponding enhanced wave growth below f may result in
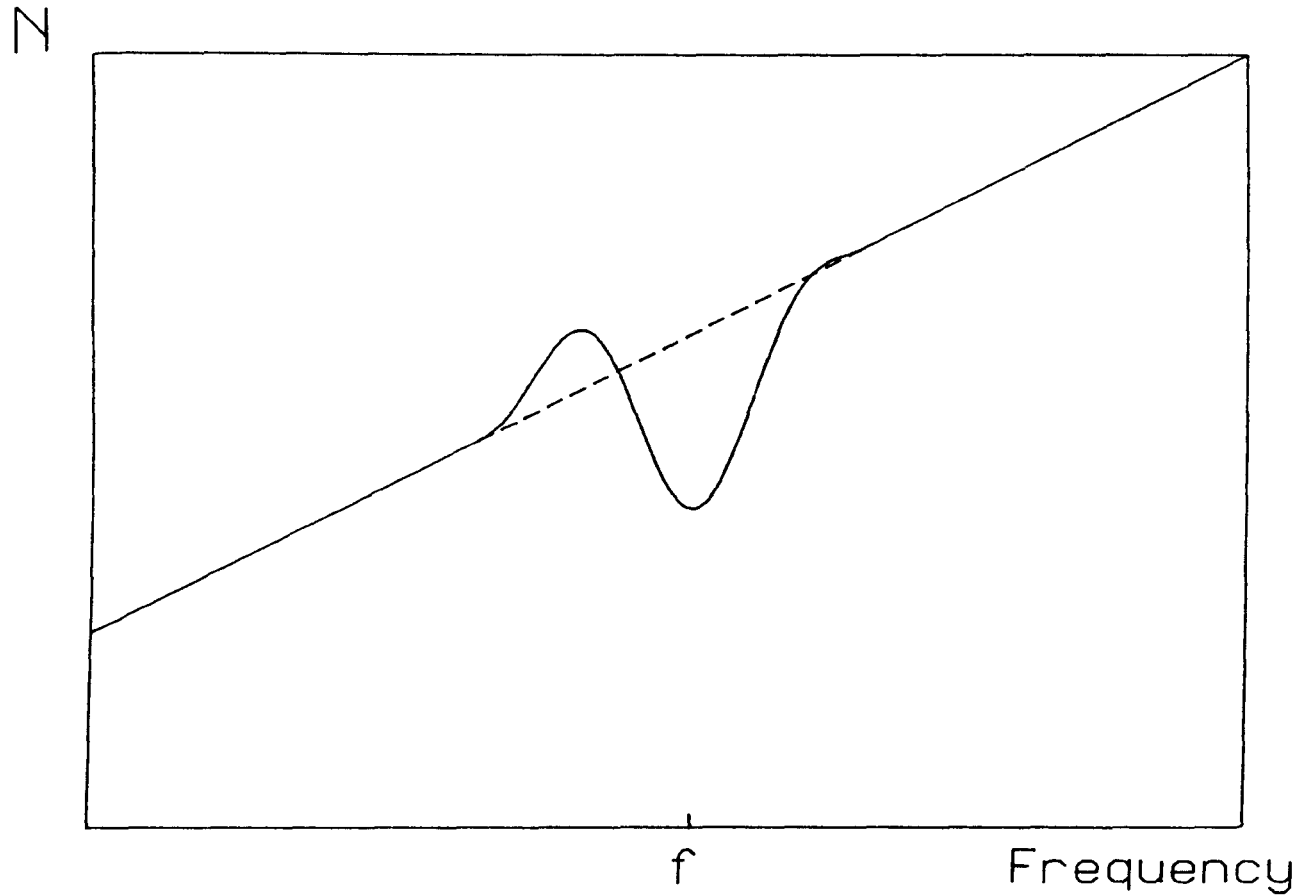
Figure 5.13 . An illustration of the effect of a whistler mode wave (f)
on the electron distribution function shown plotted against the
corresponding gyro-resonant frequency as predicted by Matthews (1982).

the generation of another line as selective amplification of background hiss occurs at this frequency on each pass through the interaction region. The process may then repeat resulting in the generation of an array of lines below the original wave. The good whistler mode echoing required for this to happen are always observed with MLR events. Hiss is also present during many MLR events.

The increased wave growth above f will result in a small upward shift in f on each pass through the interaction region and hence the gradual upward drift observed in MLR events. This assumes that the wave growth is able to dominate over the original initiating wave which is likely to be the case if the initiating wave is a power line harmonic since they are very weak.

The scale of the perturbation in the electron distribution is determined by the trapping frequency, f_t; the lower line being generated at about 2.5 f_t below f . To calculate f_t for the conditions at the time of a Halley MLR event the equation given by Matsumoto (1979) is used.

$$\omega_t \equiv 2\pi f_t = (kv_\perp \Omega_w)^{1/2} \qquad\qquad (5.3.2$$

where

$$\Omega_w = \frac{eB_w}{m_e}$$

and

$$k = (\Pi_e/c)[\omega/(\Omega_e-\omega)]^{1/2}$$

In this equation B_w is the wave amplitude, Π_e is the plasma frequency, and Ω_e is the electron gyro frequency. The following equation is used to determine Π_e from n_{eq} which may be determined from whistler analysis.

$$\Pi_e = \sqrt{\frac{n_{eq}e^2}{\varepsilon_o m}} \qquad\qquad (5.3.3$$

The values of $n_{eq} = 180$ cm^{-3} and $\Omega_e = 5\times10^4$ rads^{-1} were deduced from measurement of the dispersion of the whistler mode echoing observed in the 27 June MLR event and by assuming an equatorial interaction region. A value of 2×10^7 ms^{-1} was chosen for $v_\perp$ which is compatible with the resonant electron energy of about 1 keV estimated earlier for this event assuming a reasonably isotropic pitch angle distribution. Using the above values and putting $B_w = 2$ pT (estimated by Matthews and Yearby 1981 for MLR events with

received field strengths similar to the 27 June 1980 event) a value of f_t = 22 Hz was calculated.

The above value for f_t agrees well with the observed line spacing of about 70 Hz for the first minute of the 27 June 80 event. The line frequency drift is about 80 Hz per minute, corresponding to 1/10 f_t per one hop echo period, which is reasonable for this mechanism.

The one prediction of the successive quiet band theory for MLR generation which it has not been possible to check with observation is the way in which the lines should grow downward from the initiating wave. This has not been observed in any MLR event but since most of our VLF recordings are made on a one minute in every five minutes schedule most of the evolution of the MLR events are not recorded. Also it is possible that successive quiet band generation could start at the same time from several different initiating waves such as prominent power line harmonics.

Chapter 6   Conclusion

                    and Suggestions for Future Work

The VLF receiver comes at the front end of the analysis system for VLF emissions, and this has been improved by the correction of the peak in its frequency response, and the replacement of the single tone calibration oscillator by a digital calibration tone generator which generates five tones simultaneously. A comparison of the signals simulated by a local calibration coil (the normal means of injecting the calibration signal) with those simulated by a distant calibration coil confirmed the validity of the former method.

The next stage is the analysis of the signals received and for this a means has been developed for automatically measuring the amplitude of spectral lines. This technique has been used extensively for measuring PLHR induction lines (chapter 4) and for measuring magnetospheric line radiation (chapter 5). It has also been used by other members of the Sheffield space physics group. A technique has also been developed for deconvoluting goniometer spectra, although this has not been used in practice since the number of spectra which required processing to obtain good results could not be handled by the available hardware. Also the technique is best suited to plane polarised signals whereas most magnetospheric signals have a degree of elliptical polarisation.

In chapter 4 the measurement of VLF radiation from power lines in in Newfoundland was described together with the analysis of the results to estimate the radiated power, which for the lines measured (which should be typical of Newfoundland) was unlikely to be strong enough to cause a magnetospheric effect. It was also possible to estimate the skin depth and conductivity of the ground beneath the power lines.

A summary of all MLR events which have so for been found in the data recorded at Halley was presented in chapter 5 . Several of these are new events including one which shows definite evidence that it originated from PLHR. The intensity of PLHR required to stimulate this event was estimated to be 10^6 times the largest radiated power determined for a single line in Newfoundland. The occurrence of MLR at Halley and at Siple was compared and it was found that MLR occurred three times as frequently at Siple during the periods studied. The variation of the occurrence of MLR with magnetic activity was similar at the two stations, while the variation with local time was quite different.

The current theories of the origin of MLR events have been discussed in relation to the properties of the Halley events. Although it has not been possible to identify the mechanism causing MLR events, several of the theories explain the line structure in terms of enhanced magnetospheric wave growth at discrete frequencies due to structure in the energetic particle population. However, the cause of this structure is where the theories differ. It is

apparent that in most cases PLHR does not have a direct role in the generation of MLR .

There are still many uncertainties in the field of line radiation. Although an attempt was made in chapter 5 to explain some of the differences in MLR activity between Halley and Siple in terms of different PLHR inputs to the magnetosphere it is still uncertain what the PLHR inputs are, especially in the regions of Labrador and Quebec just to the west of Newfoundland. Radiation from power lines in this region could have a significant effect on the VLF wave activity at Halley. This uncertainty could be resolved by making a series of measurements on isolated power lines in Eastern Canada. A future series of measurements would benefit from the experience gained in obtaining and analysing the 1980 Newfoundland observations.

The question of what significance PLHR has on the magnetospheric wave activity in general is still surrounded by controversy, and so a repeated attempt to find a weekly variation of wave activity at Halley (which would indicate a man made control) would be a very useful experiment. The experiment would have to be carefully designed to eliminate any non-magnetospheric influence on the results, such as signals from VLF transmitters.

The precise spectrum of Halley MLR events is still uncertain due to the splitting of spectral lines caused by the goniometer. It is desirable, therefore, that some recordings are made without goniometer processing at times when MLR events are likely. Also continuous recordings

126

(rather than one minute in five) would be valuable in studying the onset and evolution of individual events. This brings a problem of a much increased rate of use of recording tape. A possible solution would be to use a spectrum analyser connected to a micro-computer which could be programmed to recognise the spectrum of MLR . Also magnetic activity could be monitored to indicate times when MLR events are likely.

Appendix A   The Programmable Power Supply

A.1 Introduction

The programmable power supply (PPS) was designed to provide all power and control requirements for a portable VLF goniometer recording station, using one 12 V car battery as the power source. The power outputs to the goniometer and tape recorder may be switched on continuously or for 1 minute in 5 using the BCD time from the time code generator.

The azimuth reference signal at 9.5 kHz is generated from the 25 Hz goniometer sine output and an internal oscillator. The time code is mixed with the azimuth reference and then attenuated to a suitable level for the tape recorder.

Also provided is a 7kHz sine wave calibration output which is switched on for the first two seconds of every minute, the first four seconds of every tenth minute and, the first ten seconds of every hour. It can also be switched on manually. Its frequency is precisely controlled using the time code generator, but the amplitude may vary slightly.

A.2 Circuit Description (Power Supplies)

Fig A.1 is a circuit of this section of the unit. The 12 V power input feeds the main switch via a 3 amp fuse and the ammeter shunt. The power to the inverters is switched through the relay in the '1 in 5' mode, and directly in the 'CONT' mode. In both modes power goes
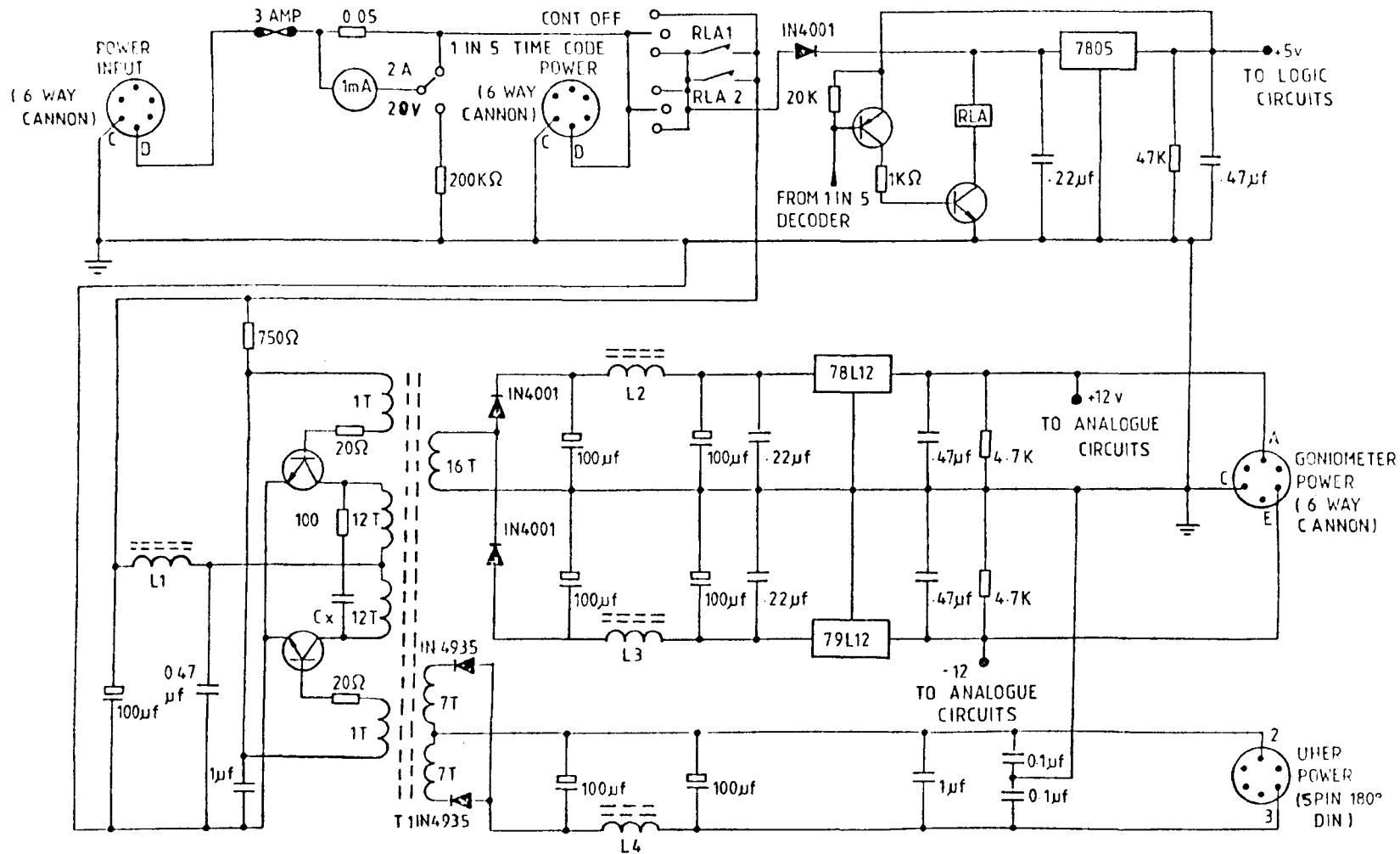
Figure A.1   ONE IN FIVE RELAY AND POWER SUPPLIES

directly to the relay and the 5 V regulator which supplies the digital circuits in the programmer (the IN4001 diode provides reverse polarity protection), since these are required for the 1 in 5 decoding.

The two TIP41C transistors, the transformer, and associated components form a DC to DC converter that is used to supply power to the Uher tape recorder and the goniometer. A standard push-pull inverter circuit is used, with the exception that all the bias current for the transistors is provided from the positive supply via the 750 ohm resistor. This is done so that when the inverter is first switched on, it will provide sufficient current to start the tape recorder motor, which when stationary presents a very heavy load to the circuit. Also the biasing is such that no current will flow if the power is applied with incorrect polarity, and that excessive current will not flow if the output is shorted, so no additional protection is required. The transformer is wound on a Mullard LA1138 ferrite core with all windings of 23 SWG wire.

The two secondary windings provide a full wave rectified 6 V (at up to 500 mA) supply for the Uher tape recorder. This is DC isolated from the rest of the supplies.

The 16 turn secondary winding feeds two half wave rectifiers giving ± 15 V. Integrated circuit regulators reduce this to ± 12 V (at 100 mA) for the goniometer and also the analogue circuits in the PPS.

Extensive decoupling is employed on both the input and output of the inverter to reduce the possibility of interference to the VLF recordings.

A.3 Circuit Description (Control Circuits)

Figure A.2 is a circuit of this section of the PPS. The parallel BCD outputs for 1, 2, 4 and 8 minutes drive a 74LS42 BCD to decimal decoder with active low outputs. The 0 and 5 outputs are connected to the relay driver on the power supply board via 4.7 K resistors, energising this relay when the minutes read 0 and 5.

The calibration tone decoder switches on the calibration tone for 10 seconds on the hour (when the minutes are zero), for 4 seconds every 10 minutes (when the unit minutes are zero), and for two seconds on every other minute. A series of NOR gates are connected to give high outputs when digits are zero. The unit seconds are split into two parts, one gate is high for seconds 0, 4 and 8 and the other for seconds 0, 1, 2 and 3. Three NAND gates are connected to decode the three calibration tone functions from the outputs of the NOR gates. The outputs are connected together using a wired OR connection. A switch is also connected between the node and 0 V to manually switch on the calibration tone. The node gates the 1 kHz carrier output from the time code generator from which the seventh harmonic is filtered out to produce the calibration tone. A two pole LC filter followed by a variable gain high input impedance amplifier is used, with the latter adjusted using VR1 for a

FIGURE A.2 . ONE IN FIVE DECODER AND CAL. TONE GENERATOR.
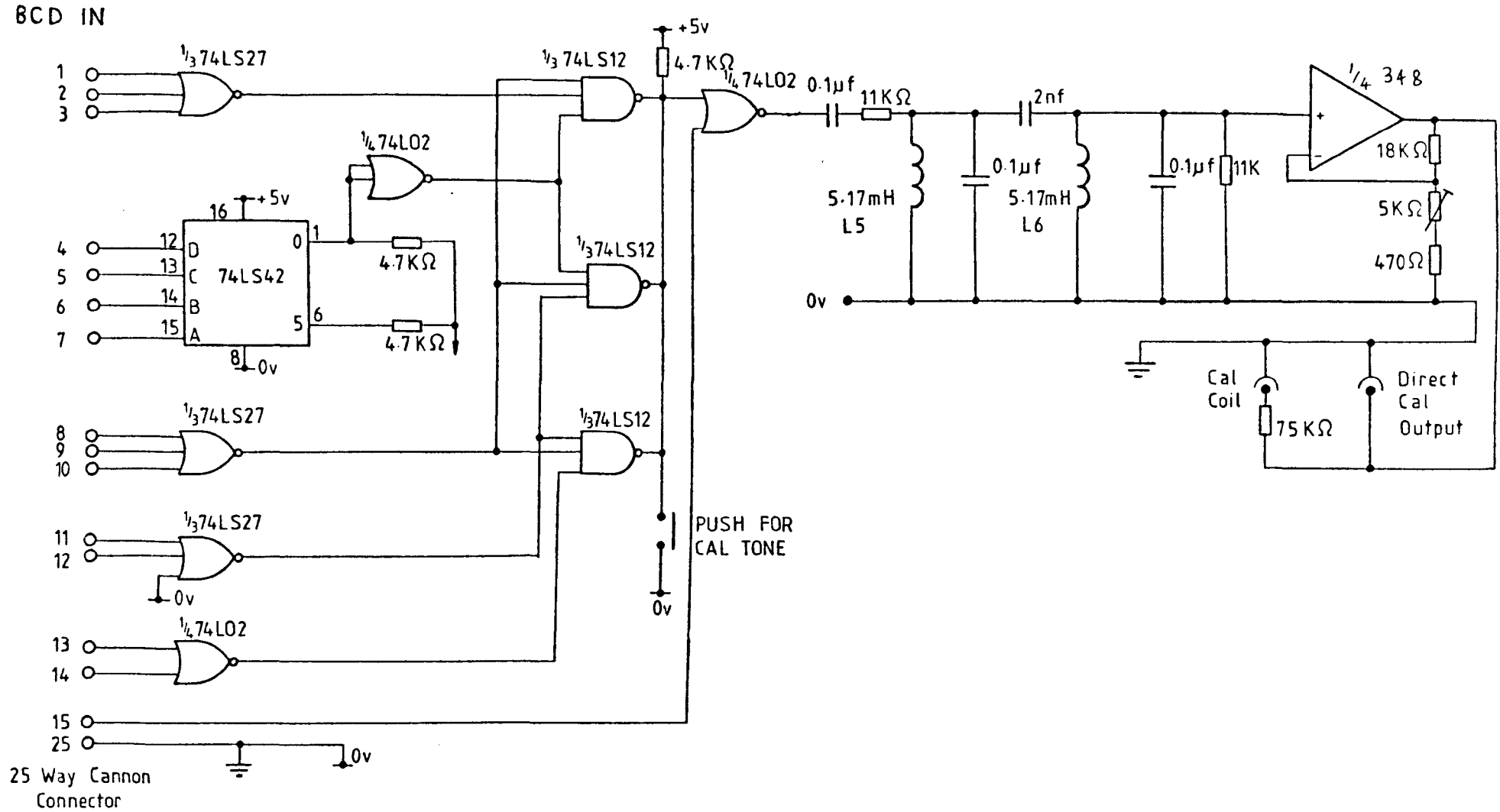
1 V RMS calibration tone amplitude. As well as the direct output, an output for the calibration coil is provided with a 75 kΩ series resistor (for small loop aerials).

A.4 Circuit Description (Azimuth Reference Oscillator)

The 25 Hz SINE output from the goniometer double side band modulates a suppressed 9.5 kHz carrier using the circuit in figure A.3 .

The 7555 astable oscillator provides a 19 kHz square wave which is divided by two in the 4027 JK flip flop giving two antiphase square waves of 1:1 mark space ratio. These drive the enable inputs of a DG201 quad analogue switch which switches the 25 Hz sine wave alternately to the two inputs of the differential amplifier while grounding the unused input. The frequency response of the differential amplifier falls off above 10 kHz to reduce the amplitude of the odd harmonics of 9.5 kHz. There are no even harmonics. The resulting output is equivalent to the 25 Hz sine multiplied by a 9.5 kHz sine wave. The time code is passed through a 2 kHz low pass filter and then mixed with the azimuth reference using a summing amplifier. Finally it is attenuated to a level suitable for feeding the tape recorder CH2 input.

FIGURE A.3 . AZIMUTH REFERENCE MODULATOR AND TIME CODE MIXER.

Appendix B Transfer of Digital Data from the Unigon
Spectrum Analyser to the M6800 microprocessor

B.1 Hardware

The digital data from the Unigon FFT spectrum analyser is output as two 12 bit words, one for the magnitude or imaginary part of the spectrum (depending on which mode the analyser is used in) and one for the real part of the spectrum. The spectral amplitudes are encoded on these words as complemented offset binary. A clock input is available for stepping the digital output through each point in the spectrum in turn. When the analyser is used in complex mode (to output real and imaginary components of the spectrum) two clock pulses are required to step from one point in the spectrum to the next, the first steps the real output on to the next point and the second the imaginary.

The hardware consists of two multiplexers, one to connect either the real or imaginary outputs to the microprocessor (input lines A0 to A7 and B0 to B3 of an M6820 PIA integrated circuit) and one to connect the spectrum analyser clock input either to the microprocessor (CA2 output) or to the existing source within the whistler analyser. Figure B.1 is a circuit of the interface.

The multiplexers are constructed using 74LS01 dual input NAND gates. Since they invert the data the input to the microprocessor is just offset binary rather than complemented offset binary. The multiplexers are controlled using bits B4 to B7 of the microprocessor port as shown in

132

Figure B.1 . Circuit of the FFT interface.
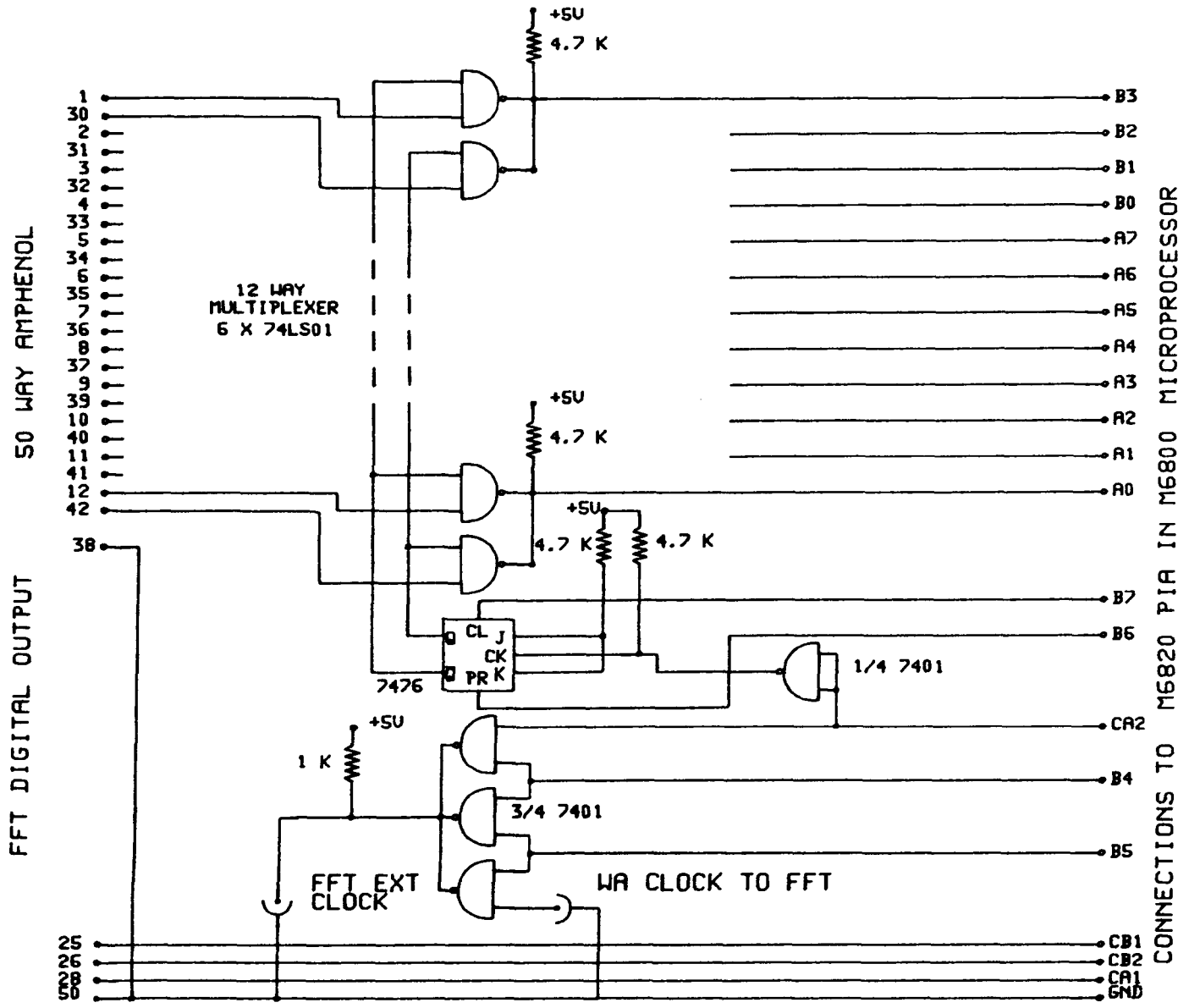
the tables below.

B4	B5	Clock Input
0	0	High
1	1	Low
1	0	$\overline{CA2}$
0	1	$\overline{EXT}$

B6	B7	Data to Microprocessor
0	1	Real
1	0	Imaginary or Magnitude
1	1	Changes on CA2 +ve Transition
0	0	Not Defined

In use the outputs B4 to B7 would normally be set as follows; B4=1, B5=0, B6=1, B7=0. This connects the magnitude data to the microprocessor and the CA2 output to the clock input. By suitably programming the microprocessor input port so that a pulse is generated on the CA2 output automatically when the microprocessor reads the data, a series of processor reads will read consecutive points in the spectrum. When used in complex mode, B6 and B7 may be set to one so that a series of processor reads will access the real and imaginary components of the spectrum alternately.

To synchronise the reading of the spectra with their calculation, two control signals are provided by the spectrum analyser. The sync output is a square wave which has a low to high transition one clock pulse before the data output addresses the first point in the spectrum (DC). This

133

is connected to the CB1 input of the microprocessor port. The calculation complete output is high while the FFT calculation is in progress and low otherwise. When the analyser is in the free run mode this output is a square wave, high for 33 ms and low for 9.5 ms. The transfer of data into the output memory takes place during the latter period, therefore, the microprocessor must wait for the next low to high transition before reading the data. The situation is more complicated when the analyser is used in transient capture mode. Then, just a single spectrum is processed and the calculation complete output is low during the data input, high for 33 ms and then low. The transfer of data to the output buffer is not complete, however, until 9.5 ms after the final transition and so the microprocessor must wait until then (using a timer routine) before reading the spectrum. Finally the strobe output, which is a square wave with the digital output data valid on the low to high transition and changing on the high to low transition, is connected to the CA1 input. However, the present software does not make use of this signal.

B.2 Software

A set of subroutines has been written in 6800 assembly language to control the transfer of data from the analyser to the microprocessor. They are not listed here since they would not be meaningful to anyone not familiar with the 6800 microprocessor. Instead a brief description of what the routines do is given.

The subroutines SYNC and CALC provide the synchronisation required between the generation and transfer of spectra. When the subroutine SYNC is entered a series of external clock pulses are sent to the FFT until a low to high transition occurs on the sync output, after which control returns to the calling program. Calling subroutine CALC causes the program to wait for a low to high transition on the calculation complete output, after which the new spectrum is available for transfer.

The two subroutines MGREAD and CPREAD are the main routines used to transfer magnitude and complex spectra respectively from the analyser to the microprocessor's memory. Each routine contains a trigger segment to allow transfer of spectra to be started a set time after the amplitude at a certain frequency in the current spectrum exceeds a set threshold. The number of spectra to be transfered and the frequency range of the spectra may be specified subject to the limit on the total number of spectral points that can be accommodated in the available memory. Also, if a time resolution less than that provided by the analyser is required, it is possible to skip several spectra between each one that is transfered. Magnitude spectra only may be averaged, either over a number of adjacent spectra or over several repeatitions of the whole routine. No provision for averaging complex spectra is provided since it is not usually meaningful to do this without considerable preprocessing which cannot be done in real time (see sections 3.2 and 3.3).

To access the spectra stored in the memory, routines are provided for printing out the spectra in numerical form, for plotting the spectra on an XY plotter, and for further processing using the BASIC interpreter.

The program is incorporated into the M6800 operating system for the whistler analyser.

C.1 Peak Finder

The   following   program   runs   on   the   M6800
microprocessor using a BASIC interpreter and the co-resident
operating system COMSYSMK3.1 which contains the machine code
programs   for   transfer   of   data   from   the   FFT   analyser
discussed   in   appendix   B.   Two   machine   code   routines   are
called   via   the   USR   function,   the   address   of   the   routine
first being stored at absolute address 287 (high   byte)   and
288   (low   byte)   using   the   POKE   instruction.   The   first,
MGREAD,   (at 80(high),9(low)) is used   to   read   a   block   of
spectra   from   the   FFT   analyser   to   the   microprocessor's
memory. This routine does not use the   argument   to   USR   or
return a result. The second (at 80(high),   3(low)) allows the
spectral   amplitudes   to   be accessed as if the spectra were
packed end to end in a one dimensional array called USR,   by
accepting   an   array index as the argument and returning the
spectral amplitude   as   the   result.   The   operating   system
(COMSYSMK3.1)   of   the M6800 allows the output from BASIC to
be redirected to a different port by storing a vector to the
port at absolute address 20470 . This was used to   send   the
output   of this program to a port connected to the Sheffield
work-station on the SRC computer network   for   the   work   in
chapter   4   and to the PDP 11 computer in the VLF laboratory
for the work in chapter 5.

```
1 REM FFTSPECTRUM PEAK FINDING PROGRAM TO RUN WITH COMSYSMK3.1
4 PA=20470
5 REM FFTPROG PARAMETERS MUST BE SET FOR READ MODE REQUIRED
8 DEF FNA(V)=INT(10*V+0.5)/10
```

```
9 INPUT"PORT NO.";PT:REM GET OUTPUT PORT
10 INPUT"SING/MULT/READ";IN$
12 IF IN$="SP"GOTO 180
14 IF IN$="S"GOTO 185
16 IF IN$="MP"GOTO 70
18 IF IN$="M"GOTO 60
20 IF IN$<>"R"GOTO 10
24 REM READ FFT SPECTRA IN TO MEMORY
25 GOSUB 9900
30 GOSUB 1000:REM READS FFT THEN SETS USR VECTOR FOR MGREAD
40 INPUT"TIME";TM
50 GOTO 10
59 REM MULTIPLE PEAK FINDING ROUTINE
60 IF FM<>0 GOTO 90
69 REM GET PARAMETERS
70 INPUT"RANGE,N,F0";FM,NM,F0
80 INPUT"LF,HF";LF,HF
90 NF=INT(LF/FM*500+0.5)-N
95 N=NM:YF=FM
100 FF=HF/FM*500
110 IF FF>PEEK(20493)+PEEK(20492)*256 THEN GOTO 80
120 POKE PA,PT*4:REM SET OUTPUT PORT
122 PRINT-205;TAB(8);TM
125 PRINT -207;TAB(8);FM
130 GOSUB 2000 :REM GO FIND A PEAK
140 IF NF>FF THEN POKE PA,PEEK(PA-2):GOTO 10
150 NF=NF+N+1
160 PRINTFNA(AP);TAB(8);FNA(F);TAB(16);FNA(AB);
164 IF F0>0 THEN PRINTTAB(24);FNA(F/F0);
166 PRINT
170 GOTO 130 :REM GO AND FIND NEXT PEAK
179 REM SINGLE PEAK FINDING ROUTINE
180 INPUT"RANGE,N,FREQ";FS,NS,SF
185 IF FS=0GOTO 180
190 NF=INT(SF/FS*500+0.5)-N
195 N=NS:YF=FS
200 FF=500
210 GOSUB 2000 :REM GO AND FIND PEAK
220 POKE PA,PT*4 :REM SET OUTPUT PORT
225 PRINT-205;TAB(8);TM
230 PRINT -206;TAB(8);FS
240 PRINTFNA(AP);TAB(8);FNA(F);TAB(16);FNA(AB)
250 POKE PA,PEEK(PA-2):GOTO 10
999 REM READ SPECTRUM FROM FFT
1000 POKE 287,80:POKE 288,9
1010 X=USR(0):POKE32794,32
1019 REM SET USR VECTOR TO SPECTRAL AMPLITUDE FUNCTION
1020 POKE 287,80:POKE 288,3
1030 RETURN
1989 REM PEAK FINDING SUBROUTINE
1990 NF=NF+1:IF NF>FF THEN RETURN
2000 P=0:PB=0:PF=0
2005 IF USR(NF)<2 GOTO 1990
2010 FOR I=NF-N TO NF+N
2015 IF USR(I)<0 THEN PRINT"OVERFLOW":END
2019 REM DO SUMMATIONS TO MEASURE CANDIDATE PEAK
```

```
2020 P=P+USR(I)*USR(I)
2030 PF=PF+USR(I)*USR(I)*(I-NF)
2040 PB=PB+USR(I)*USR(I)*(I-NF)*(I-NF)
2050 NEXT
2060 IF P=0 THEN NF=NF+N:GOTO 1990
2070 AF=PF/P
2079 REM CHECK IF FREQUENCY OFFSET SMALL ENOUGH
2080 IF AF>0.5 GOTO 1990
2090 IF AF<-0.51 GOTO 1990
2099 REM CHECK IF WIDTH SMALL ENOUGH
2100 IF PB/P>N*(N+1)/4 GOTO 1990
2104 REM CORRECT WIDTH FOR ANALYSER RESOLUTION
2105 PB=PB-P*(0.333+AF*AF):IF PB<0 THEN PB=0
2109 REM CALCULATE FREQUENCY AMPLITUDE AND BANDWIDTH
2110 F=YF*(NF+AF)/500:AP=SQR(P):AB=YF*SQR(PB/P)/250
2120 RETURN
9899 REM WAIT FOR ANY KEY TO BE PRESSED
9900 POKE 20466,0:PRINTCHR$(7)
9910 IF PEEK(20466)=0 GOTO 9910
9920 POKE 20466,0:RETURN
```

C.2 PLRANL

This program was run on the IBM 370 computer at Daresbury to produce tables of field strength for each harmonic as a function of distance from the power line for the work in chapter 4.

```
C PROGRAM TO PROCESS UNCORRECTED AMPLITUDES AND FREQUENCIES
C TO PRODUCE A TABLE OF FIELD STRENGTHS AS A FUNCTION OF
C SITE NUMBER, HARMONIC NUMBER AND RECORDING TYPE
      REAL AMP,FUNDO,LHN
      DIMENSION AMP(80,10,4),FUNDO(10,4),AMPCOR(10,4),AFCOR(80)
      DIMENSION FDA(18),ADA(18)
C INITIALIZE AMPLITUDES TO -999.0 (NO VALUE)
C AND FUNDAMENTAL FREQUENCIES TO 0.0
      DATA AMP/3200*-999.0/,FUNDO/40*0.0/
      LOGICAL LCAL
      DATA LCAL/.FALSE./
      REAL FCOR,A,B,CALF
      INTEGER SITE,TYPE,HN,TYP1
C SET STARTING HARMONIC NUMBER, SITE, AND RECORDING TYPE.
      DATA HN/1/,SITE/1/,TYPE/1/
C SET FUNDAMENTAL FREQUENCY TO 59 HZ INITIALLY
      DATA FUND/59.0/
C READ NUMBERS FROM NFPLR.. (PROBABLY AMPL. AND FREQ. )
   10 READ(7,*)A,B
C CHECK IF CONTROL COMMANDS
      IF(A.EQ.-205.0) GOTO 10
      IF(A.EQ.-206.0) GOTO 50
      IF(A.EQ.-207.0) GOTO 60
      IF(A.EQ.-999.0) GOTO 80
      IF(LCAL)GOTO 70
C IF NOT CONTROL CHECK IF FREQUENCY IS LESS THAN CURRENT HN
   20 IF(B.LE.FUND*HN+5)GOTO 30
      HN=HN+1
      GOTO 20
C CHECK IF A HARMONIC AND AMPLITUDE HIGH ENOUGH
   30 IF(B.GE.FUND*HN-5.AND.A.GE.2)GOTO 40
C WRITE OUT UNUSED DATA
      B=B/FUND
      WRITE(8,*)A,B
      GOTO 10
C STORE AMPLITUDE IN MAIN ARRAY
   40 AMP(HN,SITE,TYPE)=20.0*ALOG10(A)
C IF HARMONIC NO. 7 THEN RESET FUNDAMENTAL FREQUENCY
      IF(HN.EQ.7)FUND=B/7.0
      GOTO 10
C
C SET FLAG TO INDICATE CALIBRATION FOLLOWING
   50 LCAL=.TRUE.
      GOTO 10
C READ CALIBRATION INFO FROM PLRAUX..
   60 READ(5,*)SITE,TYPE,CALF
```

```fortran
      LCAL=.FALSE.
      HN=1
      GOTO 10
C PROCESS CALIBRATION DATA TO GET AMPLITUDE AND FREQUENCY
C CORRECTION FACTORS
  70  FCOR=7000.0/B
      AMPCOR(SITE,TYPE)=20.0*ALOG10(CALF/A)
      WRITE(8,*)AMPCOR(SITE,TYPE),FCOR,HN,SITE,TYPE
      FUNDO(SITE,TYPE)=FCOR*FUND
      GOTO 10
C COME HERE WHEN ALL DATA READ TO APPLY CORRECTIONS
C AND WRITE OUT RESULTS
C
  80  DO 150 TYPE=1,3,2
C READ FREQUENCY RESPONCE DATA FROM PLRAUX..
      DO 160 I=1,18
      READ(5,*)FDA(I),ADA(I)
 160  CONTINUE
      I=1
C CALCULATE AMPLITUDE CORRECTIONS FOR EACH HARMONIC
      DO 130 HN=1,80
      LHN=ALOG10(HN*60.0)
      IF(LHN.GT.FDA(I+1))I=I+1
      AFCOR(HN)=ADA(I)+(LHN-FDA(I))*
     *(ADA(I+1)-ADA(I))/(FDA(I+1)-FDA(I))
 130  CONTINUE
      WRITE(8,*)AFCOR
C APPLY CORRECTIONS TO AMPLITUDES IN ARRAY
      DO 150 SITE=1,8
      DO 150 HN=1,80
      TYP1=TYPE+1
      DO 150 I=TYPE,TYP1
      IF(AMP(HN,SITE,I).EQ.-999.0)GOTO 150
      AMP(HN,SITE,I   )=AMP(HN,SITE,I)+AMPCOR(SITE,I)-AFCOR(HN)
 150  CONTINUE
C WRITE OUT TABLES
      DO 120 TYPE=1,4
      WRITE(6,800)TYPE
      WRITE(6,802)(N,N=1,8)
      DO 110 HN=1,75
      WRITE(6,801)HN,(AMP(HN,SITE,TYPE),SITE=1,8)
 110  CONTINUE
      WRITE(6,803)(FUNDO(SITE,TYPE),SITE=1,8)
 120  CONTINUE
      STOP
 800  FORMAT(1H1,I4,30X,'SITE NO')
 802  FORMAT('H NO.',8I8)
 801  FORMAT(I4,8F8.1)
 803  FORMAT(1H0,'FUND',8F8.3)
      END
```

C.3 <u>PLRRAT</u>

This program, which was also run on the IBM 370 computer at Daresbury, produced tables of field strength ratios using the output produced by PLRANL.

```
C PROGRAM TO CALCULATE AMPLITUDE RATIOS
C OF 2 SETS OF RESULTS PRODUCED BY PLRANL
      INTEGER TYPE,HN,I,N
      REAL A,B,C
      DIMENSION A(8),B(8),C(8)
      DO 30 TYPE=1,4
      WRITE(6,601)TYPE,(I,I=2,8)
      DO 30 HN=1,75
C READ AMPLITUDES FROM INPUT FILES
      READ(5,500)N,(A(I),I=1,8)
      READ(7,500)N,(B(I),I=1,8)
      DO 40 I=1,8
      IF(A(I).EQ.-999.0) B(I)=0.0
      IF(B(I).EQ.-999.0) A(I)=0.0
C SUBTRACT TO CALCULATE RATIO SINCE AMPLITUDES LOG.
      C(I)=A(I)-B(I)
  40  CONTINUE
      WRITE(6,500)N,(C(I),I=1,8)
  30  CONTINUE
 500  FORMAT(I4,8F8.1)
 601  FORMAT('TYPE ',I1,4X,'1',7I8)
      END
```

142

C.4 Control commands for PLRANL

The following command file was used to link files (known as datasets on the IBM 370) to the program PLRANL and then to initiate execution of the program. The base name of the input files was NFPLR and that of the output files PLROUT. An extension to the file name was passed as a parameter to this command file to complete the filenames for a particular set of measurements. The files of base name PLRAUX contained data that described the conditions of the individual sets of measurements.

```
PROC 1 LC
ALLOC FILE(FT05F001) DA(PLRAUX&LC..DATA)
ALLOC FILE(FT06F001) DA(PLROUT&LC..DATA)
ALLOC FILE(FT07F001) DA(NFPLR&LC..DATA)
ALLOC FILE(FT08F001) DA(*)
LOADGO PLRANL FORTLIB
END
```

References

Akaike, H., Fitting Autoregressive Models for Prediction, Ann. Inst. Statist. Math., 21, 243-247, 1969

Albertson, V.D., J.M. Thorson, Jr., and S.A. Miske, J., The Effects of Geomagnetic Storms on Electrical Power Systems, Trans. Paper No. T-73-370-4, IEEE-PE5 Summer Meeting, Vancouver, Canada, July 15-20, 7pp, 1973

Ashour-Abdalla, M., Amplification of Whistler Waves in the Magnetosphere, Planet. Space Sci., 20, 639-662, 1972

Barr, R., ELF Radiation from the New Zealand Power System, Planet. Space Sci., 27, 537-540, 1979

Bernard, L.C., A New Nose Extension Method for Whistlers J. Atmos. Terr. Phys. 35, 871-880, 1973

Blackman, R.B. and J.W. Tukey, The Measurement of Power Spectra, Dover, New York, 1958

Boerner, W-M. and J.B. Cole, Interaction of Natural and Man-made Sources with the Geo-electromagnetic Environment - Overview, Presented at URSI, Washington DC, August 1981

Bullough, K. and J.L. Sagredo, VLF Goniometer Observations at Halley Bay, Antarctica - 1. The Equipment and Measurement of Signal Bearing, Planet. Space Sci., 21, 899-912, 1973

Bullough, K., A.R.L. Tatnall, and M. Denby, Man-made ELF/VLF Emissions and the Radiation Belts, Nature, 260, 401-403, 1976

Bullough, K. and T.R. Kaiser, Ariel 3 and 4 Studies of Power Line Harmonic Radiation, Wave Instabilities in Space Plasmas, p37-50, Ed: P.J. Palmadesso and K. Papadopoulos, D. Reidel Publishing Co., 1979

Bullough, K., Satellite Observations of PLHR, Review paper presented at the URSI Conference, Washington, August 1981

Bullough, K., and A. Cotterill, Ariel 4 Observations of Power-Line Harmonic Radiation Over North America and its Effect on the Magnetosphere, Proceedings 6th International Symposium on EMC, Wroclaw, June 1982, (cancelled)

Burg, J.P., Maximum Entropy Spectral Analysis, PhD. Thesis, Stanford Univ., Stanford, CA, 1967

Cagniard, L., Basic Theory of the Magnetotelluric Method of Geophysical Prospecting. Geophysics, 18, 605-635, 1953

Carson, J.R., Wave Propagation in Overhead Wires with Ground Return, Bell System Tech. J., 5, 539-544, 1926

Cooley, J.W. and J.W. Tukey, An Algorithm for the Machine Calculation of complex Fourier Series, Math. of Comput., 19, 297, 1965

Coroniti, F.V., R.W. Fredricks, C.F. Kennel and F.L. Scarf, Fast Time Resolved Spectral Analysis of VLF Banded Emissions, J. Geophys. Res., 76, 2366-2381, 1971

Dazey, M., Kafjord, Norway Transmission Line VLF Antenna Tests, 1979-1980. Aerospace Corporation Report No. SD-TR-82-22,1982

Dowden, R.L., A.D. McKay, L.E.S. Amon, H.C. Koons, and M.H. Dazey, Linear and Nonlinear Amplification in the Magnetosphere During a 6.6-kHz Transmission, J. Geophys. Res., 83, 169-181, 1978

Dowden, R.L., Non-Linear Magnetospheric Amplification of VLF Transmissions, Adv. Space Res., 1, 173-182, 1981

Fougere, P.F., A Solution to the Problem of Spontaneous Line Splitting in Maximum Entropy Spectrum Analysis, J. Geophys. Res., 82, 1051-1054, 1977

Francis, C.R., Satellite and Ground-Based Studies of ELF/VLF Wave-Particle Interactions, PhD Thesis, University of Sheffield, 1979

Garnier, M., G. Girolami, H. Koons and M. Dazey, VLF Iransmissions from Kafjord (Norway) to SCATHA. Adv. Space Res. 1, 213-216, 1981

Hargreaves, J.K., The Upper Atmosphere and Solar-Terrestrial Relations, Van Nostrand Reinhold Co. Ltd., 1979

Hayashi, K., T. Oguti, T. Watanabe, K. Tsuruda, S. Kokubun, and R.E. Hovita, Power Harmonic Radiation Enhancement During the Sudden Commencement of a Magnetic Storm, Nature, 275, 627-629, 1978

Helliwell, R.A., Whistlers and Related Ionospheric Phenomena, Stanford University Press, 1965

Helliwell, R.A., J.P. Katsufrakis, T.F. Bell, and R. Raghuram, VLF Line Radiation in the Earth's Magnetosphere and Its Association with Power System Radiation, J. Geophys. Res., 80, 4249-4285, 1975

Helliwell, R.A., D.L. Carpenter, and T.R. Miller, Power Threshold for Growth of Coherent VLF Signals in the Magnetosphere, J. Geophys. Res., 85, 3360-3366, 1980

Hutton, V.R.S., M.R. Ingham, and E.W. Mbipom, An Electrical Model of the Crust and Upper Mantle in Scotland, Nature, 287, 30-33, 1980

Jones, D., Pattern Recognition for VLF Studies, Radio Science, 8, 467-473, 1973

Jones, D., Auto and Cross-Correlation Analysis Techniques on-board Spacecraft, Ann. Telecommunic., 34, 187-195, 1979

Kodera, K., R. Gendrin, and C. de Villedary, Analysis of Time-Varying Signals with small BT Values, IEEE Trans. Acoust., Speech, Signal Processing, ASSP-26, 64-76, 1978

Koons, H.C., M. Dazey, and B.C. Edgar, Satellite Observation of Discrete VLF Line Radiation Within Transmitter-Induced Amplification Bands, J. Geophys. Res. 83, 3887-3889, 1978

Koziar, A. and D.W. Strangway, Shallow Crustal Sounding in the Superior Province by Audio Frequency Magnetotellurics, Can. J. Earth Sci., 15, 1701-1711, 1978

Lashinsky, H., T.J. Rosenberg, and D.L. Detrick, Power Line Radiation: Possible Evidence of Van Der Pol Oscillations in the Magnetosphere, Geophys. Res. Letts., 7, 837-840, 1980

Lefeuvre, F. and K. Bullough, Ariel 3 Evidence of Zones of VLF Emission at Medium Invariant Latitudes which Co-rotate with the Earth, Space Research XIII, Akademie-Verlag, Berlin, 699-706, 1973

Luette, J.P., C.G. Park and R.A. Helliwell, Longitudinal Variations of Very-Low-Frequency Chorus Activity in the Magnetosphere: Evidence of Excitation by Electrical Power Transmission Lines, Geophys. Res. Letts., 4, 275-278, 1977

Luette, J.P., C.G. Park, and R.A. Helliwell, The Control of Magnetospheric Chorus by power Line Radiation, J. Geophys. Res., 84, 2657-2660, 1979

Luette, J.P., C.G. Park, and R.A. Helliwell, Comment on 'On Possible Causes of Apparent Longitudinal Variations in OGO 3 Observations of VLF Chorus' by C.T. Russell, J. Geophys. Res., 85, 1343-1344, 1980

Lyons, L.R., A Comment on the Effects of Man-made VLF Waves on the Radiation Belts, E.O.S. Trans. AGU, 59, 362, 1978

Matsumoto, H., Nonlinear Whistler-Mode Interaction and Triggered Emissions in the Magnetosphere: A Review, P.J. Palmadesso and K. Papadopoulos (eds.), Wave Instabilities in Space Plasmas, D. Reidel Co., 163-190, 1979

Matthews, J.P., VLF Measurements in Antarctica, PhD Thesis, University of Sheffield, 1980

Matthews, J.P., and K. Yearby, Magnetospheric VLF Line Radiation Observed at Halley, Antarctica, Planet. Space Sci. 29, 97-106, 1981

Matthews, J.P., A Theory of VLF Emissions Triggered by Non-ducted Waves and an Interpretation of Magnetospheric Line Radiation Phenomena, Submitted to J. Geophys. Res., 1982

Matthews, J.P., Y. Omura and H. Matsumoto, A Study of Particle Trapping by Whistler Mode Waves in the Geomagnetic Field: A New Theory of the VLF Quiet Band Phenomenon, Submitted to J. Geophys. Res., 1982

Park, C.G., Methods of Determining Electron Concentrations in the Magnetosphere from Nose Whistlers, Stanford Electronic Laboratories Tech. Rpt. No. 3454-1, 1972

Park, C.G., VLF Wave Acivity During a Magnetic Storm: A Case Study of the Role of Power Line Radiation, J. Geophys. Res., 82, 3251-3260, 1977

Park, C.G., and R.A. Helliwell, Whistler Precursors: A Possible Catalytic Role of Power Line Radiation, J. Geophys. Res., 82, 3634-3642, 1977

Park, C.G. and D.C.D. Chang, Transmitter Simulation of Power Line Radiation Effects in the Magnetosphere, J. Geophys. Res. Letts., 5, 861-864, 1978

Park, C.G., and R.A. Helliwell, Magnetospheric Effects of Power Line Radiation, Science, 200, 727-730, 1978

Park, C.G., and T.R. Miller, Sunday Decreases in Magnetospheric VLF Wave Activity, J. Geophys. Res., 84, 943-950, 1979

Park, C.G., Generation of Whistler-Mode Sidebands in the Magnetosphere, J. Geophys. Res., 86, 2286-2294, 1981

Park, C.G., and T.R. Miller, Reply, J. Geophys. Res., 86, 1642-1644, 1981

Park, C.G., and R.A. Helliwell, Power Line Radiation in the Magnetosphere, Adv. Space Res. 1, 423-437, 1981

Paschal, E.W., Design of Broad-band VLF Receivers with Air-core Loop Antennas, Stanford Electronics Laboratories Report, September 1980

Pileggi, D.J., N.H. Chandra, and A.E. Emanuel, Prediction of Harmonic Voltages in Distribution Systems, IEEE Trans. Power Apparatus and Systems, PAS-100, No. 3, 1307-1315, 1981

Radoski, H.R., P.F. Fougere, and E.J. Zawalick, A Comparison of Power Spectral Estimates and Applications of the Maximum Entropy Method, J. Geophys. Res., 80, 619-625, 1975

Raghuram, R., T.F. Bell, R.A. Helliwell, and J.P. Katsufrakis, A Quiet Band Produced by VLF Transmitter signals in the Magnetosphere, Geophys. Res. Lett., 4, 199-202, 1977

Russell, C.T., On Possible Causes of Apparent Longitudinal Variations in OGO 3 Observations of VLF Chorus, J. Geophys. Res., 85, 1341-1342, 1980

Rycroft, M.J. Gyroresonance Interactions in the Outer Plasmasphere, J. Atmos. Terr. Phys., 38, 1211-1214, 1976

Smith, A.J., I.D. Smith, A.M. Deeley and K. Bullough, A Semi-Automated whistler Analyser. J. Atmos. Terr. Phys. 41, 587-600 1979

Stiles, G.S., Digital Spectra of Artificially Stimulated VLF emmisions, Stanford Electronics Laboratories, Tech. Rpt. No. 3465-3 1974

Stiles, G.S., Comment on 'Fast Time Resolved Spectral Analysis of VLF Banded Emissions' by F.V. Coroniti, R.W. Fredricks, C.F. Kennel and F.L. Scarf, J. Geophys. Res. 80, 4401-4403, 1975

Tatnall, A.R.L., A Satellite Study of Power Line Harmonic Radiation, Thunderstorm Noise and Associated Magnetospheric Phenomena, PhD Thesis, University of Sheffield, 1978

Tatnall, A.R.L., J.P. Matthews, K. Bullough, and T.R. Kaiser, Power-Line Harmonic Radiation and the Electron Slot, Scientific Report 1978 No. 1, Sheffield University Space Physics Group, 1978

Thorne, R.M., and B.T. Tsurutani, Comment on 'Sunday Decreases in Magnetospheric VLF Wave Activity' by C.G. Park and T.R. Miller, J. Geophys. Res. 86, 1639-1641, 1981

Tsurutani, B.T., S.R. Church, and R.M. Thorne, A Search for Geographic Control on the Occurrence of Magnetospheric ELF Emissions, J. Geophys. Res., 84, 4116-4124, 1979

Tsurutani, B.T., and R.M. Thorne, A Skeptic's View of PLR Effects in the Magnetosphere, Adv. Space Res. 1, 439-444, 1981

Ulrych, T.J. and T.N. Bishop, Maximium Entropy Spectral Analysis and Autoregressive Decomposition, Rev. Geophys. and Space Phys., 13, 183-200, 1975

Wedepohl, L.M., and A.E. Efthymiadis, Wave Propagation in Transmission Lines over Lossy Ground: a new, Complete Field Solution, Proc IEE, 125, No. 6, 505-510, 1978

Yearby, K.H., J.P. Matthews and A.J. Smith, VLF Line
Radiation Observed at Halley and Siple, Adv. Space
Res., 1, 445-448, 1981